Internet Data Transport

From the Perspective of Discrete Mass Transport Modeling

Vom Fachbereich Physik
der Universität Duisburg-Essen
(Campus Duisburg)
zur Erlangung des akademischen Grades eines
Doktors der Naturwissenschaften
genehmigte Dissertation von

Torsten Huisinga
aus
Düsseldorf

Referent: Prof. Dr. rer. nat. Michael Schreckenberg
Korreferent: Prof. Dr. rer. nat. Joachim Krug
Datum der mündlichen Prüfung: 30.01.2006

Contents

Abstract

In recent years a new class of one-dimensional cellular automata (CA) models has attracted much attention. These so-called mass transport models can be characterized as non-equilibrium stochastic processes.
In the presented thesis a new model of this class, the Asymmetric Multi Occupation Process (AMOP) is considered. This CA model was first introduced with open boundary conditions to simulate Internet data transport. It is defined on a one-dimensional lattice equipped with buffers of finite size that can be occupied by at most B particles. The local dynamics are implemented by the totally asymmetric shift of discrete mass variables respectively particles under consideration of hard-core repulsion and parallel dynamics.

In the first part of this work the AMOP with periodic boundary conditions is investigated by means of numerical as well as analytical considerations. Regarding deterministic model dynamics the influence of finite buffer and system sizes onto the fundamental diagram (FD), i.e., flow-density relation is analyzed. Furthermore, for stochastic movement the FDs obtained by numerical simulations are compared with analytical results derived by Mean-Field (MF) approaches and a 2-cluster approximation.
In the second part the AMOP with open boundary conditions is investigated in the context of boundary induced phase transitions. In case of deterministic bulk dynamics an analytical exact representation of the system inflow as well as the outflow is presented in dependence of the buffer size. As a result the deterministic phase diagram derived by numerical simulations could be verified by analytical considerations. Regarding stochastic particle movement the phase diagram is obtained by Monte Carlo simulations. In both cases it is shown that the jammed phase is strongly enlarged for increasing buffer sizes.
Finally, in the third part of this thesis the influence of interacting boundaries on the model dynamics is analyzed. Therefore, a new *fall back* inflow strategy is introduced in order to stabilize high flow states and thus prevent the system from a complete jamming. Precisely, the inflow is determined by the state of the last site of the system. As a result the phase diagrams of the deterministic and the stochastic model obtained by means of numerical simulations are presented. Two new phases could be identified a free-flow as well as a jammed phase both characterized by a striped microscopic pattern. Especially in the arising striped jammed regime system flow and mean velocity are drastically enlarged compared to generic inflow strategies. Here, the fall back strategy is capable to prevent the system from a complete jamming. Thus, the introduced inflow procedure represents an effective strategy for establishing reliable connections.

1 Preface

1.1 Introduction

Information exchange is one of the most important requirements in modern societies. Today the accessibility of information combined with the possibility to interact in seconds with systems and people around the whole world opens a new dimension of private and business life and has become a key element for a prosperous economic growth in a more and more global world. The communication structure behind the Internet, is considered to be the most rapidly growing and complex artificial system in the entire world. First introduced at the University of California in Los Angeles in 1969 as a project of the US Department of Defense, the Internet started a rise in information systems without comparison. In short times large companies recognized the enormous possibilities and participated in the development and further extensions of the Network. As a result nowadays the Internet has become a common media for almost everyone in the entire world. E-business and E-commerce are only two catchwords which represent the immense importance of this medium.

However, the enormous growth and the rapid expansion of the Internet combined with the demand of unrestrained capacity is accompanied by enormous challenges. Thus there are problems and obstacles leading to data losses because of capacity bottlenecks inducing Internet jams, an inhomogeneous infrastructure providing routing as well as compatibility problems and delays in the travel times of data packets and many more. So almost everybody using the Internet is familiar with annoying waiting times or web-site breakdowns and the necessity of transmission improvements[1]. In order to improve the connectivity and provide a more stable communication there are engineers and specialists with different scientific background working on the fields of Internet data transport, routing and network connectivity.

Also for physicists the Internet exhibits a wide field of scientific potential since transportation processes, many body systems and network structures are basic physical investigation fields. Therefore, the concepts of statistical physics are suitable methods to investigate the phenomena appearing in real data as well as the possibility to develop efficient models providing the important characteristic features of the Internet. On the basis of these models simulations can help to understand the basic phenomena leading to the characteristics of data transport in the Internet. Moreover, it becomes practicable to investigate and simulate scenarios and concepts introduced in order to solve the problems appearing in reality on large system scales with the focus on microscopic measurands as for example data packets in contrast to macroscopically defined measurement categories as flow or density. By means of the obtained results evaluations of the introduced models become practicable. Assumed that a realistic model approach exists, new concepts become applicable and therewith expensive misleading hardware enhancements as well as software design problems could be prevented or at least reduced.

[1] An overview of current Internet traffic can be found at *http://www.internettrafficreport.com.*

Especially in the field of transportation processes physicists recently introduced effective simulation methods originally developed for many-body system. A common and very popular simulation approach is a class of cellular automata (CA) models that provides simple applicability and an enormous potential for the investigation and analysis of complex systems. For example in the fields of vehicular traffic and pedestrian movement [24, 48, 69, 75, 82], granular media [63, 102, 120] and many other so called many body systems [22] where hundreds of thousands of vehicles, persons or particles have to be moved or updated, CA-models are widely used. Here, especially the discrete nature of this model class allows a rather simple implementation as well as the possibility to simulate a large amount of particles in extensive network environments much faster than real time compared to other simulation models like fluid dynamical approaches.

In general CA-models are predestined to help understanding interdisciplinary problems which are mostly representations of underlying non-equilibrium processes. In contrast to equilibrium systems where the probability distribution can be calculated for known energy functions or hermitian Hamiltonian non-equilibrium systems are defined by *local* rules and do no provide a hermitian Hamiltonian. These models can be categorized in systems relaxing into a thermal equilibrium and such ones in a stationary state far from thermal equilibrium. In this work the focus lies on a CA-model with local dynamics far from equilibrium. The model, introduced to simulate Internet data transport is investigated in the context of recent result and techniques adopted from equilibrium theory which are effectively introduced with slightly modifications.

1.2 Outline

The outline of this thesis is as follows: In the first part of chapter 2 the experimental facts and model approaches are recalled. The focus lies herby on the results derived by the statistical analysis of high resolution traffic data in order to reveal the statistical properties of real Internet data transport. In the second part of this chapter known mass transport models as well as the results obtained by analytical and numerical investigations are recalled.

The main focus is here the Asymmetric Simple Exclusion Process (ASEP) and the analytical results derived by the matrix product ansatz. Moreover, another mass transport model namely the discrete version of the Asymmetric Random Average Process (ARAP) is recollected in order to show the main differences between these two kinds of model types.

The main part of this thesis deals with a discrete mass transport model introduced in the scope of this work in order to simulate data transport in the Internet. The model can be classified as a combination of the ASEP and the ARAP.

In the third chapter the model with periodic boundary conditions is introduced and investigated by the help of numerical and analytical investigations.

The introduced model with open boundary conditions is investigated in chapter 4. Here the deterministic as well as the stochastic model is analyzed in the context of boundary induced phase transitions. In this context for deterministic particle movement the system inflow and outflow is calculated by analytical calculations. Moreover the phase diagrams

for the two model dynamics are derived by the help of numerical simulations.

In chapter 5 a new inflow strategy is introduced in order investigate the influence of flow control policies realized by reduced inflow rates. It will be shown that this new inflow strategy exhibits completely different system dynamics in case of deterministic as well as in case of stochastic movement. With regard to this finally the phase diagrams for both system dynamics are introduced.

In the last chapter finally a discussion and a summery will be given where the introduced model characteristics and features will be recalled and discussed.

2 Empirical Findings and Model Approaches

2.1 Introduction to Internet Data Transport

Data transport in the Internet is the basis for all computer applications dealing with the connectivity or the information exchange in any computer network. On the basis of so called internet protocols [1] small data packets denoted as *datagram* are guided autonomously throughout the complete network with all its complex sub-networks consisting of a widely heterogeneous hardware structure. Hereby, each data packet is treated by the basic *Transmission Control Protocol/Internet Protocol* (TCP/IP) individually at each single autonomously operating router. The arriving data packet contains all information needed by each of the enormous number of routers to be guided without the control of a superior monitoring unit through the entire network from source to destination host. Therefore, this protocol layer is called autonomous system level. Just as in any other complex network system a striking problem is the appearance of transportation or, as in this case, transmission failures caused by bottlenecks as routers and gateways no being able to cope with temporary growing bursts of demand of capacity or bandwidth. As a result, Internet jams induced by extraordinary Internet traffic at these bottlenecks or hardware failures lead to data losses or communication errors. Moreover, there are problems caused by the enormous growth and the heterogeneous character of the network as routing problems and the therewith associated data losses. Considering all these problems and difficulties that are causing an enormous economic loss, obviously there is a high potential for optimizing and improving the Internet data transport on the basis of scientific investigations. Consequently, the Internet has become an extremely interesting object of preference for scientists from different fields like physicists, mathematicians, network and computer engineers, but also for psychologists and other fields of humanities.
In order to get an impression of the complexity of the Internet in fig. 2.1 the location of almost every class C networks is mapped by the OPTE project [1] in November 2003.

2.2 Empirical Data

Reliable empirical data is the fundamental basis of all scientific investigations since the evaluation of physical properties as well as the model design can only be as exact as the collected data. In case of the Internet a large amount of empirical data has been gathered over the last years in the diverse scientific fields and plenty of surprising phenomena have been found. Outstanding features are self-similarity, long-range correlations occurring in Internet data traffic as well as scaling behavior in the connectivity of Internet nodes. These empirical findings are of special interest because of the fact that the arrival process of data packets was considered to follow an exponential distribution as described by Paxon et al. [89] and Crovella et al. [27]). Therefore, Internet data transport was regarded to obey a simple Poisson process [45, 67, 83] and thus modeled by queuing systems which of course

[1] Official specification documents of the Internet Protocol suite that are defined by the Internet Engineering Task Force (IETF) and the Internet Engineering Steering Group (IESG) are recorded and published as standards track RFC's and realize the communication of computers, routers and gateways.

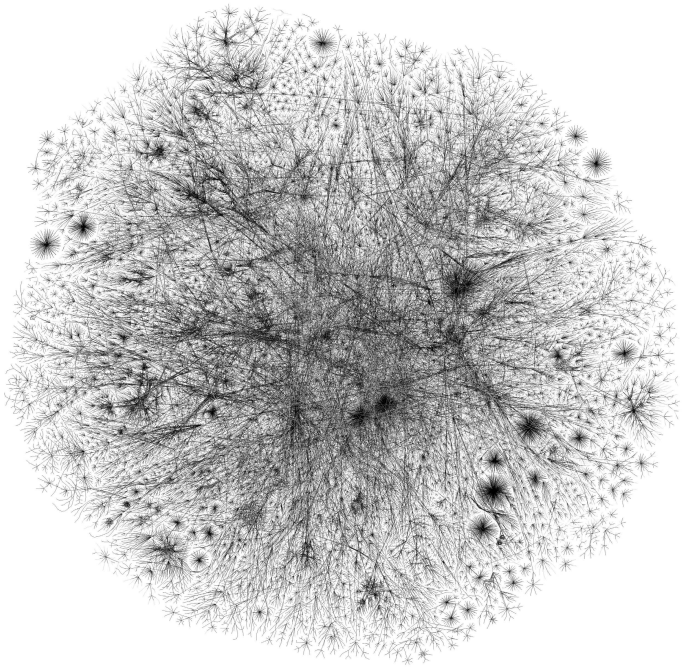

Figure 2.1: Visualization of the Internet (about 50 mio. edges) in Nov. 2003 taken from the OPTE project *http://www.opte.org*. Every edge represents a network while the nodes represent the mostly used paths between neighboring edges.

do not exhibit long-range correlations.
This was found to be in totally disagreement with empirical findings by Leland et al. [77, 78] and Willinger et al. [117] who extensively investigated high resolution traffic load data at single routers. This investigations revealed fractal behavior and therewith long-range correlations. Independent from these results there were investigations of Ping-experiment[2] time-series exhibiting $1/f$-noise [28, 54, 107, 108] also verifying the existence of long-range correlations in Internet data transport.

2.2.1 Time-Series Analysis

Empirical data often exhibits time dependent properties or correlations allowing the evaluation of characteristic system features. Therefore, the statistical analysis of time-series data is a basic investigating methods to find essential systems properties. In the notation and evaluating of discrete data sets or time-series a covariance stationary stochastic process X, i.e., the process is characterized by a constant mean $\mu = E[X_t]$ and a finite

[2]The *ping* command is a simple unix program sending an Internet control packet to dedicated Internet hosts. Hereby, the bidirectional travel time between the source and the destination host, i.e., the round trip time, is measured and used for the statistical analyze.

variance $\sigma^2 = E[(X_t - \mu)^2]$, of a set of random variables $\{X_t : t \in \tau\}$ usually defines a probability space τ where t represents a discrete time-step and X_t the state of the system at that time. A basic analyzing method to investigate the characteristics of discrete arbitrary time-series $x(t)$ is the analysis of the power spectrum $S(f)$ which is generated by applying the discrete Fourier-transform (DFT) on $x(t)$. The discrete Fourier-transform $F(f)$ for a time series $x(t)$ of length T with $t = 0, 1, ..., T$ is given by:

$$F(f) = \sum_{t=0}^{T-1} x(t) e^{2\pi i t f/T}, \tag{2.1}$$

while the inverse discrete Fourier transform is given by:

$$x(t) = \frac{1}{T} \sum_{f=0}^{T-1} F(f) e^{-2\pi i t f/T}. \tag{2.2}$$

The power spectrum or power spectral density S(f) reveals the dominant time constant in the system and is related to the autocorrelation function AC via the Wiener-Khinchin-Theorem:

$$AC(k) = F(S(f)), \tag{2.3}$$

with

$$S(f) = |F(f)|^2 \tag{2.4}$$

and

$$AC(k) = \frac{E[(X_t - \mu)(X_{t+k} - \mu)]}{E[(X_t - \mu)^2]}. \tag{2.5}$$

Here, E represents the expectation. For detailed explanations see [83, 93]. A stochastic process then is called *long range dependent* if its auto-correlation function decays to zero as a power-law in so far that $\lim_{k\to\infty} |AC(k)| = \infty$ which means that there is a kind of memory existing in the system dynamics leading to a significant dependence between distant values.
Self-similarity on the other hand means that certain properties of a stochastic process arise independent from scaling in space and time. Precisely a stochastic process is self-similar for

$$x(at) = a^H x(t), \qquad a > 0 \tag{2.6}$$

where a is a scaling factor. H is called *Hurst exponent* representing a persistent system for $1/2 < H < 1$ while an Hurst exponent of $H < 1/2$ characterizes an anti-persistent one (Markov or ARMA processes). Otherwise, in case of $H = 1/2$ the system describes a random walk problem (see [45, 60, 61, 81]). As shown above, the autocorrelation function is related to the power spectrum via the Wiener-Khinchin-Theorem. Considering a power spectrum in log-log scale a $1/f$-trend appears as a straight line with slope $\xi = -1$. For a fractal or self-similar time-series there is a simple relation between the slope ξ and the Hurst exponent given by:

$$\xi = 2H - 1. \tag{2.7}$$

Summarizing this section it is to mention that slowly decaying variances, long-range dependence and a power-spectrum obeying a power-law behavior are different manifestations of fractal or self-similar behavior of the underlying stationary stochastic process.

2.2.2 Internet Traffic Data and Analysis

The first evidence of self similar behavior in Internet traffic was found by Leland et al. in 1994 [77]. In order to characterize the properties of Internet traffic consequently detailed investigations of the system flow (precisely the amount of data packets per time) at single network nodes were conducted. The collected data were extensively evaluated in the context of time-series analysis. It was found that the variability was invariant compared to the observed time scale indicating self-similarity or long range dependence, i.e., with autocorrelation functions decaying like a power law [27, 77, 78, 117]. Precisely, Leland and colleges found bursts of data packets at network nodes which show similar statistical behavior in time intervals of $10^{-2}s, 10^{-1}s, 1s, 10s$ and $100s$. The existence of long-range dependence in Internet data traffic was confirmed by Paxon and Floyd [89] by investigating Telnet and FTP packet arrival times. The collected data exhibits heavy-tailed distributions of the packet inter-arrival times and was characterized by higher variability indicating that Poisson processes underestimate the variability. Moreover, Willinger et al. [117] investigated the packet flow at single network nodes and identified so called heavy-tail distributed ON/OFF sources, i.e., active and less active time periods and by this investigations also confirmed self-similar behavior at the macroscopic investigation level. Further investigations of end-to-end data as well as further flow measurement data confirmed the existence of long-range dependence and the self-similar character. The different power-law behavior revealed by the investigations were then used as a characterization method to identify traffic patterns [4, 27, 44, 84, 98, 113].

Independent from the investigations of Leland in 1994 in the same year Csabai [28] also found self similar behavior, namely $1/f$-noise in fluctuations of the round-trip-times (RTT-times) derived by Internet Ping-experiments. In this experiment the travel times of single data packets between two designated Internet hosts were measured representing indirectly the state of congestion along the considered path. Later these results were confirmed by Takayasu et al. [107, 111] and Huisinga et al. [54] who also found critical behavior, i.e. $1/f$-noise, in the power spectra of ping experiment data. Detailed analysis of RTT-data sets revealed that the power spectra of the RTT time series exhibit white noise for paths without congestions while there is a $1/f$-dependence for routes with critical load. Further investigations exhibit that congested paths on the other hand are characterized by a $1/f^{\xi}$-dependence with $\xi \approx 1/2$ of the arriving times of the data packets as described in [54, 55].

A typical time series showing self-similar properties is depicted in fig. 2.2 while the corresponding power-spectrum is given in fig 2.3. Clearly, the $1/f$-noise can be identified for low frequencies respectively for long time scales while for short time scales white noise dominates the power-spectrum. For the sake of completeness in fig 2.4 and fig 2.5 typical power-spectra for congested and free flow paths are depicted. Here, the power spectrum in fig. 2.4 corresponds to a path without congestions. Consequently, white noise dominates over all time scales. Contrary, for paths with strong congestions in fig. 2.5 there is a $1/f^{1/2}$-dependence at large time scales while white noise dominates at short time scales.

Summarizing this, the results found by time series analysis of packet flow measurements and Ping-experiment data clearly confirmed the fractal or self-similar character of Internet transport processes. However, the exact origin of the statistical properties of the underlaying mechanism are not yet exactly known. But there are investigations and model approaches describing these phenomena in the context of dynamical phase transition behavior [56, 59, 109, 110].

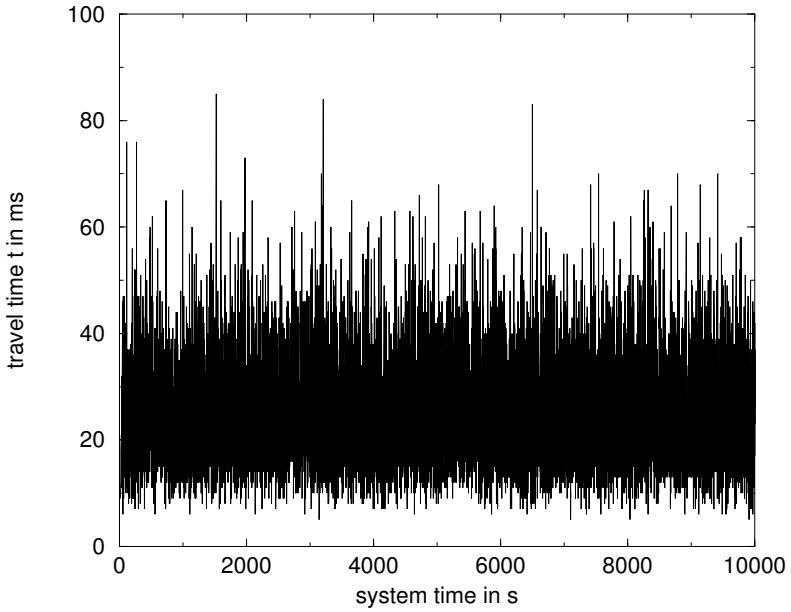

Figure 2.2: Typical RTT time-series for a system with critical load taken from [55]. The abscissa shows the time the data packet was broadcast while the ordinate represents the travel time of the data packet.

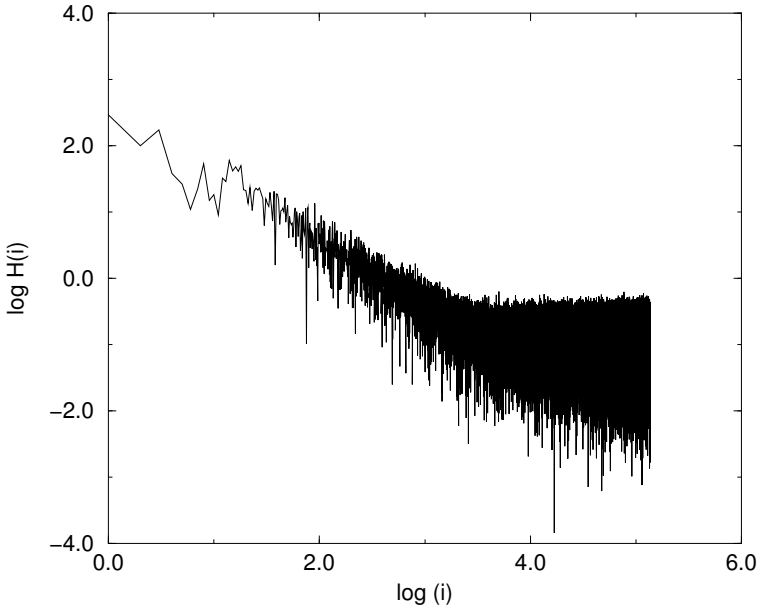

Figure 2.3: Corresponding power spectrum of a path at critical load in log-log scale. There is a $1/f$-dependence for low frequencies while larger frequencies exhibit white noise.

Another important research field in the framework of Internet data transport are investigations concerning the topology and the expansion of the Network. In order to develop effective simulation models a detailed knowledge of the underlying network structure and evolution is of prime importance [90]. Moreover, developing routing strategies and algorithms adjusted to the topology and the protocols realizing the data transport are of

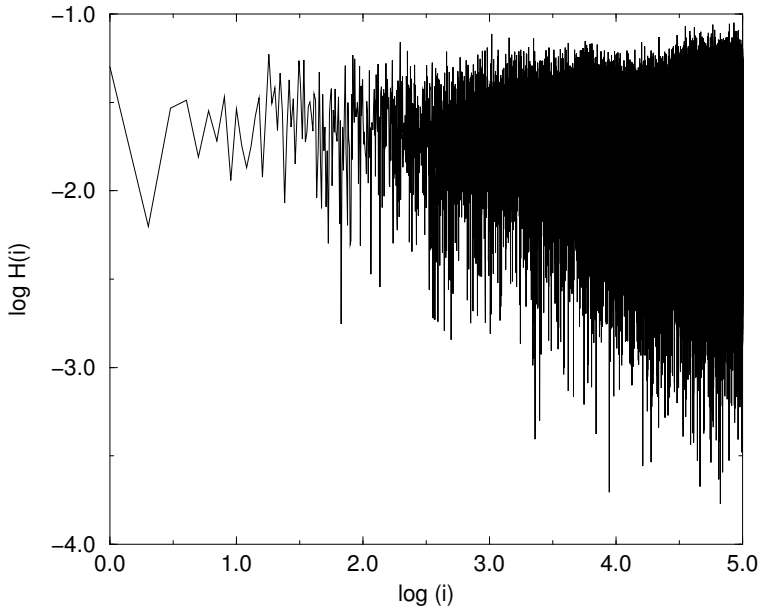

Figure 2.4: Power spectrum of a internet path without any congestion. The complete frequency range is dominated by white noise.

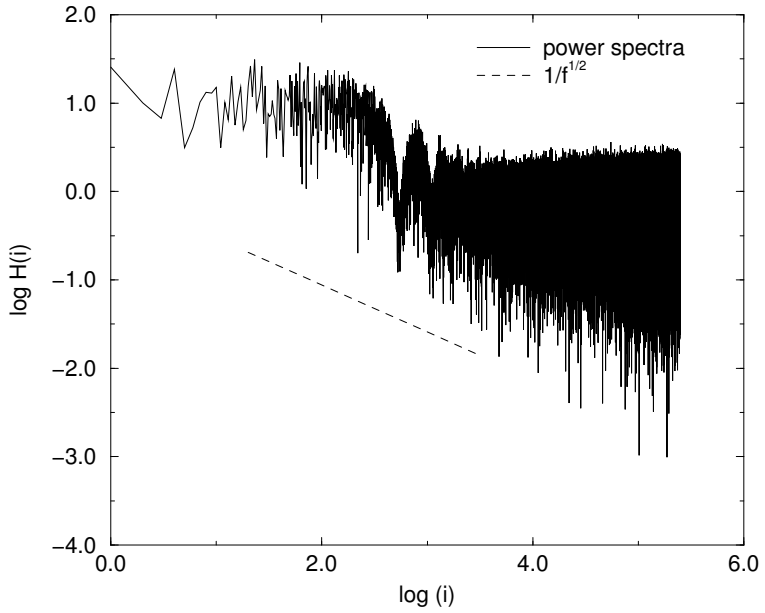

Figure 2.5: Power spectrum of the RTT data of a congested path. There is a $1/f^{1/2}$-dependence at small frequencies while the higher frequencies are also dominated by white noise.

special interest. The Internet is hereby a typical example of a growing complex network [5, 6, 36, 87, 106] showing sophisticated phenomena such as *small-world* characteristics [11, 106, 116], i.e., the average separation between clustered vertices grows slowly with the total number of vertices, or the power-law distributed behavior of the node degree $P(r) \propto r^{\xi}$, where r corresponds to the number of edges incident to a vertex or node and ξ a certain network specific exponent. Networks showing these power-law distributed node degree are called *scale-free* networks [12, 13, 37, 43, 85, 86] and can be found in

different fields, e.g., physics, biological systems and many more. For a deeper insight, see [38, 88] and references therein. And last but not least there were investigations of the social structures or the *human factor* [53] describing the user behavior and the influence on data traffic and traffic demand.

2.3 Simulation Methods

In order to determine the nature of the phase transition behavior in real data measurements of RTT time-series Takayasu et al. [110] introduced a cut off threshold between congested and free flow travel times and analyzed the *congestion duration length* to determine the cumulative distribution of the *jammed* states where the travel times are found larger than the dedicated threshold. As a result it was found that the congestion duration distribution length follows a power law distribution with exponent $\xi = -1$ corresponding to $1/f$-noise in the power-spectra at critical load. Moreover, it was shown that the free flow regime is characterized by an exponential decay while the jammed state is delineated by an exponent $\xi < 1$. Therewith, the existence of two phases could be confirmed, in particular because of the fact that the congestion duration probability shows self similarity as well as a tendency to a divergence of the auto-correlation function for RTT intervals near the defined threshold (see [46, 47, 110] and references therein).

With the aim to get an deeper insight into the statistical system behavior of Internet data transport and the real mechanism of phase transition behavior the first model proposals were based on the assumption that the data transport in the Internet could be simulated by queuing models following the statistics of Poisson processes. This model approach was effective applied in traditional traffic theory [26, 27, 89]. However, as mentioned before the statistics of such Poisson processes do not exhibit long range correlations at all and consequently this model approach becomes ineffective and is only marginally applied for simulations of Internet data transport.

Nowadays, a widely used tool for simulating and evaluating Internet data transport is the *Network Simulator Vers. II* (ns2) [2], a highly complex free software package used by many researchers in order to investigate detailed protocol influences onto the statistics of the transport process. The detailed implementation of the simulator tool with an immense degree of freedom, i.e., detailed definition of the capacity, propagation delay, queuing size, queuing management, sender and receiver specific rule-sets and many others, becomes a strongly limiting factor with regard to the complexity of the network topology as well as the scenarios which can be analyzed. Therefore, there are newer and in particular smaller simulation tools basing on the ns2-simulator with limited libraries in order to simulate larger networks less detailed [115].
With regard to this, cellular automaton models with their well known advantages for the simulation of complex many body systems might be a very useful and efficient tool in order to get excellent results concerning the detailed analysis of transport processes in the Internet even in case of large scale simulations.

2.4 CA-Models Simulating Transportation Processes

In the field of statistical physics cellular automata models have become a very useful tool for investigating complex many-body systems. Their flexibility and in particular their simple applicability for computer simulations predestine these models for investigating topics

of inter-disciplinary fields like biochemical systems, vehicular traffic or especially in this case Internet data transport. Hereby, the main advantage is the ability to handle complex network topologies and in particular an immense number of particles. This features have made cellular automaton models a common and efficient simulation method.
First introduced in the 1960's by von Neumann [114] who was working on self replicating systems[3], Cellular Automaton models (CA models) were introduced as a infinite, regular grid of cells where each cell can take on a finite number of states. All cells were updated according to universal rule sets synchronously and in discrete time steps. About 20 years later John Horton Conway introduced a two dimensional cellular automaton model called "game of life" [49]. This game of life drew much attention after an article in "Scientific American" and was widely investigated upon the development of micro computers, which are in fact, regarding the utilized logic, von Neumann machines. The simple game of life CA with its very simple deterministic interacting rules exhibits an immense diversity of behaviors, as fluctuations between randomness and order or the appearance of so called gliders, stable structures moving across the grid with the ability to interact and so perform logical operations. Later in the 1980s Stephen Wolfram published systematical investigations of an elementary class of CA models (see [121–123] and references therein). The introduced CA model class was defined on a one-dimensional grid of cells where each cell exhibits two neighbors and also two different states. This means that there are $2^3 = 8$ dedicated configurations a neighborhood can take on. This as a results leads to $2^8 = 256$ possible rule sets and so Wolfram introduced a classification of the resulting CA models after the binary name of the chosen rule set.

Nowadays, CA models are widely used in diverse scientific fields since further model development like the introduction of stochastic rule sets (see [94]) or open boundaries exhibit a rich dynamic behavior as self-organized criticality [9, 10, 105, 123] or boundary induced phase transitions (see [23, 72] and references therein). Especially CA models with open boundaries that can be classified as driven lattice gas models (DLG) first introduced to simulate and understand the effect of the electric field on the ordering processes to admit a directed particle movement [34, 64, 65] have become common simulation models due to their relevance for real world problems. A well understood DLG-model describing transportation processes is the Asymmetric Exclusion Process (ASEP) [72], a lattice gas automaton (see [23] and references therein) with slight changes first introduced to simulate biological systems as the kinetics of polypeptide synthesis [80] or later vehicular traffic (Nagel-Schreckenberg Model [82]). In case of the ASEP with open boundary conditions particles move according to a driving force from one reservoir at one end to another reservoir at the other end of the system. In contrast to periodic systems with a conserved number of particles, these systems reside in a state far from equilibrium and therefore can not be described in the context of statistical equilibrium mechanics. Recently, another class of cellular automaton models have attracted much attention. These so called mass transport-models [41, 73] are characterized by multi-occupation of sites, i.e, each site can be occupied by an arbitrary amount of particles in the discrete picture or a arbitrary mass variable in the continuous picture (see [41, 73] and references therein). This rather artificial model class exhibits a close relation to the so called q-model [25] describing the structure of forces responsible for the solid structure of granular materia.

[3] By the use of a two dimensional CA with nearest neighbor interactions and 29 states per cell, von Neumann introduced a simplified model of the physics of the universe which acted like a self replicating machine making endless copies of itself.

2.5 Asymmetric Simple Exclusion Process (ASEP)

The ASEP as mentioned before was introduced to simulate the kinetics of polypeptide synthesis and was originally formulated in mathematical literature in continuous time where particles are situated at the sites of a d-dimensional lattice. In this formulation dynamics are introduced by allowing the particles to move to the next neighboring empty sites with random rates. For a deeper insight see [79, 103, 104, 112] and references therein.

The one-dimensional derivative of the asymmetric exclusion process can be characterized as the prototype model for a driven diffusive system [35, 64, 65] where exact analytical results can be found by using the matrix product ansatz for different kinds of update procedures [32, 96, 97], moving directions [33] and boundary conditions [30, 39, 40, 42]. Moreover, there are analytical results derived with the help of the Bethe-Ansatz describing the influence of defects [31] and many more. For more details see [23] and references therein.

In the following the model variant with open boundary conditions as depicted in fig. 2.6 and hardcore repulsion where particles move because of an internal driving force from one reservoir at one end in a dedicated direction to another reservoir at the other end of the system is recalled because of its relevance for the further investigation.

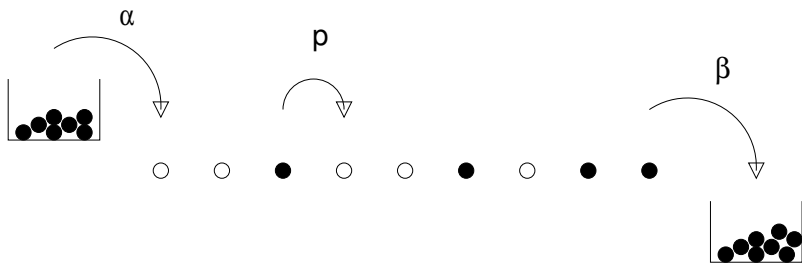

Figure 2.6: Figure of the ASEP with open boundary conditions. Particles are inserted at the left hand side with probability α. They move with probability p throughout the entire system and are removed at the right end with probability β.

For the sake of completeness the definition of the model with open boundary conditions and parallel update dynamics is described in the following:

Consider a one-dimensional lattice of $i = 1, ..., L$ sites where each site i can be empty ($\tau_i = 0$) or occupied ($\tau_i = 1$) by one single particle. The system configuration is then represented by the n-tuple $\tau = (\tau_1, ..., \tau_L)$ of the single site configurations τ_i. The inflow is realized by inserting particles at the left boundary (site $i = 1$) with a certain probability α while the outflow is implemented by removing particles at the right end of the system (site $i = L$) with probability β.
The system dynamics with parallel update procedure is applied by moving the particles at site $i = 1, ..., L-1$ synchronously with probability p to the next neighboring site at the right as far as this site is not occupied. In case of an occupied next neighboring site the particle rests at its current position (hard-core repulsion).

The ASEP with open boundary conditions and random sequential dynamics has been solved analytically by Derrida et al. [30, 32] by representing the weights of any possible

configuration in the steady state by non-commuting matrices, a technique introduced on *lattice animal problems* [112] and anti-ferromagnetic spin chains [68]. Hereby, the transition probability ϕ for a Markov-Process from any arbitrary probability distribution $P_L(\{\tau\}, t)$ with the states $\{\tau\} = \{\tau_1, \tau_2, \tau_3, ..., \tau_L\}$ of each lattice cell at time t to the probability distribution $P_L(\{\tau'\}, t + \delta t)$ at time $t + \delta t$ can be described by the master equation:

$$\frac{\partial P(\{\tau\}, t)}{\partial t} = \sum_{\{\tau'\}} \phi(\{\tau'\} \to \{\tau\}) P(\{\tau'\}, t) - \sum_{\{\tau'\}} \phi(\{\tau\} \to \{\tau'\}) P(\{\tau\}, t). \tag{2.8}$$

It turns out that the master equation of the stationary state of the ASEP can be exactly solved by analytical investigations for different kinds of update procedures with the help of the matrix product ansatz (MPA). For more details see [32, 40, 42, 96].

In the following the exact analytical results derived by Evans et al. [42] for the parallel update rule set and open boundary conditions in terms of the quantum formalism is presented briefly.
In the steady state $P_L(\tau)$ denotes the probability to find a system of L sites in the configuration τ. Regarding not-normalized weights $f_L(\tau)$ it follows:

$$P_L(\tau) = f_L(\tau)/Z_L, \tag{2.9}$$

where

$$Z_L = \sum_{\tau} f_L(\tau) \tag{2.10}$$

represents the sum over all possible configurations. The matrix product ansatz is introduced by writing $f_L(\tau)$ as the scalar product of operators $\mathbf{E}$ and $\mathbf{D}$ where $\mathbf{E}$ represents an empty site and $\mathbf{D}$ an occupied one. The vectors $\langle W|$ and $|V\rangle$ then represent the boundary conditions and have to preserve the stationary state weights. As a result the weights are given by:

$$f_L(\tau) = \langle W| \prod_{i=1}^{L} ((1 - \tau_i)\mathbf{E} + \tau_i \mathbf{D}) |V\rangle. \tag{2.11}$$

Moreover, the operators $\mathbf{E}$ and $\mathbf{D}$ as well as the vectors $\langle W|$ and $|V\rangle$ have to satisfy algebraic rules given in the following. In the bulk one gets:

$$\begin{aligned}
\mathbf{EDEE} &= (1-p)\mathbf{EDE} + \mathbf{EEE} + p\mathbf{EE}, \\
\mathbf{EDED} &= \mathbf{EDD} + \mathbf{EED} + p\mathbf{ED}, \\
\mathbf{DDEE} &= (1-p)\mathbf{DDE} + (1-p)\mathbf{DEE} + (1-p)\mathbf{DE}, \\
\mathbf{DDED} &= \mathbf{DDD} + (1-p)\mathbf{DED} + p\mathbf{DD}.
\end{aligned}$$

Furthermore the interaction of the boundary vectors has to be considered. The rules involving two sites next to the boundaries are given by:

$$\begin{aligned}
\mathbf{DD}|V\rangle &= \frac{p(1-\beta)}{\beta}\mathbf{D}|V\rangle, \\
\mathbf{ED}|V\rangle &= \frac{p}{\beta}\mathbf{E}|V\rangle, \\
\langle W|\mathbf{EE} &= \frac{p(1-\alpha)}{\alpha}\langle W|\mathbf{E}, \\
\langle W|\mathbf{ED} &= \frac{p}{\alpha}\langle W|\mathbf{D}.
\end{aligned}$$

Moreover for the interaction with the three sites next to the boundaries it has to be valid:

$$\begin{aligned}
\mathbf{DDE}|V\rangle &= (1-\beta)\mathbf{DD}|V\rangle + (1-p)\mathbf{DE}|V\rangle + p(1-\beta)\mathbf{D}|V\rangle, \\
\mathbf{EDE}|V\rangle &= (1-\beta)\mathbf{ED}|V\rangle + \mathbf{EE}|V\rangle + p\mathbf{E}|\mathbf{V}\rangle, \\
\langle W|\mathbf{DEE} &= (1-\alpha)\langle W|\mathbf{EE} + (1-p)\langle W|\mathbf{DE} + p(1-\alpha)\langle W|\mathbf{E}, \\
\langle W|\mathbf{DED} &= (1-\alpha)\langle W|\mathbf{ED} + \langle W|\mathbf{DD} + p\langle W|\mathbf{D}.
\end{aligned}$$

The complete rule sets for the algebra can be solved by introducing suitable operators, i.e., rank four tensors, for $\mathbf{D}$ and $\mathbf{E}$ and vectors $\langle W|$ and $|V\rangle$ of the same dimension to generate quadratic rules as follows.

$$\mathbf{D} = \begin{pmatrix} D_1 & 0 \\ D_2 & 0 \end{pmatrix}, \qquad \mathbf{E} = \begin{pmatrix} E_1 & E_2 \\ 0 & 0 \end{pmatrix} \tag{2.12}$$

and

$$\langle W| = (\langle W_1|, \langle W_2|), \qquad |V\rangle = \begin{pmatrix} |V_1\rangle \\ |V_2\rangle \end{pmatrix}. \tag{2.13}$$

Here, $D_1, D_2, E_1, E_2, V_1, V_2, W_1, W_2$ are of arbitrary (usually infinite) dimension. Now it is possible to derive an expression for the normalization constant Z_L as:

$$Z_L = \langle W|\mathbf{C}^L|V\rangle \tag{2.14}$$

with

$$\mathbf{C} = \mathbf{D} + \mathbf{E} = \begin{pmatrix} C_1 & E_2 \\ D_2 & 0 \end{pmatrix} \tag{2.15}$$

and $C_1 = D_1 + E_1$.

Therewith, the exact flow J_L, the density profile or one-point correlation function $\langle\tau_i\rangle_L$ as well as the higher correlation functions, e.g., the two point correlation function $\langle\tau_i(1-\tau_j)\rangle_L$ can be calculated by the help of the introduced algebra as:

$$J_L = p\frac{\langle W|C^{i-1}DEC^{L-i-1}|V\rangle}{Z_L}, \tag{2.16}$$

$$\langle\tau_i\rangle_L = \frac{1}{Z_L}\langle W|C^{i-1}DC^{L-i}|V\rangle \tag{2.17}$$

and

$$\langle \tau_i(1-\tau_j)\rangle_L = \frac{1}{Z_L}\langle W|C^{i-1}DC^{j-i-1}EC^{L-j}|V\rangle. \tag{2.18}$$

It turns out that one can find an one-dimensional representation for $\mathbf{D}, \mathbf{E}, \langle W|$ and $|V\rangle$ only if $\alpha + \beta = p$. Only in this case the mean field results become exact whereas in all other cases the matrices are infinite-dimensional. The knowledge of the system flow J in dependence to α, β, p and the exact shape of the density profiles allows to calculate the phase diagram depicted in fig. 2.7 and moreover with regard to the shape of the density profiles the nature of the phase transitions that occur in the system can be determined.

In case of deterministic movement with $p = 1$ the only stochastic elements are the inflow and outflow rates α and β respectively. Here, two phases can be identified, a low density free flow phase and a high density jammed phase.

In the low density regime ($\alpha < \beta$) the free flow J_- is given by:

$$J_- = \frac{\alpha}{1+\alpha} \tag{2.19}$$

and the density profile $< \tau_i >_L$ obeys:

$$< \tau_i >_L = \frac{\alpha}{1+\alpha}(1 + \frac{1-\beta}{\beta}e^{(L-i)\ln(\alpha/\beta)}). \tag{2.20}$$

Contrary, in the high density regime ($\beta > \alpha$) the system flow J_+ is given by:

$$J_+ = \frac{\beta}{1+\beta} \tag{2.21}$$

and here the density profile is given by:

$$< \tau_i >_L = \frac{1}{1+\beta}(1 - (1-\alpha)e^{i\ln(\beta/\alpha)}). \tag{2.22}$$

At the transition line ($\alpha = \beta$) the density becomes linear as,

$$< \tau_i >_L = \frac{\alpha}{1+\alpha}(1 + \frac{(1-\alpha)i}{\alpha L}) \tag{2.23}$$

indicating a first order phase transition.

In contrast thereto in case of stochastic movement($p \neq 1$) the phase-diagram of the ASEP is depicted in fig. 2.7 in dependence to α and β for fixed hopping probability $p = 0.5$. Three phases can be distinguished, a low density phase (AI, AII) a high density phase (BI, BII) and a maximum current phase (C). Characteristic density profiles of the corresponding phases are depicted in the insets and can be consulted in order to reveal the nature of the phase transitions in the system. As a result one finds a first order phase transition between jammed and free-flow phase while there are continuous (second order) phase transitions between jammed and maximum current as well as between free flow and maximum current phase respectively. For more details see [42].

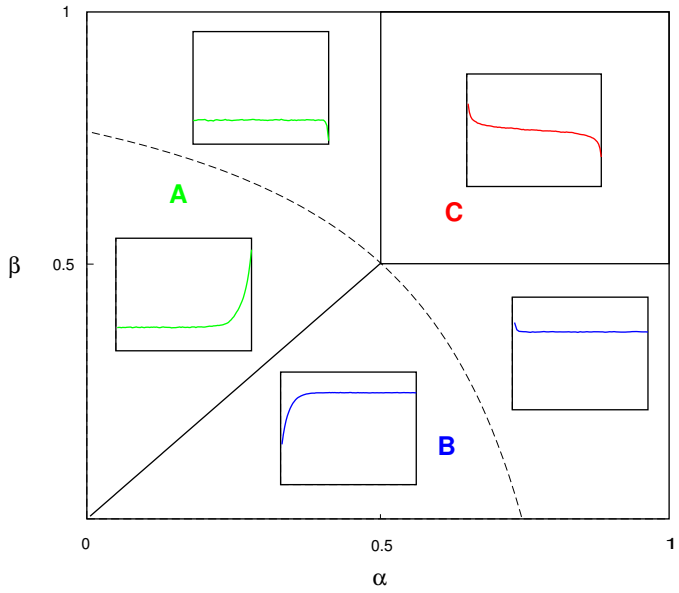

Figure 2.7: Exact phase diagram of the ASEP derived by analytical investigations. The exact mean field results with $\alpha - \beta = p$ are given by the dashed line. The picture is taken from [42].

2.6 Mass Transport Model Approach

Recently, investigations of a model class describing mass transport processes have attracted much attention. Well known models are for example the Zero Range Process (ZRP) [41] or the Asymmetric Random Average Process (ARAP) [73, 95]. A characteristic feature of these model class is the stochastic transport of so called *masses* in continuous (ARAP) or discrete (ZPR) representation along a chain of sites. Usually, one considers periodic boundary conditions whereas there are no restrictions or limitations for the mass transport from one site to another one, i.e., unbound state space. In contrast to the ASEP or other discrete transportation models, e.g., NaSch or VDR, here multi-occupation of single sites is an essential model characteristic.

In this context the investigated Internet model can be seen as a specification of mass transport models since in the Internet model there is a limitation in the maximal mass transport from one site into the next one because of the introduction of finite buffer size. In order to develop a effective strategy to represent the periodic version of the internet model by terms of a matrix representation the results of the ARAP are recalled here.

2.6.1 Asymmetric Random Average Process

The ARAP can be regarded as an archetype of a mass transport model since this model is equipped with probabilistic nearest neighbor interaction where the mass transport is realized by chipping a continuous amount of mass m_i from one site i to the next neighboring one $i + 1$ in continuous time. Nevertheless, although the ARAP is an artificial construct its generic model definition allows the mapping to other mass transport models by slightly changes in the system rule-sets [125, 126].
The model dynamics for the ARAP with discrete mass transport in discrete times are recalled in the following in order to show the affinity between the ARAP and the Internet

model [55] that will be analyzed in this thesis.

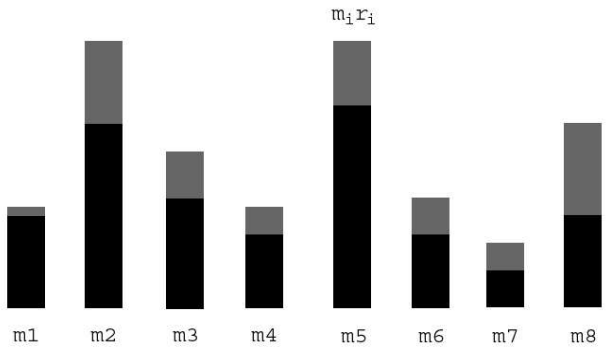

Figure 2.8: Schematic representation of the Asymmetric Random Average Process (ARAP). The model is defined on a periodic lattice with an arbitrary number of sites. Particles move according to the chosen chipping rate r_i into the next neighboring site.

For parallel dynamics the update procedure is realized by choosing a random number r_i with $r_i \in [0,1]$ to determine the amount of mass $\Delta_i = m_i r_i$ transported from site i to site $i+1$ at each discrete time step Δt. Therewith, the representation of the local mass transport is given by the following master equation:

$$m_i \to (1-r_i)m_i + r_{i-1}m_{i-1}. \tag{2.24}$$

The ARAP was solved in case of periodic boundary conditions parallel dynamics and discrete masses in terms of the matrix-product technique by Zielen et al. [126]. Therefore, the already known mean-field results [125] were reproduced by a one-dimensional representation of the matrix-algebra in consideration of the fact that the ARAP with periodic boundary conditions and parallel update scheme in the thermodynamic limit ($M, L \to \infty$ with $\rho = M/L = \text{const.}$) can be represented by a backward sequential update procedure of the MPA. The corresponding stationary state mass distribution of the system is then given by:

$$|P\rangle = Tr\left(A \otimes A \otimes ...A \otimes \hat{A}\right) \tag{2.25}$$

A and $\hat{A}$ are the state vectors of each site $i = 1, ..., L$ and are defined as:

$$A := \sum_{m=0}^{\infty} D_m |m\rangle, \tag{2.26}$$

$$\hat{A} := \sum_{m=0}^{\infty} \hat{D}_m |m\rangle. \tag{2.27}$$

Here, $|m\rangle$ spans an infinite-dimensional local state space and the matrices D_m represent the weight of m particles at each single site. Consequently, as in the calculation known

from the ASEP (where only two states exist namely D and E) the tensor product of the state vectors is given by:

$$A \otimes \hat{A} = \sum_{m,m'} D_m \hat{D}_{m'} |m, m'\rangle. \tag{2.28}$$

The dynamics are introduced by the local update operator $\hat{A}$ which is applied backward sequentially throughout the chain. $\hat{A}$ obeys the following rule:

$$t\left(A \otimes \hat{A}\right) = \hat{A} \otimes A \tag{2.29}$$

where t represents the local transfer matrix commuting A and $\hat{A}$.
Now it is possible with eq. (2.25) - (2.29) to give an expression for the local transfer matrix with

$$t|m, m'\rangle = \sum_{\Delta=0}^{m} \phi(\Delta, m)|m - \Delta, m' + \Delta\rangle \tag{2.30}$$

where $\phi(\Delta, m)$ represents the transition probability for chipping the mass Δ from the mass m to the next neighboring site.
This again leads to:

$$t\left(A \otimes \hat{A}\right) = \sum_{m,m'} \sum_{\Delta=0}^{m} \phi(\Delta, m) D_m \hat{D}_{m'} |m - \Delta, m' + \Delta\rangle. \tag{2.31}$$

Consequently, one obtains

$$\sum_{\Delta=0}^{m} \phi(\Delta, m) D_m \hat{D}_{m'} |m - \Delta, m' + \Delta\rangle = \hat{D}_{m'} D_m |m', m\rangle. \tag{2.32}$$

By replacing $m' = m - \Delta$ the algebra for the matrices D can be represented by:

$$\sum_{\Delta=0}^{m} \phi(\Delta, m) D_{m'+\Delta} \hat{D}_{m-\Delta} = \hat{D}_{m'} D_m. \tag{2.33}$$

Now a one-dimensional representation of the algebra from eq. (2.33) for the stationary state can be found only if all joint probabilities for a given chipping function ϕ factorize. In this case the D_m are real-valued and the Ansatz:

$$D_m = D_0 \mu \left(\frac{D_1}{D_0}\right)^m, \tag{2.34}$$

$$\hat{D}_m = \nu \hat{D}_0 \left(\frac{D_1}{D_0}\right)^m \tag{2.35}$$

is a non-trivial representation of the algebra from eq. (2.33).

For the Free-ARAP, where free means that there is no truncation of the transition probabilities and under consideration of ultra-local fraction densities, i.e., identical transition probability for arbitrary mass transport, the chipping function is given by:

$$\phi(\Delta, m) = \frac{1}{m}. \tag{2.36}$$

In this case mean field becomes exact (see [125, 126]) and the weights D_m respectively $\hat{D}_m$ can be calculated as:

$$D_m = \frac{1+m}{2^m} D_0 \left(\frac{D_1}{D_0}\right)^m \tag{2.37}$$

and

$$\hat{D}_m = \frac{1}{2^m} \hat{D}_0 \left(\frac{D_1}{D_0}\right)^m . \tag{2.38}$$

As mentioned above there is no restriction of the mass transport. Each particle or mass unit is shifted into the next site with a certain probability defined by the transition probability or transition rate ϕ. In contrast to the Internet model where the buffer size restriction exhibits an immense influence on the system dynamics the contemplation of the ARAP with discrete time and discrete mass transport can be seen as a special case and should therefore be regarded.

2.6.2 Proof for the Existence of a Factorized Steady State

An important factor for the explicit calculation of the stationary state by means of a mean-field approach is the existence of a factorized representation of the stationary state distribution. In this context Zia et al. [124] recently introduced a simple test on the chipping function ϕ for one-dimensional mass transport models with nearest neighbor interactions and parallel update rules to proof the existence of a factorized steady state. The factorization test of the chipping function for discrete mass transport is given by the cross-ratio

$$R(\Delta, m) = \frac{\phi(\Delta+1, m+2)\phi(\Delta, m)}{\phi(\Delta+1, m+1)\phi(\Delta, m+1)} \tag{2.39}$$

with

$$\phi(\Delta, m) = \frac{u_\Delta v_{m-\Delta}}{f_m}. \tag{2.40}$$

Here, $f_m = \sum_{\Delta=0}^{m} u_\Delta v_{m-\Delta}$ is the single weight function and u and v are non-negative functions that have to be chosen carefully. If the factorization condition in eq. (2.40) holds the cross ratio in eq. (2.39) is independent of Δ and a factorized steady state exists. Moreover, in case of the existence of a factorized steady state it is possible to calculate the exact single weight functions f_Δ with:

$$f_m = (f_0) \left(\frac{f_1}{f_0}\right)^m \left[\prod_{\Delta=0}^{m-2} \frac{1}{R(\Delta)^{m-\Delta-1}}\right] \qquad \text{for} \quad m > 2. \tag{2.41}$$

The test was performed for several kinds of discrete mass transport models in [118, 124] to proof the existence of factorized steady states in order to calculate exact mean-field approaches. Here, only the two cases of the ARAP with ultra-localized fraction densities or the so called binomial-chipping model are recalled since these model definitions without any buffer restrictions are directly related to the model investigated in this thesis. This is done for both models considering discrete mass units or particles m and parallel update procedure. The particles moves independently from the other ones with probability p into the next site $i+1$ with respect to periodic boundary conditions. In case of the binomial chipping model then the chipping probability or function is given by:

$$\phi(\Delta, m) = \begin{cases} 0 & \Delta = 0 \\ \binom{m}{\Delta} p^{\Delta}(1-p)^{m-\Delta} & \Delta \geq 1, m \geq 1 \end{cases} . \tag{2.42}$$

Inserting this into eq. (2.39) one gets:

$$R(\Delta, m) = \frac{m+2}{m+1} \tag{2.43}$$

for all $m \in \{0, 1, ...\}$. This again means that $R(\Delta, m)$ is independent from Δ and therewith a factorized steady state

$$F(m_i) = \prod_{i=1}^{N} f_i \tag{2.44}$$

can be found with the following single-weight functions:

$$f_i = f_0 \left(\frac{f_1}{f_0}\right)^m \frac{1}{m!}. \tag{2.45}$$

For further details see [124].

In case of the ARAP with ultra-localized fraction density the chipping function reads as follows:

$$\phi(\Delta, m) = \begin{cases} 0 & m = 0 \\ \frac{1}{m} & m \geq 1 \end{cases} . \tag{2.46}$$

The cross ratio from eq. (2.39) is then given by:

$$R(\Delta, m) = \frac{m^2 + 2m + 1}{m^2 + 2m} \tag{2.47}$$

and obviously independent from m which is in totally agreement with the results derived by Zielen et. al in [126] in case of ultra-localized fraction density.

3 Asymmetric Multi Occupation Process (AMOP)

Simulating and investigating the physical and statistical properties of data transport in the Internet on the packet transportation layer or as in Internet notation often used autonomous source level (AS-level) cellular automata models are predestined as a powerful tool for characterizing statistical properties of real data and explaining the appearing phenomena.

Obviously, there are many reasons for introducing a discrete model approach. First of all it is of importance to mention that there is a smallest transportation unit of fixed size, called datagram, moving from router to router where these packets are stored in buffers that can be characterized as a queuing system. Secondly, there is an immense number of these data packets traveling throughout a network of enormous size. Handling the network and treating each single data packets realistically as possible and detailed as necessary a microscopic simulation becomes a suitable and furthermore reasonable approach.
Moreover, investigations of real data showed that an Internet connection between a designated source and destination host is established along a stable and fixed path for more than hours [54]. This is an important result, since the transportation process itself is in general determined by locally defined rules (see [3]), i.e., each single router is guiding the data packets autonomously by locally defined rule-set throughout the entire network. Therefore, the strategy to introduce a one-dimensional model approach for simulating data transport in the Internet on the AS-level becomes an appropriate choice.

Although cellular automata models are an enormous generalization and simplification by considering time, space and velocity as discrete variables these models are able to describe basic statistical properties despite the mentioned extreme simplifications of real world properties and the minimal rule-set regulating the system dynamics. Consequently, these model approaches are widely used and successfully applied in highly complex application fields like vehicular traffic and granular flow [52, 102, 119].
A new cellular automaton model was introduced by Huisinga et al. in [54] in order to simulate the Internet data transport along a fixed path with regard to the statistical properties found in Internet Ping-experiment data [28, 55, 108, 111]. The presented model can be characterized as a derivative of the well known CA model for discrete transportation process with open boundaries namely the Asymmetric Simple Exclusion Process (ASEP). It should be mentioned here that the ASEP with slightly changes, i.e., particles were allowed to move with velocity $v > 1$, was introduced to simulate vehicular traffic by Nagel and Schreckenberg in 1992 [82] and is now, with a few more diversifications [75] a standard simulation model used to simulate and evaluate vehicular highway traffic. For further details see *http://www.traffic.uni-duisburg.de/autobahnnrw.htm*.

3.1 Introduction

In case of the Internet the investigated model is in fact another derivative of the ASEP. In contrast to the pristine model, in the model introduced to simulate Internet data transport [54, 55] each site can store more than one particle in a buffer of finite size (*Multi* Occupation) and thus the *Simple* Exclusion is given up. This leads to the notation of Asymmetric Multi Occupation Process, AMOP. A striking feature of the AMOP is the possibility that particles in a buffer are able to overtake each other. This is motivated by the fact that particles that get lost on their way to the destination host are sent again and therewith the other particles somehow outrun the "lost" packet. Moreover, the effective travel time of this interim "lost" packet is consequently enlarged. It turned out that this features are essential for simulating data transport in the Internet on the AS-level. So it was shown that a suitable calibration of the parameter set provided by the AMOP with open boundary conditions permits to reproduce the statistics as well as the quantitative values of the travel times of data packets [54]. Therewith, it could be confirmed that the introduced model exhibits the characteristic statistical features as long-range dependence and self-similarity in travel times found in real Internet Ping-experiment time-series [28, 55, 108, 111] making this model approach a suitable tool for further investigations.
In this work the a cellular automaton model with parallel dynamics is investigated in the context of statistical physics. First, the periodic version is investigated in detail. Here, the number of particles located in the system is conserved and the focus of the investigations lies on the global properties, e.g., the fundamental diagram representing the flow - density relation.
The main part of the work deals with the investigation of the model with open boundary conditions where inflow respectively outflow exert an immense influence on the system dynamics. Here, so called boundary induced effects are analyzed in detail.
The model version with open boundaries is identically to the model introduced to simulate data transport in the Internet and was applied to investigate the properties of Ping-experiment time-series. Moreover, it will be shown that the choice of the used inflow strategy has an enormous influence onto the system dynamics. With respect to this a diversification of the model will later be discussed with regard to real Internet transportation problems.

3.2 AMOP with Periodic Boundary Conditions

In order to understand the basic phenomena and essential features a new model exhibits, traditionally model investigations start with the simplest rule-set for the system dynamics since more advanced rule-sets usually reveal more complex system properties. Consequently, the model with periodic boundary conditions is investigated first. In this case in contrast to open boundary conditions the number of particles is preserved and there are no boundary induced effects exerting influence on the system dynamics. Moreover, neglecting boundary induced effects might give the chance to find analytical representations of the model dynamics in context of mean-field approaches. As an example it should be mentioned here that the ASEP with periodic boundary conditions can also be solved exactly by the use of the so called car oriented mean-field (COMF) approach [100]. Therefore, in contrast to the standard Mean-Field approach and the matrix product ansatz where the state of each single site is considered as the dynamical variable here the distance or gap between succeeding particles or cars is regarded. This strategy was also applied to

find analytical expressions for some derivatives of the ASEP like the Nagel-Schreckenberg (NaSch) model. Unfortunately, an exact solution could not be found but nevertheless a good approximation may reveal some basic features of the underlying dynamics. In this chapter the characteristics of the AMOP with periodic boundary conditions are investigated by numerical simulation as well as by analytical approaches.

Definition of the Model

In the framework of this thesis in following the periodic version of the model with parallel dynamics (see fig. 3.1) is presented. In this case an arbitrary amount of particles moving on a ring of length L with a certain probability p into the right neighboring site under consideration of hard-core repulsion is considered. Each site $i = 1, ..., L$ can hereby store a finite number of particles in a buffer of size B. In contrast to the open system, in the periodic version the particle number N is conserved, i.e., a constant density $\rho = \frac{N}{LB}$ is provided, and particles in in the buffer of site L move into the first site $i = 1$, obeying the dynamics introduced below.

The exact dynamics from time $t \to t + 1$ is then as follows:

At each time step t the $n_i(t)$ particles in the buffers of each site $i = 1, \ldots, L$ are picked up respectively to their time of arrival [1] and move simultaneously with probability p to the next neighboring site $i + 1$ as far as the buffer of this site is not completely occupied ($n_{i+1}(t) < B$). In case of a complete occupation of the succeeding site $i + 1$ the remaining data packets reside at their current position.

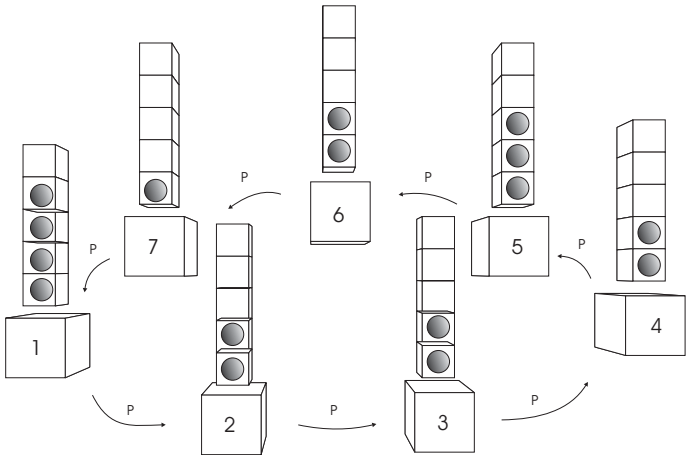

Figure 3.1: Periodic system consisting of $L = 7$ sites with buffer size $B = 5$. The system is occupied by an arbitrary amount of particle which move according to the dynamics with probability p to the right neighboring site as far as there is enough space left in the buffer of the succeeding site.

In other words this means that the buffer itself is updated sequentially obeying the rule "first in first out" whereas the particles at the bottom of each buffer are chosen to move at first. Note that all particles in a buffer are chosen to move with probability p. The entirety of extracted particles then move simultaneously, i.e., in parallel, into the next

[1] This is important only for the calculation of travel times and the their statistics, but not for the global dynamics.

neighboring site, as far as the buffer is not completely occupied. This means that at most the amount of $B - n_{i+1}(t)$ particles is able to move. This system dynamics are identical for all investigated model versions.

3.3 Fundamental Diagram

A common method to evaluate transportation systems where the main focus of interest lies on the survey of macroscopic measurements determined by the internal dynamics, is the investigation of the so called fundamental diagram (FD). The FD represents the relation between the macroscopic quantities of the mean flow and the system density $J(\rho)$. Note that mean flow $J = v\rho$ and density $\rho = \frac{N}{L \cdot B}$ are normalized variables and so the absolute values may differ drastically. As mentioned in the model definition the particles only move with velocity 1 and more important the particles are able to overtake each other in case of $B > 1$. Moreover, for the following investigations B and p are chosen identically for all sites.

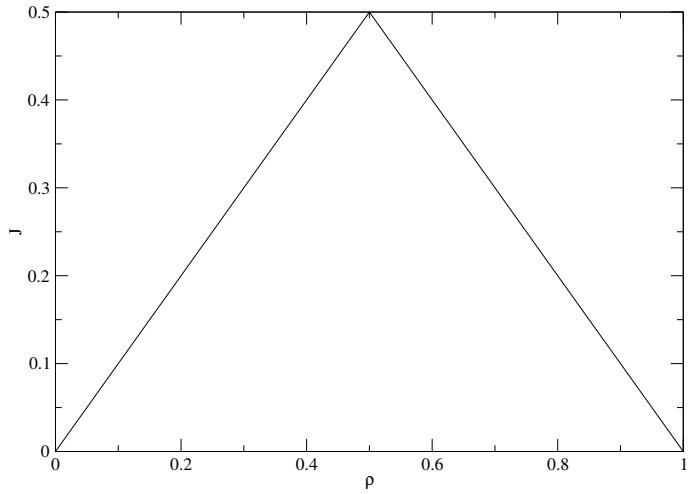

Figure 3.2: FD of a periodic system consisting of $L = 5000$ sites for arbitrary buffer sizes B and deterministic movement. Different buffer sizes do not have any influence on the shape of the FD. Here, identical densities provide identical system flows.

In order to get an impression of the system properties first the deterministic model with $p = 1$ where all fluctuations are neglected is regarded. The survey of the deterministic model reveals that in the steady state the FDs for different buffer sizes B do not exhibit any differences (see fig. 3.2) compared to the FD of the ASEP. For densities $0 < \rho \leq 0.5$ the mean system flow increases linear with the density. Particles move undisturbed through the whole system and no jams exist. At $\rho^* = 0.5$ the maximum system flow $J_{max} = 0.5$ is reached. For all particles in a buffer there is exactly the same number of free cells in the succeeding one, i.e., all particles in the system will move in the next time step. The system resides in the free flow phase.

In case of densities $\rho > 0.5$ the mean system flow decreases linearly with increasing density and jams arise in the system since particles are refused to enter the next neighboring site due to hardcore repulsion and the buffer restriction. The system has entered the jammed phase. Considering the complete FD obviously two phases can be distinguished, a low-

density phase for $\rho \leq 0.5$ and a high-density phase for $\rho > 0.5$. The FD is symmetric with regard to $\rho = \rho^* = 0.5$ because of the particle-hole symmetry. As mentioned before the buffer size B does not have any influence on the mean system flow at a fixed density. Considering the thermodynamic limit in the free flow phase the system flow is simply given by $J_{free}(\rho) = \rho$ while in the jammed phase the system flow is $J_{jam}(\rho) = 1 - \rho$.

3.3.1 Deterministic Movement, $p = 1$

Regarding the steady states of the periodic system obviously the system size affects the internal dynamics even in case of buffer size $B = 1$, i.e., for the ASEP. For an odd number of cells for example the density of $\rho^* = 1/2$ can not be adjusted. In case of the AMOP with buffer size $B > 1$ there are some more diversifications which have to be regarded in case of finite system sizes L. In this case obviously the choice of the buffer size B affects the maximal system flow as well. Coming back to the ASEP there is only one outstanding system configuration providing maximal flow represented by particle hole symmetry. For $B = 1$ this can only be realized by definition as $1|0|1|0|1|0|...|1|0$.

With respect to the AMOP one has to distinguish between odd and even values of L and B respectively. In the following the possible system configurations providing the maximal system flow in case of deterministic movement are described briefly.

Regarding even system and arbitrary buffer sizes there are $(B + 2) \mod 2$ stable system configurations providing the maximal system flow $J_{max} = 0.5$ at $\rho^* = 0.5$. The configurations are given by $n_i = B - k$ and $n_{i+1} = B - (B - k)$ with $k \in \{0, 1, ..., B \mod 2\}$. A schematic representation in case of $k = 0$ would be $B|0|B|0|...|0$.

Considering an odd number of sites there is only one stable system configuration providing the maximal system flow of $J = 1/2$ namely if B is even. Then this configuration is given by $B/2|B/2|B/2|...|B/2$. Here, any other system configuration is not capable to provide the maximal deterministic system flow since otherwise there are two succeeding buffers that will not provide a local density configuration of $\rho_{local} = 1/2$ meaning that the global density of $\rho = 1/2$ could not be adjusted because of the discreteness of the CA-model and therefore the maximal deterministic system flow can not be reached.

Here, it has to be stated that in contrast to the ASEP where the discrete model exhibits only one stable system configuration providing the maximal system flow in case of multi-occupation of sites one has to regard $(B+2) \mod 2$ configurations. This becomes relevant for analytical calculations and has therefore to be considered later.

Finally, it has to be mentioned that in contrast to the normalized considered values the maximal capacity $C(B)$, i.e., the absolute number of free flowing particles in a system, is strongly enlarged for systems with larger buffer sizes and is given in case of deterministic movement in the thermodynamic limit by $C(B) = B/2$. This means that the maximal capacity grows linearly with the buffer size.

3.3.2 Stochastic Movement, $p \neq 1$

Considering the probabilistic version of the AMOP ($0 < p < 1$) with periodic boundary conditions, a completely different behavior becomes apparent (see fig. 3.3). In contrast to the symmetric FD of the ASEP varying the buffer size exerts an immense influence onto

the system dynamics. The mean maximal system flow is strongly increased and shifted to larger densities ρ at identical moving probabilities for larger buffer sizes. Moreover detailed investigations of the system dynamics reveal a highly complex system behavior. For example, comparing the statistics of travel times between ASEP and AMOP revealed that in case of the ASEP there are only two statistical properties. The power spectra shows white noise in case of a free flow system and $1/f$-dependency otherwise.

This means that in contrast to the well studied dynamics known from the ASEP [31] the fact that particles are allowed to overtake each other in case of multi-occupation of sites ($B > 1$) leads to completely different statistical properties as shown in the introduction where the statistical properties of travel times of individual data packets were discussed (see [54, 55, 57, 58]).

With respect to the FD of the stochastic derivative as well as in the deterministic case two phases can be distinguished. At first, there is a free flow phase where the particles are moving nearly undisturbed throughout the complete system. There are only a few disturbances which dissolve quickly and no large jams exist. As depicted in fig. 3.3 larger buffer sizes provide higher system flows even in the free flow regime. On the other hand there is a jammed phase where particles are detained from moving into the next site because of the hardcore repulsion and the restriction of the buffer size. The buffer of the next site is completely occupied and jams occur in the system. Even here the system flow is enlarged at identical densities compared to smaller values of B. Clearly another influence of the increased buffer size can be identified. There is a shift of the density ρ^* of the maximal flow J_{max} to higher densities. For a moving probability of $p = 0.5$ in the limit $B \to \infty$ the density ρ^* converges to $2/3$ while the maximal system flow $J_{max}(\rho^*)$ converges to $1/3$.

Phenomenological, the system dynamics can be explained as follows. Consider a system without noise, i.e., the deterministic version where all particles in a buffer move into the succeeding one as far as there is enough free space left. The maximum flow ($J^* = 0.5$) then is obviously reached for the density $\rho^* = 0.5$ (particle-hole symmetry), i.e., the number of free cells or space in the succeeding buffer corresponds exactly with the number of particles in the regarded buffer.

Contrary, in case of stochastic movement, only a fraction of particles determined by the hopping probability p is chosen to move. Consequently, this means that the number of free buffer space in the succeeding site only has to satisfy this reduced demand, claimed by the particles chosen to move. This obviously shifts the point of the maximal flow to higher densities ($\rho^* > 0.5$). Moreover, the number of particles dedicated to move for a fixed moving probability at identical system densities obviously scales with the buffer size, so that larger buffer sizes provide higher system flows.

Regarding large buffer sizes $B \gg 1$, in the density picture ρ^* is reached if $p\rho$, representing the mass current, i.e., the flow, from one site into the following one, is equal to the free space in exactly the succeeding buffer given by $1 - \rho$. One simply gets:

$$p\rho^* = 1 - \rho^* \Leftrightarrow \rho^* = \frac{1}{1+p}. \tag{3.1}$$

In case of a moving probability of $p = 0.5$ the density of maximal system flow reads as $\rho^* = 2/3$. Considering the maximal system flow one gets $J_{max}(\rho^*) = 1/3$.

It has to be recalled that the AMOP with periodic boundary conditions is capable to provide significant higher system flows for increasing buffer sizes in case of stochastic movement (see fig. 3.3). Especially the fact that particles in a buffer which are not chosen to move because of the internal dynamics (hopping probability p) can be passed by other particles in the same buffer is, as mentioned in the introduction of great importance for the statistics of the travel times.

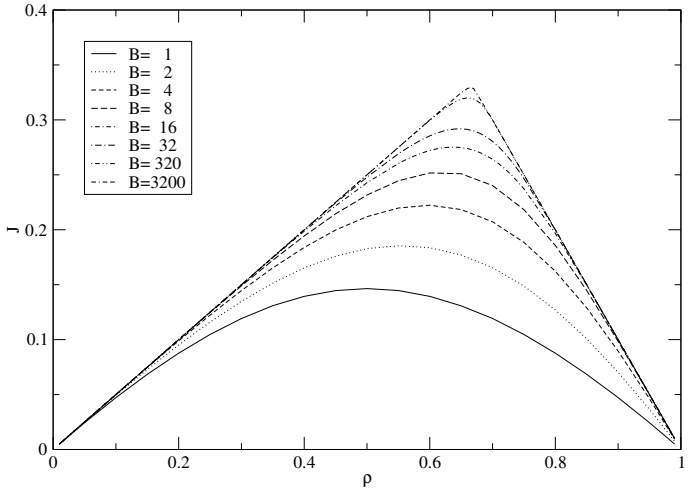

Figure 3.3: FD of a periodic system consisting of $L = 5000$ routers with buffer size $B = 1, 2, 4, 8, 16, 32, 320, 3200$ and stochastic movement ($p = 0.5$). In contrast to the case with deterministic movement here the restriction of the buffers exerts an immense influence onto the shape of the FD. Larger buffers provide strongly increased system flows compared to lower ones. Moreover the maximal system flow is shifted to larger densities.

3.4 Mean-Field Approach

An important feature of the AMOP is, as mentioned before, the restriction of the buffer size to an arbitrary value B which as a result provides a completely different behavior in the statistics of the travel times of single data packets. Considering the system flow mean field approaches are as described before a useful and common method to give a first analytical representation of a model. Nevertheless, mean field results are in most cases not exact but can be used as simple approximations and it often turned out that even phase diagrams and critical exponents can be roughly calculated [8, 62]. The main reason for the loss of exactness of the generic mean field (MF) approach is primarily due to the existence of long-range correlations which are totally neglected (random phase approximation [29]). In case of the ASEP the generic approach completely neglects nearest neighbor correlations and becomes exact only in case of a random sequential update scheme [82]. For parallel update the MF approach underestimates the correlations and thus becomes inexact. Despite this inexactness the prediction of the generic MF approach has been used as a starting point for a deeper understanding of the model. Thus, in the following the generic MF approach is applied to calculate the FD of the AMOP with periodic boundary conditions.

A starting point for the analytical investigation by the use of generic MF approaches is the consideration of the temporal evolution of the system state or mean particle density.

Therefore, the state or occupation number $\tau_i(t)$ of each site $i = 1, 2, 3, ..., L$ at time t is considered. Here, $\tau_i(t)$ can take on values of $0, 1, 2, 3, ..., B$. Remind that this is in contrast to the ASEP where $\tau_i(t) \in \{0, 1\}$ is representing a binary state space. Considering only the system flow without the internal dynamics given by the shuffled order of particles in a buffer, each buffer cell of an arbitrary site i can be seen individually occupied or not. The simplest temporal evolution of the mean particle density at a dedicated site is then given by the local master equation:

$$\frac{d\langle\tau_i(t)\rangle}{dt} = \sum_{\tau_{i-1}(t)=1}^{\min(\tau_{i-1}(t),B-\tau_i(t))} \tau_{i-1}(t)[B-\tau_i(t)] - \sum_{\tau_i(t)=1}^{\min(\tau_i(t),B-\tau_{i+1}(t))} \tau_i(t)[B-\tau_{i+1}(t)]. \quad (3.2)$$

Averaging over the stationary solutions of this local master equation (3.2) would reveal the mean occupation number of a neighborhood and therewith higher order correlations would be implied. Neglecting these correlations and applying the MF approximation the local master equation reads as follows:

$$\langle\tau_i(t), \tau_{i+1}(t)\rangle = \langle\tau_i(t)\rangle\langle\tau_{i+1}(t)\rangle. \quad (3.3)$$

This simply means that the two-point correlation of the state of succeeding sites is considered as a product measure of the states of the single site. Obviously the averages $\langle ...\rangle$ of the stationary state variables are time-independent. The average system flux at a single site can then be described by:

$$\langle j_i(t)\rangle = \frac{p}{B}\min(\langle\tau_i(t)\rangle, \langle B-\tau_{i+1}(t)\rangle). \quad (3.4)$$

Now it is possible by introducing the local density $\rho_i = \langle\tau_i(t)\rangle/B$ to give the following approximation in the continuum limit for the system flow in dependence to the density as:

$$J(\rho) = p\rho(1-\rho^B). \quad (3.5)$$

Remind that for introducing a moving or hopping probability p one has to consider a reduced transition probability for a particle to move into a free place of the next buffer. Moreover, it has to be considered that the average density ρ is represented by a real number $\rho \in [0, .., 1]$ and therefore the continuum limit for $\frac{LB}{N}$ has to be made.

Regarding the FD derived by the simple MF approximation clearly large deviations compared to the simulation results can be found (see fig. 3.4). In contrast to the case with $B = 1$ where the mean system flow J is underestimated, for higher buffer sizes $B > 1$ the flow derived by the approximation becomes much too high. Especially for $B \gg 1$ the MF approach underestimates the buffer restrictions and the FD becomes identical to the FD of the discrete ARAP [126] or the binomial chipping model [124].

Nevertheless, in contrast to large buffer sizes, for buffer size $B = 2$ the mean-field approximation seems to be qualitatively in relatively good agreement with the simulation results. The maximum system flow is enlarged and shifted to higher densities, but quantitatively the system flow is up to 20% enlarged in particular for densities $\rho > 0.6$.

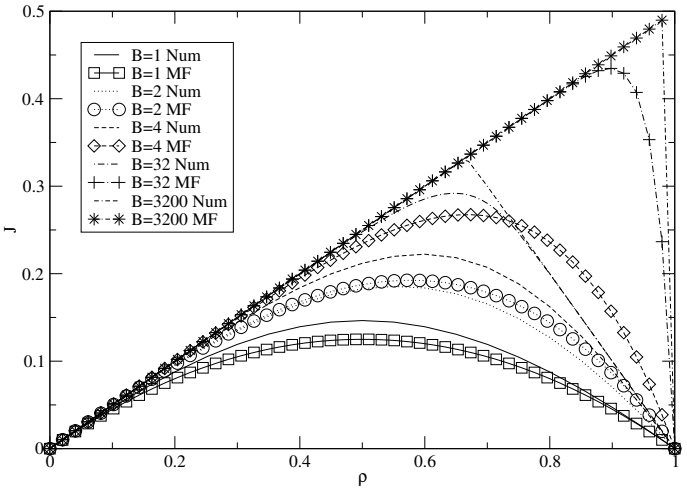

Figure 3.4: FD of a periodic system derived by mean-field approximations and the corresponding FD derived by numerical simulations for identical buffer size $B = 1, 2, 4, 32, 3200$. The moving probability in the simulation is set to $p = 0.5$ as well as considered in the mean-field case. Clearly the strong deviations of the calculated flow compared to the simulation results can be recognized especially for rising buffer sizes.

Already for $B = 4$ the results of simulation and approach diverge drastically and the approximation becomes artificial. This could be explained by the fact that in case of the generic MF approach the sequential update of the single buffer is neglected, meaning that the MF approach underestimates the conditional probabilities for all particles in a buffer to move.

Therefore, another approximation technique is used in order to get better results.

3.5 2-Cluster Approximation

As shown in the previous section the introduced generic MF approximation for the AMOP with periodic boundary conditions is not capable to give satisfactory results for the FD since all correlations in the system are completely neglected. In order to include short range correlations the n-cluster approximation technique derived in [99, 101] is used to obtain much better results. This improved mean-field approach was introduced to derive analytical results for the NaSch-model [82] for velocities $v_{max} > 1$ and is also a site oriented approximation technique.

The n-cluster approximation in general is applied by dividing the lattice of a system consisting of L sites into clusters of a arbitrary length n with $n = 1, 2, ..., L$. Hereby, there is an overlap of $n - 1$ sites for two neighboring clusters. A sketch for $B = 2$ and different cluster lengths n is given in fig. 3.5.

The probability to find a given cluster of length n in a certain state is as usually denoted by $P(\tau_i, ..., \tau_{n-1})$ where $\tau_i, i \in \{1, .., L\}$ represents the state respectively the occupation number of a single site i. Considering periodic boundary conditions the probability dis-

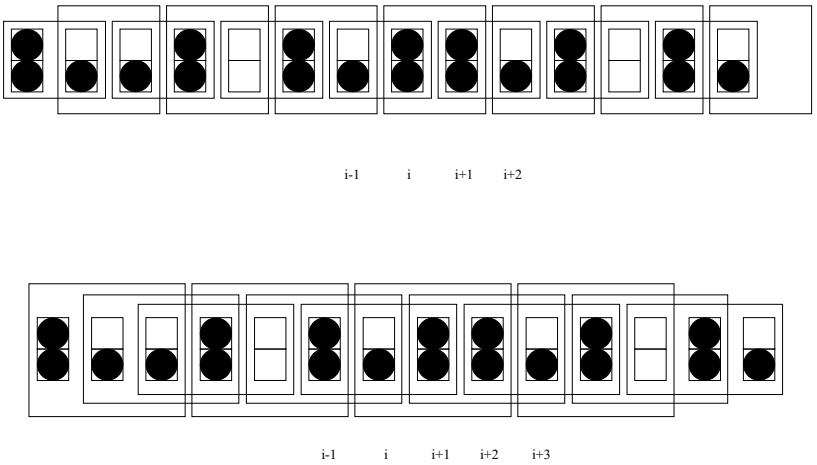

Figure 3.5: Schematic representation of the $n = 2$ at the top and $n = 3$-cluster approximation at the bottom for a periodic system with buffer size $B = 2$. The smallest possible cluster size is $n = 1$ which is identical to the generic mean field case were any correlations are neglected. For a increasing cluster length long-range correlations are considered since the overlap is also increased.

tribution for the transition of a $n + 2$-cluster system from configuration $(\tau'_{i-1}, ..., \tau'_{i+n})$ to the configuration of a n-cluster system $(\tau_i, ..., \tau_{i+n-1})$ then reads as follows:

$$P_n(\tau_i, ...\tau_{i+n-1}) = \sum_{\{\tau'\}} W(\tau_i, ..., \tau_{i+n-1}|\tau'_{i-1}, ..., \tau'_{i+n}) \times P_{n+2}(\tau'_{i-1}, ..., \tau'_{i+n}). \tag{3.6}$$

Here, $\sum_{\{\tau'\}} W(\tau_i, ..., \tau_{n-1}|\tau'_{i-1}, ..., \tau'_{i+n})$ represents the sum over all the transition rates for all possible configurations of the $n + 2$-cluster probability $P_{n+2}(\tau'_{i-1}, ..., \tau'_{i+n})$ to the n-cluster probability $P_n(\tau_i, ...\tau_{i+n-1})$. Note that in contrast to the NaSch-model here the particles are only allowed to move with velocity $v = 1$ and therefore only the next neighboring sites τ_{i-1} on the left and τ_{i+n} on the right of a dedicated cluster of size n have to be considered for the calculation of the steady state probability distribution.

Now it is possible to write the conditional probability by the decomposition of the $n + 2$-clusters as:

$$P(\tau_i|\underline{\tau_{i+1}, ..., \tau_{i+n-1}}) = \frac{P_n(\tau_i, ..., \tau_{i+n-1})}{\sum_{\tau_i} P_n(\tau_i, \tau_{i+1}, ..., \tau_{i+n-1})} \tag{3.7}$$

and

$$P(\underline{\tau_i, ..., \tau_{i+n-2}}|\tau_{i+n-1}) = \frac{P_n(\tau_i, ..., \tau_{i+n-1})}{\sum_{\tau_{i+n-1}} P_n(\tau_i, ..., \tau_{i+n-2}, \tau_{i+n-1})}. \tag{3.8}$$

As a result the n-cluster approximation gives:

$$\begin{aligned} P_{n+2}(\tau_{i-1}, \tau_i, ..., \tau_{i+n-1}, \tau_{i+n}) &= P(\tau_{i-1}|\underline{\tau_i, ..., \tau_{i+n-2}}) \\ &\times P(\tau_i, ..., \tau_{i+n-1}) \\ &\times P(\underline{\tau_{i+1}, ..., \tau_{i+n-1}}|\tau_{i+n}). \end{aligned} \tag{3.9}$$

It is well known that in the limit $n \to \infty$ the approximation becomes exact for infinite system size ($L \to \infty$), first shown by Kikuchi et al. [66]. For further details about this

$n, n-1$-cluster approximation method see [19] and references therein.

In the following the results for the $n = 2$-cluster approximation for a periodic system with buffer size $B = 2$ are presented. In this case the 2-cluster approximation is given with eq. (3.6) and eq. (3.9) by:

$$\begin{aligned} P_2(\tau_i, \tau_{i+1}) &= \sum_{\tau'} W(\tau_i, \tau_{i+1}|\tau'_{i-1}, \tau'_i, \tau'_{i+1}, \tau'_{i+2}) \\ &\times P(\tau'_{i-1}|\underline{\tau'_i}) \times P(\tau'_i, \tau'_{i+1}) \times P(\underline{\tau_{i+1}}|\tau'_{i+2}). \end{aligned} \tag{3.10}$$

In order to calculate the temporal evolution $P_2(\tau|\tau')$ one has to determine all transition probabilities $W(\tau|\tau')$ for all possible system states along the ring of two succeeding sites. As a result one gets:

$$P_2(\tau) = \sum_{\tau'} W(\tau|\tau') \cdot P(\tau') \tag{3.11}$$

with

$$W(\tau|\tau') = \prod_{i=1}^{L} W(\tau_i, \tau_{i+1}|\tau'_i, \tau'_{i+1}). \tag{3.12}$$

In the considered case with $B = 2$ one has already to take into account 81 initial configurations whereas the non-vanishing local transition probabilities and the local transition probabilities $\neq 1$, $W(\tau_i, \tau_{i+1}|\tau'_i, \tau'_{i+1}) \neq 0, 1$ contributing to the resulting transition probability $W(\tau|\tau')$ reads as follows:

$$\begin{aligned} W(1,0|1,0) &= 1-p, \\ W(2,0|1,0) &= 1-p, \\ W(0,1|1,0) &= p, \\ W(1,1|1,0) &= p, \\ W(1,1|1,1) &= 1-p, \\ W(1,0|1,1) &= 1-p, \\ W(2,1|1,1) &= 1-p, \\ W(2,0|1,1) &= 1-p, \\ W(0,2|1,1) &= p, \\ W(0,1|1,1) &= p, \\ W(1,2|1,1) &= p, \\ W(1,1|1,1) &= p, \\ W(2,0|2,0) &= (1-p)^2, \\ W(1,1|2,0) &= 2p(1-p), \\ W(0,2|2,0) &= p^2, \\ W(2,1|2,1) &= (1-p)^2, \\ W(1,1|2,1) &= p^2 + 2p(1-p), \\ W(1,2|2,1) &= p^2 + 2p(1-p). \end{aligned} \tag{3.13}$$

Now, with the knowledge of the resulting transition probability the use of the Kolmogorov consistency conditions [50] given by

$$\sum_{\tau} P_2(\tau_i, \tau) = P(\tau_i) = \sum_{\tau} P(\tau, \tau_i) \tag{3.14}$$

and the normalization

$$\sum_{\tau} P(\tau_i, \tau_{i+1}) = 1 \tag{3.15}$$

it is possible to derive the exact probabilities for all configurations $P(\tau, \tau')$. Therewith, again it is possible to calculate the system-flow in dependence to the density in order to give a representation of the FD $J(\rho)$. The density of moving particles ρ_m can be derived by extensive calculations with:

$$\rho_m = P(\tau, \tau_{i+1}) \tag{3.16}$$

and the system flow then is identical to the calculated density.

The results of the non-trivial calculations of the FD are depicted in fig. 3.6 in comparison to the simulation results and the generic MF approach. Clearly one finds that the results derived by the 2-cluster approximation produce much better results compared to the generic MF case. However, as expected the $n = 2$ cluster size neglects longer correlations and therefore the results are not exact. Consequently, one has to consider larger cluster sizes in order to find a more suitable representation but that is in fact very extensive because of the complex structure of the equations representing the probabilities for the configurations of succeeding sites albeit in the case of $n = 2$.

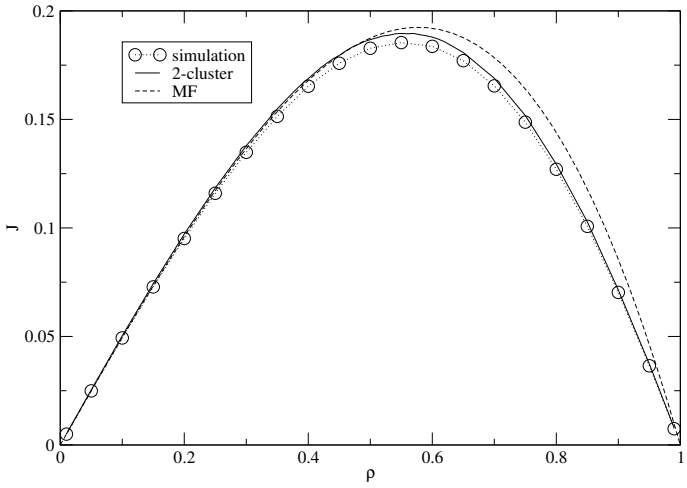

Figure 3.6: FDs derived by the two-cluster approximation, the generic MF approach and by Monte Carlo simulations for a system of buffer size $B = 2$ and moving probability $p = 0.5$. Clearly the results derived by the two-cluster approximation are qualitatively much better then the results derived with the generic MF approach. Nevertheless, in order to get a more accurate representation one has to consider larger clusters sizes $n > 2$.

3.6 Discussion

In this chapter the AMOP with periodic boundary conditions was investigated by numerical and analytical representations of the fundamental diagram. It was shown by numerical simulations that the AMOP exhibits strong deviations compared to the ASEP and the ARAP which are somehow special cases of the presented model.

On the one side there is the ASEP with $B = 1$ where particles are not allowed to pass each other and the system flow is determined by the distance to the next particle. The dynamics can be solved exactly by the matrix product technique (see chapter 2) as well as by the use of an advanced MF approach. In case of this *particle oriented* MF ansatz in contrast to the generic (site oriented) MF approach, the distance between succeeding particles is considered as the dynamic variable. It was shown in [100] that the results become exact in the case of a maximum velocity of $v_{max} = 1$. For higher velocities, i.e., in case of the NaSch model there are strong deviations and the MF approaches become inexact (for more details see [23] and references therein). With regard to the AMOP this advanced MF ansatz was found to be ineffective because of the varying distances caused by the reordering due to the passing of particles within an update step.

On the other hand the discrete ARAP is representing the AMOP with infinite buffer size ($B \to \infty$). This model was also shown to be exactly solvable in terms of the matrix product ansatz under consideration of the exact results known from generic MF approach and continuous masses. Unfortunately, in the discrete case a straightforward representation of the transfer matrices could not be given. Moreover, it turned out that a restricted buffer size leads to a highly complex algebra and could not be solved as well.

However, in order to give a suitable analytical result the cluster approximation method was applied to the AMOP. This method was shown to be effective and provides very good results in case of the NaSch model [101] ($v_{max} > 1$). In this method correlations are taken into account by considering overlapping clusters of various sizes n. The results are known to become exact in case of infinite cluster size [66]. For the AMOP already the results derived by a cluster size of $n = 2$ are showing good agreement with the numerical simulations compared to the generic MF results. Nevertheless, there are deviations which can only be reduced by increasing the cluster size n. A known disadvantage of this method is the numbers of initial configurations that have to be considered in order to calculate the resulting weight of each single configuration and therewith the transition probabilities. As mentioned above in case of $B = 2$ there are already 81 initial configurations and for $B = 16$ there would be 83521 for the 2-cluster approximation. Moreover, it is to mention that even in the assumed simple case with $B = 2$ and $n = 2$ there is no trivial solution and some extensive calculations are needed to derive the exact results for density and flow. As a consequence the combination of larger cluster and buffer sizes are making this approach hardly to handle analytically and therefore numerical simulations are preferable in order to get meaningful results especially for large buffer sizes.

Summarizing this, the results derived by the numerical simulations point out some apparent differences compared to the results known from ARAP as well to the ASEP and the NaSch model. The restriction of the buffer sizes are hereby of prime importance as one can see in the FDs in fig. 3.3. Compared to the ASEP increasing the buffer size leads to higher system flows at higher densities which is also in contrast to the NaSch model

where increasing the maximal velocity also increases the maximal system flow but in fact for smaller densities. Regarding the ARAP the unbounded state space at each single site leads to rather simple dynamics in comparison to the AMOP.

4 AMOP with Open Boundary Conditions

In the previous chapter some general features of the periodic version of the Asymmetric Multi Occupation Process (AMOP) were presented. The main focus of interest was hereby the shape of the FD and the differences to other well known CA models with periodic boundary conditions. Therefore, numerical investigations were compared with analytical results. It turned out that the analytical results derived by simple mean field approximations, i.e., neglecting correlations, become rather inaccurate already for $B \geq 2$. Therefore, an improved mean field approach was consulted to produce much better compliance with respect to the numerical investigations. It was shown exemplarily for a buffer size $B = 2$ that the results derived by the $n = 2$-cluster approximation for the calculation of the FD are in relatively good agreement compared to the simulation results. Nevertheless, only for large n the results are hardly to distinguish from the numerical simulations and the number of configurations which have to be considered in order to calculate the probability distribution are hardly to determine.

In this chapter now, the AMOP with open boundary conditions is investigated in detail. In the field of statistical physics these models with open boundary conditions are denoted as driven lattice gas models (DLGs) where the main system (here a discrete lattice of finite length) is coupled to particle reservoirs at the boundaries. Especially this feature exhibit much versatile system dynamics compared to the periodic derivatives of the model, e.g., boundary induced phase transitions [72]. As a consequence analytical results for systems with open boundaries are in most cases not exact except for a few exceptions. An outstanding example for this exceptions is the ASEP with open boundaries where exact analytical results can be found (see [23, 42] and references therein).

Nevertheless, DLGs enjoy great popularity especially because of their relevance for realistic simulations and investigations in many scientific fields where the conservation of the particle is not granted at all. In case of the data transport in the Internet open boundaries are of special interest data packets obviously travel from a source to a destination host passing more or less occupied respectively jammed sites which are actually queuing systems equipped with a buffer of finite size where the arriving particles are stored or buffered in order to be processed. In the following the influence of open boundary conditions and multi allocation of sites onto the phase diagram is investigated.

4.1 Model Definition

In contrast to the model with periodic boundary conditions, in case of open boundary conditions there is a particle current from one reservoir at one end of the system where particles are inserted with a given probability to another reservoir at the other end of the system where the particles are removed with another probability. Within the system the particles move according to local defined rules to the next neighboring site $i + 1$. The definition of the investigated model with open boundary conditions and parallel dynamics (see fig. 4.1) is then as follows:

Consider a one-dimensional lattice of $i = \{1, 2, 3, ..., L\}$ sites with open boundaries, whereby each site can be empty or store a maximum amount of B particles in a buffer. At one site of the system, for convenience reasons let us choose the left one ($i = 1$), a reservoir is introduced from which particles are inserted into the first buffer as far as the buffer is not completely occupied. From here the particles move stochastically throughout the complete system to the right boundary ($i = L$) where the particles are removed at once from the system.

The exact dynamics are introduced below:

At each time step t particles corresponding to a given inflow rate α are inserted at the left boundary (site $i = 1$) as far as there is space left in the buffer while particles corresponding to the outflow parameter β are removed at the right end of the system.

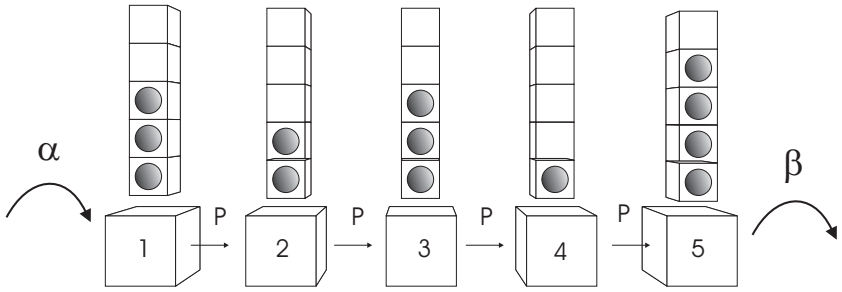

Figure 4.1: Open system consisting of $i = 5$ routers with buffer size $B = 5$. Particles are inserted from the reservoir at the left site of the system into the first site according to the inflow rate α. From there they move to the right end with probability p. At the right end of the system the particles are removed according to the outflow rate β. Note that with regard to the parallel dynamics the particles only move once at each time step.

The parallel update of the system $t \rightarrow t+1$ for all particles in all buffers of site $i = 1 \rightarrow L-1$ is then as follows:

At time t the $n_i(t)$ particles in the buffer of site $i = 1, \ldots, L-1$ are picked up sequentially with respect to their time of arrival at i and move with probability p to the next neighboring site $i + 1$ as far as the buffer of this site is not completely occupied ($n_{i+1}(t) < B$). In case of a complete occupation of the succeeding site $i + 1$ the remaining data packets reside at their current position. This means that at most $B - n_{i+1}(t)$ are able to move into the next site $i + 1$.

Note, that inflow, outflow and bulk dynamics are applied simultaneously and that particles are updated only once at each time step. Moreover, it has to be mentioned that due to the stochastic character of the update in the case of the multi occupation ($B > 1$), particles are able overtake each other. For $B = 1$ this model is identically to the ASEP with periodic respectively open boundary conditions.

4.2 Definition of the Boundaries

Comparing the diverse known cellular automaton models with open boundary conditions there are many different insertion respectively removing strategies leading to diverse and sometimes artificial system dynamics. For example there were investigations of the NaSch model where the chosen inflow strategy could not provide the maximal system flow. As a result the derived phase diagrams are incomplete [20, 21]. On the other hand, Barlović et al. [15] introduced an efficient new inflow strategy by introducing a mini system at the inflow providing boundary. Therewith, it was possible to assure also the realization of the maximal system inflow and the complete phase diagram of some CA models exhibiting velocities $v_{max} > 1$ could be derived. Moreover, the exact system inflow could be calculated analytically by considering a sequence of Bernoulli trials [45]. Hence, in the following the exact inflow strategy for the AMOP is illustrated in detail to prevent misunderstandings.

For a fixed buffer size B the inflow into the first site is realized by choosing each of the B particles in the reservoir with probability α to move into the buffer of the first site as far as there are empty cells left. Because of a maximal velocity of one site per time step this insertion strategy provides that the maximal deterministic system flow ($J^* = 1/2$) can be reached and therewith it is possible to analyze the complete spectrum of system states. In the simulations this is realized by coupling a reservoir of size $B_{res} = B$ to the left boundary which is filled up completely before each update step.

On the other side of the system the outflow dynamics are implemented by choosing each particle in the buffer of the last site $i = L$ with probability β to be removed, i.e., the reservoir at the right end of the system is always empty. Note, that due that due to the parallel update scheme only these particles are removed that have not already been moved in the actual time step.

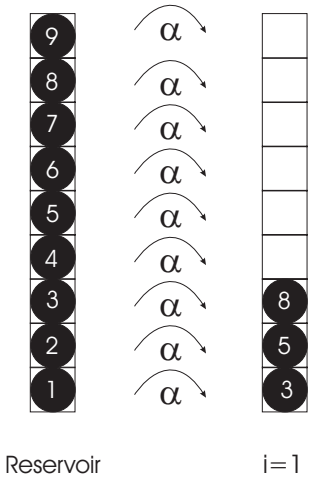

Figure 4.2: Schematic representation of the coupling of the completely filled up reservoir of size $B = 9$ onto the left boundary providing an inflow-rate of α. This is realized by choosing each particle in the reservoir with probability α to be inserted into the first site of the system, i.e., $i = 1$.

In fact the inflow at each update step is realized by choosing an identically independent distributed (i.i.d) random variable for each particle in the reservoir at the left side of the

system. The selected particles are then inserted sequentially into the first site of the system as far as there are empty cells. This means that for $\alpha = 1$, all particles in the reservoir at the left hand side try to move into the buffer of the first site until the buffer is completely occupied. An inflow rate of $\alpha = 0.5$ on the other hand is implemented by selecting each particle in the reservoir sequentially with the given probability α to move into the buffer of the first site. Remind, that the reservoir at left is completely filled up before each new update step. A schematic representation of the inflow procedure is given in fig. 4.2.

Contrary, an outflow rate $\beta = 1$ denotes, that all particles in the last router that have not already moved in the actual time step will be erased immediately while an outflow rate of $\beta = 0.5$ is realized by erasing these particles with probability $\beta = 0.5$.

4.3 Extremal Current Principle

Considering CA-models with open boundary conditions the shape of the FD is of special interest since in [7, 51, 70, 71, 92] a rather general theory was presented allowing to associate the shape of the phase diagram of the open system with the fundamental diagram of the periodic system.

This extremal current principle can be comprised as described in the following:

$$J = \begin{cases} \max_{\rho\in[\rho_R,\rho_L]} J(\rho) & \text{for} \quad \rho_L > \rho_R, \\ \min_{\rho\in[\rho_L,\rho_R]} J(\rho) & \text{for} \quad \rho_L < \rho_R. \end{cases} \tag{4.1}$$

The meaning of the equations above can simply be summarized as follows. The system flow J of the open system is related to the corresponding system flow $J(\rho)$ of the periodic system with density ρ_R at the right boundary resp. ρ_L at the left one of the open system. These boundary densities are then determining the bulk flow.

Moreover, it was shown that a domain wall approach can be use to predict the nature of the phase transitions determined by the extremal current principle. Therefore, simply the movement of the domain wall itself and the *collective velocity*, the movement of the center of mass of small fluctuations are considered [70]. The approach was successfully applied to various kinds of cellular-automaton models. Here, the number of phases observed in the open system depends on the number of maxima/minima of the FD of the periodic system.

As a starting point the phase diagram of the ASEP could be predicted and further investigations revealed that the phase diagram of the NaSch-model [82] exposes similar characteristics as the one of the ASEP [42, 92]. Moreover, it could be shown that even for CA models with meta-stable system states, like the VDR-model [17], the extremal current principle holds [15] and that the domain wall approach could be used to derive the complete phase diagram of the model.

With regard to the AMOP comparing the FD of the periodic system with the FD of the open one it is clearly shown in fig. 4.3 that the complete FD of the periodic system (full lines) can be reproduced by the open system for an appropriate choice of the parameters α and β. Here, exemplarily the FDs of the AMOP with different boundary conditions are depicted for identical moving probabilities $p = 0.5$ and buffer size $B = 4$.
In detail, with regard to the open system the free flow states are generated by keeping the outflow rate fixed to $\beta = 1$ in order to provide a maximal outflow. Thus, the mean

system flow and the mean system density is regulated by choosing an arbitrary inflow rate α. Contrary, the high density states are generated by setting $\alpha = 1$ in order to provide a maximal system inflow. Mean system flow and mean density are adjusted by varying the outflow rate β.

Since it was shown in the previous chapter that the FD of the periodic version of the AMOP exhibits only one single maximum for all buffer sizes the ASEP can be seen as a special case of the AMOP with buffer size $B = 1$ and the extremal principle (see eq. (4.1)) can be utilized and allows to give a phenomenological description of the shape of the phase diagram for the open system as well as the nature of the phase transitions with respect to the exact results known from the ASEP.

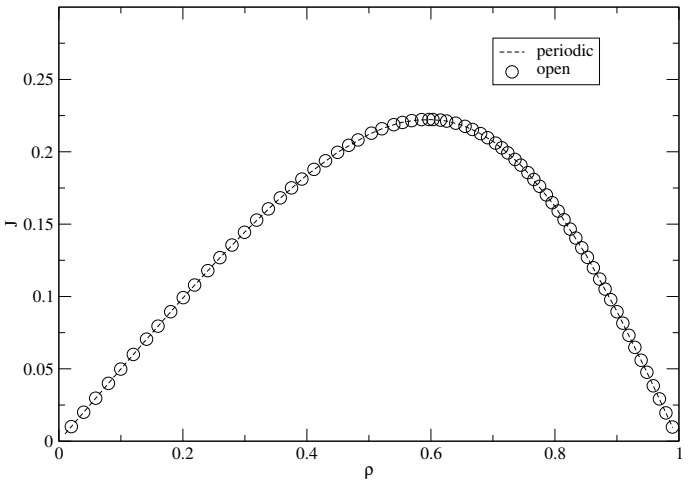

Figure 4.3: FD of a system with $N = 1600$ sites, buffer size $B = 4$ and $p = 0.5$. The dotted line corresponds to the simulation results of a periodic system while the symbols represent the simulation results of an open system for a suitable choice of parameters α and β.

4.4 Analytical Results, $p = 1$

In this section now an exact analytical representation of the system inflow respectively outflow is presented in case of deterministic system dynamics. As described in the introduction for the ASEP with open boundaries and parallel dynamics the shape of the phase diagram is exactly known from analytical investigations [32, 42]. Moreover, it was shown in the previous chapter that in case of periodic boundary conditions and under consideration of stochastic movement exact analytical results could not be found with the help of the presented approaches.

Considering an open system with deterministic movement within the system stochastic elements are introduced in particular at the boundaries. Actually for a fixed maximal inflow rate ($\alpha = 1$) and variable β respectively fixed maximal outflow rate ($\beta = 1$) and variable α, it will be shown next that it is possible to give exact analytical solutions for the system flow J in dependence of the appropriate in- and outflow parameter α respectively β. First the case of variable inflow rate is explained in detail.

4.4.1 Calculation of the Inflow, $\beta = 1$

Assuming a fixed buffer size B and maximal outflow rate $\beta = 1$ the system flow J is determined by the inflow rate α into the first site from which the particles move deterministically throughout the entire system until they are removed at the right boundary with probability $\beta = 1$. This means that the right boundary does not have any effect onto the system dynamics and the investigations can be reduced to a single site problem where only the first site has to be regarded in order to determine system flow and density.
The system flow $J(\alpha)$ or in particular the flow throughout the first site can be calculated by considering the occupation probability distribution for each single cell in the first site. Remind that the dynamics obey parallel update rules and that the actual inflow into the first site is determined by the number of particles chosen with probability α to be inserted form the reservoir coupled at the left side of the system as well as by the actual state of the first site given by the actual inflow the time step before.

Now in the following the probability to find exactly n particles in the buffer of the first site at time t is denoted by $P_n(t)$. In order to calculate the temporal evolution of $P_n(t)$ from time step t to $t+1$, all possible configurations of the inflow into the first site are analyzed.

Precisely, this means that one has to consider the transition probability of all configurations of $P_n(t)$ for $n = 0, ..., B$ particles in the first site to all possible configuration in the next time step $P_n(t+1)$.

In order to get an impression of the calculations exemplarily the case of a buffer size $B = 2$ is recapitulated for the case $P_1(t)$, i.e., there is one single particle in the first site at time t. At time $t = t+1$ this state can evolve into a new state representing 0,1 or 3 particles with corresponding probabilities $P_0(t+1)$, $P_1(t+1)$ and $P_2(t+1)$.

- $P_0(t+1)$, the first site is empty at time $t+1$, i.e., non of the two particles in the reservoir are chosen to be inserted into the first site given by the probability $(1-\alpha)^2$.
- $P_1(t+1)$, there is one single particle in the first site, i.e., one has to distinguish the cases that both particles in the reservoir are chosen to be inserted into the first site (probability α^2) whereas only one particle will actually be moved due to the parallel dynamics (one particle is positioned in the first site at time t). And finally the case that either the first or the second particle in the reservoir is chosen to move into the first site given by the probability $2\alpha(1-\alpha)$. As a result the complete transition probability for this case is then denoted as $\alpha^2 + 2\alpha(1-\alpha)$.
- $P_2(t+1)$, there are two particles present in the first site at time $t+1$. This means that the two particles in the reservoir are chosen to be inserted into the first site which is in fact impossible, due to the parallel dynamics, since one particle is already situated in the first site. The probability for this case is then given by 0.

Obviously the probabilities add up to 1 as shown below:

$$(1-\alpha)^2 + \alpha^2 + 2\alpha(1-\alpha) = 1. \tag{4.2}$$

Similar investigations have to considered for the two remaining cases $P_0(t)$ and $P_2(t)$. Namely that no particles are present in the buffer of the first site at time t as well as the

case that the first site is completely occupied, i.e., there are two particles present in the first site at time t.

As a result for arbitrary buffer sizes in the stationary state for $t \to \infty$, considering all possible system configurations, transition probabilities and the normalization

$$\sum_{n=0}^{B} P_n = 1 \tag{4.3}$$

one gets the following rules to set up an equation system:

$$P_0 = \sum_{n=0}^{B-1} P_n (1-\alpha)^B + P_B, \tag{4.4}$$

$$P_B = P_0 \alpha^B, \tag{4.5}$$

$$P_{n,B>n>0} = \sum_{k=0}^{B-n-1} P_k \binom{B}{n} \alpha^n (1-\alpha)^{B-n} + P_{B-n} \sum_{k=n}^{B} \binom{B}{k} \alpha^k (1-\alpha)^{B-k}. \tag{4.6}$$

Solving this system of equations leads to the occupation probability distribution of the first site. Therewith, the flow throughout the first site can be calculated with

$$J = \frac{1}{B} \sum_{n=1}^{B} n P_n \tag{4.7}$$

in dependence of the buffer size B which, in fact is identically to the complete system flow because of the deterministic movement within the remaining system.

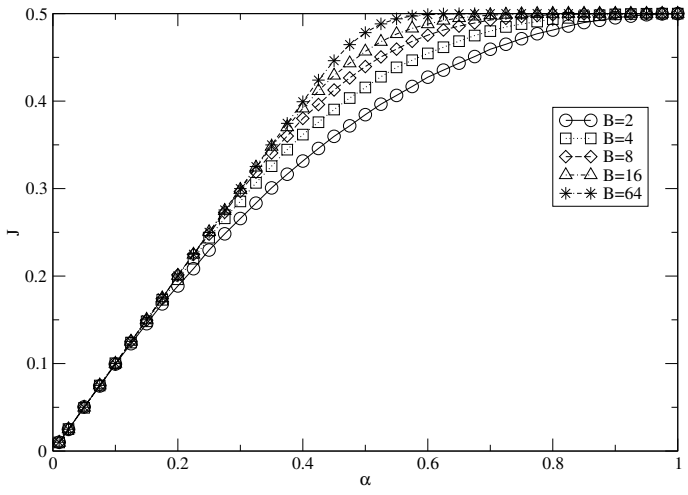

Figure 4.4: Flow J in dependence of the inflow rate α for the deterministic model ($p = 1$) with $\beta = 1$ and buffer size $B = 1, 2, 4, 8, 16, 32, 64$. The lines represent the analytical solution while the symbols correspond the numerical results.

Note that the binomial coefficient in the calculations is a relict of the possible occupation numbers of the first site at time t. In order to get an impression of the complexity of the

calculations exemplarily the results for the system flow $J(\alpha)$ for buffer size $B = 2$ and $B = 3$ are given in the following:

$$J_{B=2}(\alpha)\frac{\alpha(-1\alpha^4 - \alpha^2)}{1 + \alpha + \alpha^2 - \alpha^3}, \tag{4.8}$$

$$J_{B=3}(\alpha)\frac{\alpha(-3\alpha^4 + 3\alpha^3 - 4\alpha^2 - \alpha - 1 + 8\alpha^5 - t\alpha^6 + 2\alpha^7)}{(-1 + 2\alpha^3 - 3\alpha^2)(\alpha^5 - 2\alpha^4 + \alpha^3 + \alpha^2 + \alpha + 1)} \tag{4.9}$$

4.4.2 Calculation of the Outflow, $\alpha = 1$

In analogy to the calculation of the case with maximal outflow rate $\beta = 1$ it is also possible to give an exact analytical expression for a fixed inflow rate of $\alpha = 1$ and arbitrary outflow rates β. Hereby the occupation probability distribution of the last site is analyzed in the same way as described in the case above. Similar to the previous case here only the last site in the system has to be considered since the remaining part of the system preserves deterministic movement which provides that the inflow into the last site is equal to the system inflow $\alpha = 1$. In case of outflow rates $\beta < 1$ the system resides in the jammed phase. In the stationary state the buffer of the last site is completely filled up and then provides B particles to be chosen to leave the last site with probability β.

Consequently, one gets the following rule set for the occupation probabilities P_n of the last site:

$$P_n = \binom{B}{n}\frac{\beta^{B-n}}{(\beta+1)^B} \tag{4.10}$$

with $n = 0, 1, 2, ..., B$.
Considering the flow throughout this last site one gets the following expression:

$$J = \frac{1}{B}\sum_{n=1}^{B} nP_{B-n} = \frac{\beta}{\beta+1} \tag{4.11}$$

which is, in fact independent to the buffer size B. As in the previous considerations the system flow is now given by the calculated outflow.

4.4.3 Analytical Results, $p = 1$

In fig. 4.4 and fig. 4.5 the flow J of a system with deterministic motion in the bulk ($p = 1$) is depicted in dependence of the inflow rate α for a fixed maximal outflow rate $\beta = 1$ respectively the outflow rate β for a fixed maximal inflow rate $\alpha = 1$. Obviously, for inflow rates larger than the capacity of the right boundary the maximal system flow is determined by the outflow rate and the system is situated in the high density regime. For inflow rates less than the capacity of the right boundary the system resides in the low density regime because the particles are hardly constrained at the right boundary of being absorbed.

In case of an maximal inflow rate of $\alpha = 1$ the variation of the buffer sizes does not affect the bulk flow (see fig. 4.5), since jams evolve at the right boundary for any kind of outflow rates $\beta < 1$. In case of the chosen scenario the outflow is the decisive parameter. For $\beta = 1$ the system is completely deterministic and the maximal system flow of $J_{max} = 1/2$ is reached. There are no restrictions resulting in a limitation of the maximal inflow.

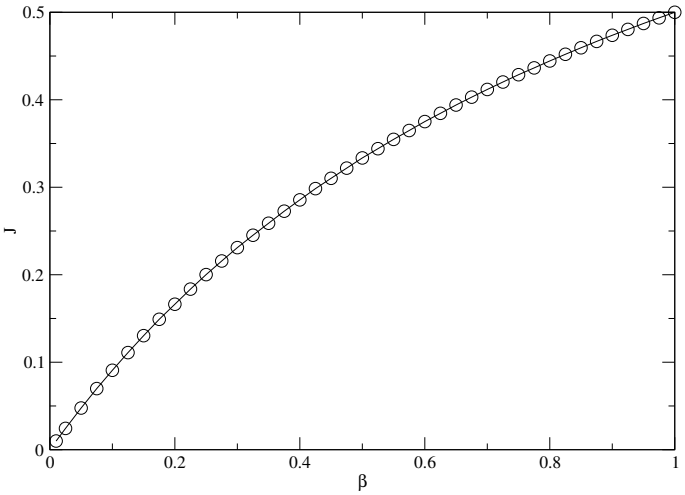

Figure 4.5: Flow J in dependence of the outflow rate β with $p = 1$ and maximal inflow ($\alpha = 1$). The graphs are identical for all buffer sizes. The solid line represent the analytical solution while the symbols correspond to the numerical results.

On the other hand for $\beta < 1$ in fact an identical outflow parameter provides an identical system flow for arbitrary buffer sizes B as shown in the analytical analysis. This is caused by the fact that in the stationary state the buffer of the last site is filled up at each time step and the outflow is then determined by choosing each particle in the buffer of the last site, that have not been moved, to be vanished with probability β (see section 4.2). The system outflow respectively the bulk flow is then given by eq. (4.11).

In contrast thereto, for maximal outflow rates ($\beta = 1$), i.e., all particles arriving in the last buffer will be deleted in the next time step, it becomes apparent that the variation of the buffer size shows an immense influence on the system flow. For larger buffer sizes the maximal flow ($J_{max} = 1/2$ in the deterministic case) is reached at lower inflow rates (see fig. 4.4). The system flow can exactly be calculated with (4.11) by solving the equations in (4.6) to determine the occupation probability distributions of the first site.
Evidently, the explanation given in the introduction of the model can be consulted again. The stochastic character of the inflow provides an identical system flow for larger buffer sizes and at higher densities. It is important to mention here, that although the maximal system flow for increasing buffer sizes is reached for lower inflow rates, a considerable augmentation of the flow compared to smaller buffers becomes apparent exceptionally in the region of medium inflow rates. Comprising it is to say that the analytical results for these special cases are in totally agreement with the results obtained by the numerical simulations (see fig. 4.4 and fig. 4.5).

4.4.4 Numerical Results, $p = 1$

In order to get a deeper insight into the model dynamics ruled by the inflow and outflow rates, in fig. 4.6 and fig. 4.7 the bulk flow is depicted in dependence of the inflow respectively the outflow exemplarily for a fixed buffer size $B = 32$ and deterministic particle motion.

As known from the ASEP a restriction of the outflow leads to plateau formation (see

fig. 4.6) for an inflow larger than the capacity of the right boundary. This is caused by the fact that jams are formed immediately at the right end of the system. The bulk density and thus the maximal system flow is determined by ρ_R respectively the outflow rate β and thus can be calculated with eq. (4.11) for $\alpha = 1$. This corresponds to the intersection of the graphs from fig. 4.6 with $\alpha = 1$ and represents the maximal system flow given by the outflow rate β in the jammed system state.
Considering an inflow rate less than the capacity of the right boundary the bulk density is given by ρ_L and the system flow can thus be calculated with eq. (4.7) which corresponds to the solid line for $\beta = 1$ and represents the free flow regime. Therewith, it is possible to derive the complete diagram $J(\alpha)$ by analytical calculations.

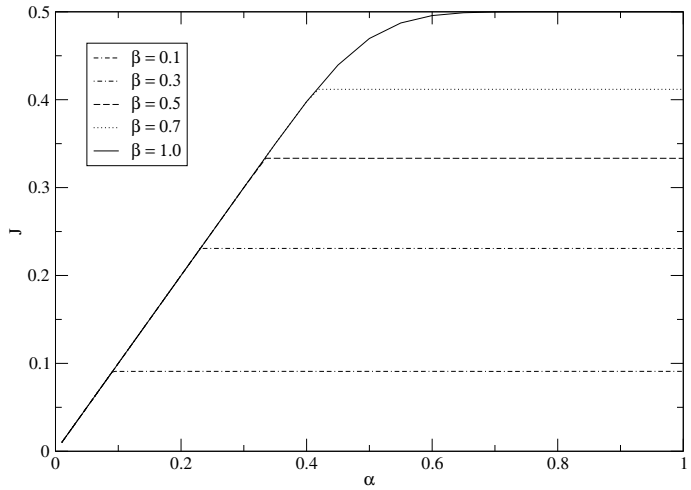

Figure 4.6: System flow J in dependence of the inflow rate α in the deterministic model ($p = 1$) and buffer size $B = 32$ for outflow rates of $\beta = 0.1, 0.3, 0.5, 0.7$ and 1. The solid line corresponds to the calculations from eq. (4.7). Clearly, the restricting influence of the reduced outflow rate can be recognized determining the maximal system flow given by eq. (4.11).

Similar to the considerations above on the other hand is also possible to calculate $J(\beta)$. Here, for restricted inflow rates plateau formation arises (see fig. 4.7). In this case the inflow rate respectively, ρ_L determines the bulk flow and the outflow parameter has no limiting influence for outflows larger than the given inflow. The system flow and therewith the plateau value can be calculated with eq. (4.7) representing the intersection of the graph with $\beta = 1$ and thus corresponds to the free flow phase.
Considering an inflow rate larger than the capacity of the right boundary, ρ_R determines the system flow. The solid line here corresponds to the case of $\alpha = 1$ and thus can be calculated with eq. (4.11) representing the high density phase.

This means that it is possible to give an analytical description of the system flow J in dependence of the inflow respectively outflow rate α and β for deterministic bulk movement ($p = 1$). With the help of the corresponding densities ρ_L and ρ_R at the boundaries it is now possible to calculate the point of maximal flow by equating eq. (4.7) and eq. (4.11) for arbitrary buffer sizes. Consequently, by applying the maximal current principle the phase diagram can easily derived in case of deterministic particle movement.

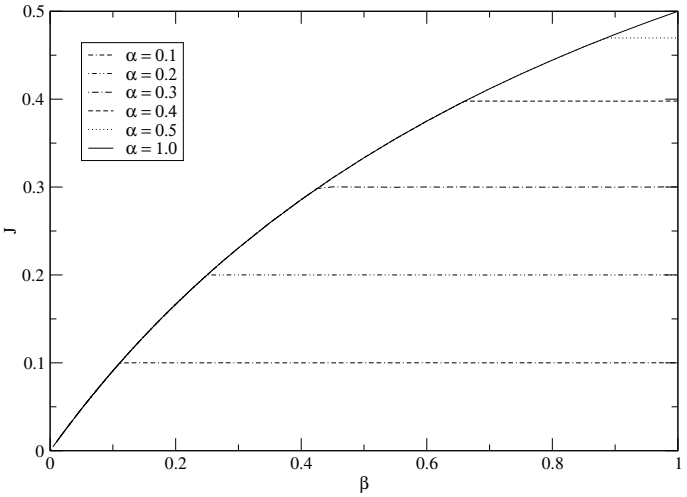

Figure 4.7: System flow J in dependence of the outflow rate β for fixed inflow rates $\alpha = 0.1, 0.2, 0.3, 0.4, 0.5$ and 1 and buffer size $B = 32$. The solid line corresponds to the calculations from eq. (4.11). Here, the restricting influence of the reduced inflow rate can be identified affecting the maximal system flow as given by eq. (4.7).

4.4.5 Phase Diagram

The phase diagram derived by analytical calculations of the model with deterministic movement and open boundary conditions is depicted in fig. 4.8 exemplarily for buffer sizes $B = 1, 2$ and $B = 32$. The deterministic case with $p = 1$ reflects the expected results namely the existence of two phases, a free flow phase A where the system flow is determined by the particle inflow and a jammed phase B where the system flow is dominated by the particle outflow.

The survey of the phase diagram in fig. 4.8 clearly reveals the influence of varying the buffer size. Especially at medium inflow rates ($\alpha \approx 0.5$), the phase boundary is shifted to larger outflow rates so that the jammed phase is highly enlarged for larger buffers. Comparing this with the results from fig. 4.4 and fig. 4.5 it has to be mentioned here that albeit the jammed phase is drastically enlarged, the system throughput at the same parameter set of in- and outflow rates on the other hand is strongly enlarged for lager buffers.

With respect to the phenomenological approach introduced by Kolomeisky et al. [70] the analytical results are in total agreement with the theory. Therefore, the phase transition between the low density and the high density phase which conform to earlier investigations of phase transitions in DLG-models (see [23, 70] and references therein) are separated by a first order phase transition. By the use of eq. (4.7) and eq. (4.11) it was shown that is possible to calculate the phase diagram for arbitrary buffer sizes B.

4.5 Stochastic Model Dynamics, $p \neq 1$

In this section the model with random bulk movement of the particles, i.e., $0 < p < 1$ is investigated. In the presence of noise a completely different system behavior becomes apparent. Here, in contrast to the deterministic system, particles can overtake each other within the system whereas in case of deterministic movement this is only possible at the last

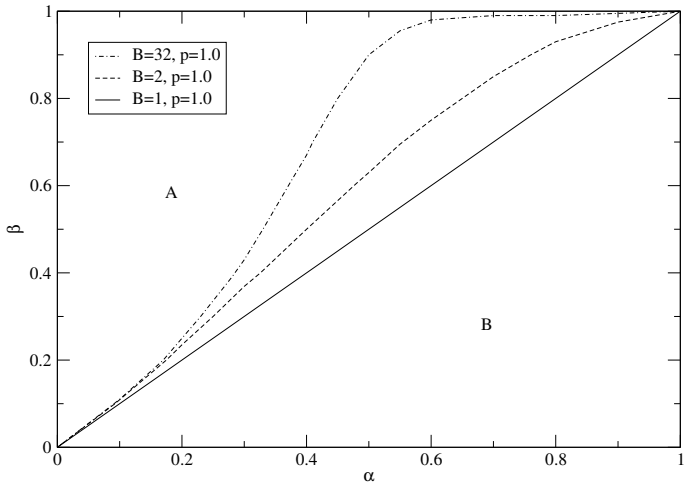

Figure 4.8: Phase diagrams for the deterministic version of the AMOP with open boundary conditions for buffer size $B = 1, 2$ and 32. There are two phases, a free flow phase A in the top left part where the system flow is determined by the inflow rate α and a jammed phase B in the lower right part of the diagram where the dominant system parameter now is the outflow rate β. One clearly finds that the jammed phase is strongly enlarged for increasing buffer sizes compared to the ASEP ($B = 1$).

site where the particles are chosen to be removed with probability β. However, one finds that similar to the investigations known form the ASEP three phases can be distinguished as depicted in the space-time plots in fig. 4.9.
Note that in contrast to space-time plots known from other investigations (especially traffic simulations) here the occupation number and not the velocity is colored. This means that sites with higher occupancy are represented by darker colors.

Regarding the left plot in fig. 4.9 first of all there is a low density or free flow phase A where particles move nearly undisturbed throughout the entire system. Small density fluctuations dissolve quickly and no large jams exist. The system flow is determined by the inflow rate α at the left boundary while the hopping probability p and the outflow rate β do not have any restricting influence onto the system dynamics. The bulk density corresponds to the density at the left border ρ_L. Note that one can recognize forward moving density waves in the free flow regime. This is in total agreement with the asymmetric shape of the FD for buffer size $B > 1$ and can although be found in the velocity dependent randomization (VDR) model [14] with $v_{max} = 1$ or in other fields of transportation problems like granular materia [76, 119], where laminar flow is also a well known phenomena.

On the other hand there is a high density phase B where large backward moving jams of various sizes are mostly induced at the right boundary, i.e., the outflow rate β restricts and therewith determines the maximal bulk flow. Here, the bulk density is given by the density at the right border ρ_R. Up to here the system dynamics can be directly related to the dynamics known from the deterministic model.

Finally, there is a new high flow phase or more precisely maximum current phase C which can not be found in the deterministic model. In this phase the bulk flow is determined by the internal hopping probability p. The inflow rate α is larger than the capacity of the

first site and so the system is overfed. On the other hand the outflow rate β is also larger than the maximal system flow provided by p. This leads to small high density regions at the left boundary while on the other side of the system the right boundary does not have any restrictive effect onto the system flow. The bulk flow is less than the capacity of the right boundary and corresponds to the system outflow given by the density at the right boundary ρ_R.

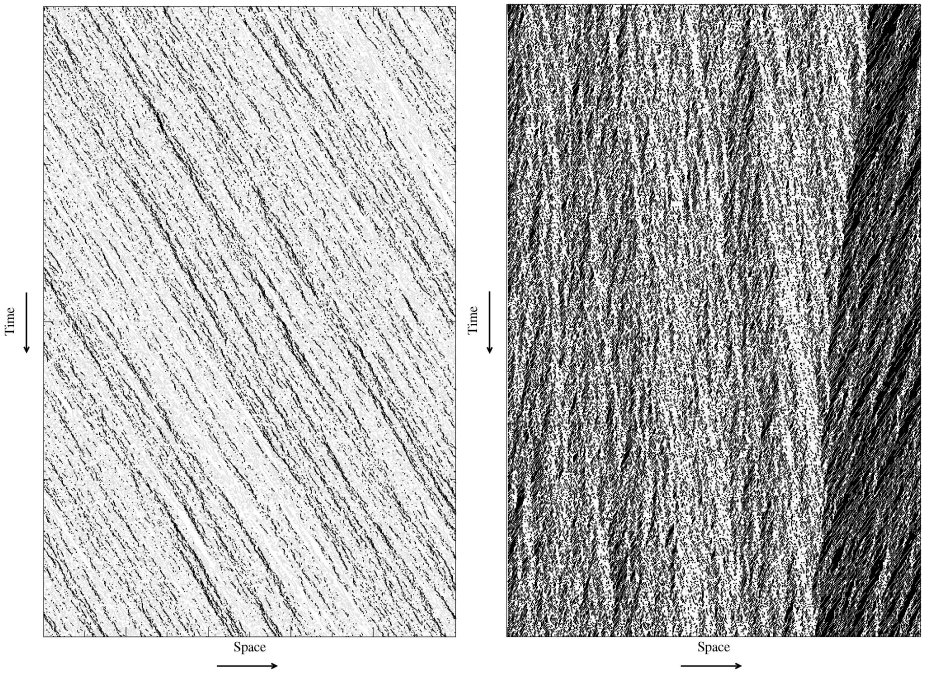

Figure 4.9: Space-time plots of a system with $N = 500$ sites, buffer size $B = 5$ and hopping probability $p = 0.5$. **Left:** System in low density state. Particles are inserted at the left boundary with $\alpha = 0.1$ and move mostly undisturbed to the right end where they are removed with $\beta = 1$. **Right:** System in high density regime. Here, the inflow rate is set to $\alpha = 1$ meaning that the system is overfed and the left part of the system resides in the maximum current phase. Because of the restriction of the outflow to $\beta = 0.3$ the right part of the system is situated in the high density phase which is growing to the left boundary.

In order to reveal the special characteristics of the models, e.g., the multi-occupation of sites combined with the buffer restriction, the influence of increasing the buffer size onto the shape of the phase diagram is investigated. Hence, the system flow is analyzed in dependence of the inflow respectively the outflow rates. As shown in section 4.3 the extremal current principle from eq. (4.1) holds and can be used to predict the shape of the phase diagram since the FD of the periodic system exhibits only one single maximum and moreover can be reproduced by the open version of the model as shown in fig. 4.3. These two points are crucial for the applicability of the approach. This again leads to the result that the shape of the phase diagram of the investigated CA model has to be qualitatively similar compared to the one of the ASEP [30, 42, 72].

Note that in order to prevent misunderstandings, for the following investigations q_{out} represents the actual flow throughout the last site provided by the outflow rate β while q_{in} is determined by α and represents the actual flow into the first site. In all diagrams the system properties are normalized and depicted in relation to these rates. Moreover, it has

to be mentioned that if not stated otherwise the moving probability within the system is set to $p = 0.5$.

4.5.1 Numerical Results

Compared to the deterministic variant in the presence of noise there are distinctive differences concerning the system behavior induced by the inflow rate α and the outflow rate β as shown in fig. 4.10 and fig. 4.11. As mentioned before varying α respectively β by keeping the other one fixed to 1 allows to scan all possible system states. Therewith, the complete FD of the periodic system can be reproduced for an appropriate choice of the parameters even in case of stochastic movement.

Provided a fixed outflow rate $\beta = 1$ for all buffer sizes there is an increase of the bulk flow in dependence of the inflow rate α until the maximal system flow $J_{max}(\alpha^*)$ is reached (see fig. 4.10). This means that for $\alpha \leq \alpha^*$ the system is in the low density regime and the system flow is given by q_{in}. In case of an inflow rate $\alpha \geq J_{max}(\alpha^*)$ a plateau is formed immediately since the system is overfed and can not cope with the inflow provided by α. The maximal bulk flow is reached which is completely determined by the hopping probability p and the buffer size B. The system enters the maximum current phase. Note that in contrast to the ASEP the buffer size is of special interest for the maximal system flow because of the fact that the flow is increased in case of larger buffers as known from the investigations of the periodic system (see fig. 4.2).

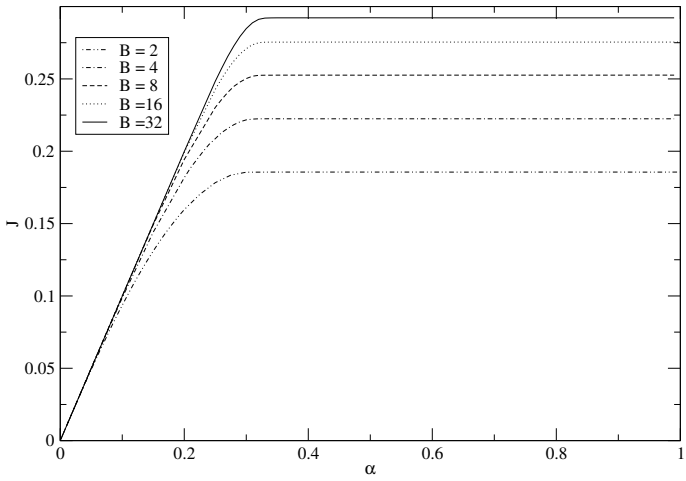

Figure 4.10: Global flow J vs. inflow rate α for a maximal outflow rate ($\beta = 1$) and stochastic movement with $p = 0.5$ for buffer size $B = 2, 4, 6, 16$ and 32. For low inflow rates the system is situated in the free flow regime while for inflow rates larger than the capacity of the system the maximal current phase is entered.

As well as in the previous case varying β by setting $\alpha = 1$ constant one finds distinctive diagrams for different buffer sizes as shown in fig. 4.11. As long as the outflow is less than the maximal bulk flow $J_{max}(\beta^*)$ which depends on the buffer size B and the chosen hopping probability p, the diagram shows an almost linear increase of the system flow for increasing outflow rates. The system resides in the high density phase since the outflow is limiting the complete system flow to q_{out}. Increasing the outflow further than the maximal bulk flow, plateau formation for all values of $\beta \geq \beta^*$ arises, since the outflow is not longer restricting the bulk flow. Here, the maximal system flow is reached which is as mentioned

before depending on the buffer size, and so obtained for different values of β. The maximum current phase is entered and the system flow is given by the effective inflow q_{in}.

Note that as well as for the investigations of $J(\alpha)$ in fig. 4.10 and $J(\beta)$ in fig. 4.11 increasing the buffer size provides a highly increased maximal system flow at identical inflow respectively outflow rates compared to smaller buffer sizes. This could be found for low inflow rates ($\alpha < \alpha^*$) and more distinctive for low outflow rates ($\beta < \beta^*$) whereas the transition into the maximum current phase is shifted for both cases to larger vales of α and β respectively. This means that the maximum current phase is explicitly reduced for increasing buffer sizes. Remind that in contrast to the case with deterministic movement here $J(\beta)$ strongly depends on the chosen buffer size B whereas otherwise the buffer size does not have any influence.

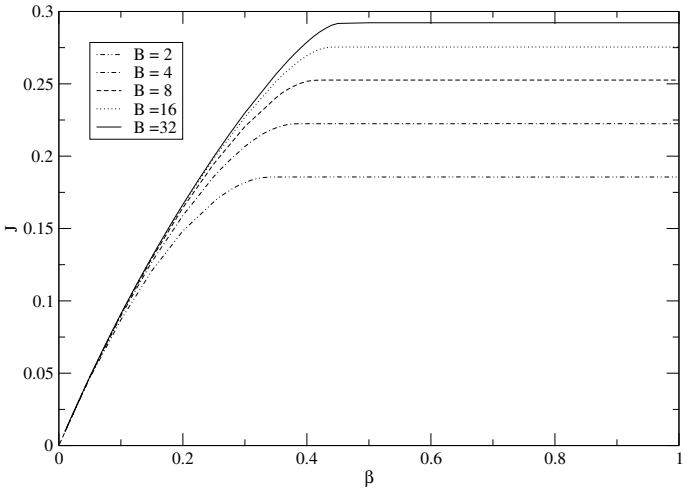

Figure 4.11: System flow J vs. outflow rate β for buffer size $B = 2, 4, 6, 16$ and 32 at maximal inflow rate $\alpha = 1$ for stochastic movement provided by $p = 0.5$. In case of outflow rates less than the capacity of the system the jammed regime is entered while for outflow rates larger than the system capacity the system is situated in the maximal current phase.

In the following investigations the influence of varying the inflow as well as the outflow rates in case of stochastic system dynamics for a system with a fixed buffer size is investigated. Therefore, conform to the investigations of the deterministic system the buffer size is set to $B = 32$. The influence of the inflow and outflow rates onto the system flow is illustrated in fig. 4.12 and fig. 4.13. Obviously, in this case the restriction of the hopping probability leads to plateau formation for $J(\alpha)$ as well as for $J(\beta)$.

In fig. 4.12 the system flow is depicted in dependence of the inflow rate α. Here, the limiting parameters are the hopping probability p and the regarded fixed outflow rate β. In contrast to the previous investigations where either the outflow or the inflow were unbound, i.e., $\alpha = 1$ or $\beta = 1$ respectively, now one has to take into account the interplay between these two rates.
The results derived by numerical investigations show that for an inflow rate less than the maximal system flow and less than the outflow rate ($\alpha < \alpha^*$, $\alpha < \beta$), the system resides in the low density phase and the bulk flow is determined by ρ_L. The inflow affects the system flow since the system as well as the right boundary are able to cope with the amount of inserted particles respectively the effective inflow q_{in}. Here, α^* denotes the inflow rate that

provides the maximal system flow respectively the inflow at which the maximum current phase is entered.

Increasing the inflow rate further more the system flow is increased as well until either the flow is restricted by the outflow ($\alpha > \beta$, $\beta < \alpha^*$) or the hopping probability p is limiting the bulk flow ($\alpha > \alpha^*$, $\beta > \alpha^*$). In the first case this means that the system enters the jammed phase and the bulk flow given by the outflow q_{out} is ruled by ρ_R while on the other hand the system enters the maximum current phase where the bulk flow is given by ρ_L again.

Summarizing this, one finds that in case of an inflow rate larger than the maximal system flow the outflow rate determines whether the system enters the maximal current or the jammed phase. In the maximal current phase the system flow is given by the maximal system inflow while in the jammed phase the bulk flow given by the system outflow.

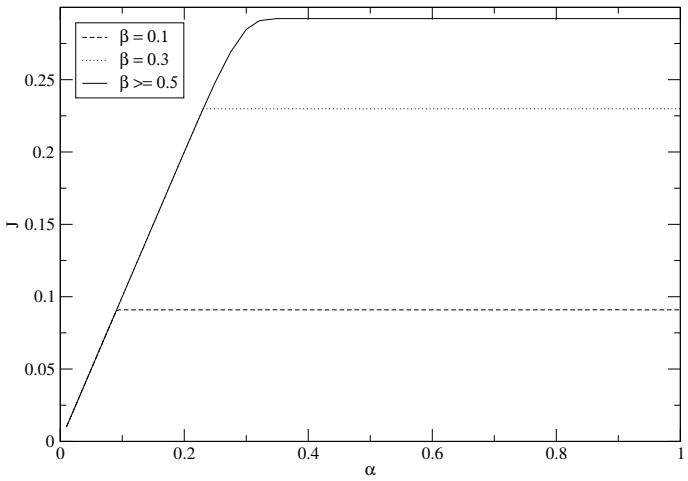

Figure 4.12: System flow in dependence of inflow rate α for a fixed buffer size $B = 32$ and hopping probability $p = 0.5$. The outflow rate is set to $\beta = 0.1, 0.3, 0.5$ and 1. For inflow rates $\alpha < 0.5$ the inflow is restricting the maximal flow while for outflow rates $\beta \geq 0.5$ the hopping probability is the distinctive parameter regulating the bulk flow. In case of an outflow less than the inflow and the maximal system flow the jammed phase is entered.

In fig. 4.13 the influence of the outflow rate β onto the system flow J_β is depicted for fixed inflow rates $\alpha = 0.1, 0.3, 0.5$ and 1, buffer size $B = 32$ and moving probability $p = 0.5$. Here, in case of outflow rates larger than the provided inflow and an inflow rate less than the maximal system flow ($\alpha < \beta$, $\alpha < \alpha^*$), the system is situated in the free flow phase. In this case the bulk flow is dominated by ρ_L and hence given by q_{in}.

Limiting the outflow further more plateau formation arises since the system enters the jammed phase ($\beta < \alpha$). In the jammed phase the system flow is determined by the restriction at the right boundary and therefore given by ρ_R. Consequently, the system flow corresponds to the system outflow q_{out}.
In case of inflows less than the by β provided maximal possible outflow and larger than the by p provided maximal system flow ($\alpha < \beta$, $\alpha^* < \beta$) the system resides in the maximum current phase. Here, the system flow is stated once again by ρ_L and is therewith given by

the maximal system inflow q_{in}^{max}.

As well as in the previous case the interplay between inflow, outflow and maximal system flow is determining the system state. Here, in case of an inflow higher than the maximal system flow the outflow rate determines whether the maximal current or the jammed phase is entered. Consequently, in the jammed phase the bulk flow is given by q_{out} while in the maximal current phase the bulk flow corresponds to the maximal system inflow q_{in}^{max}.

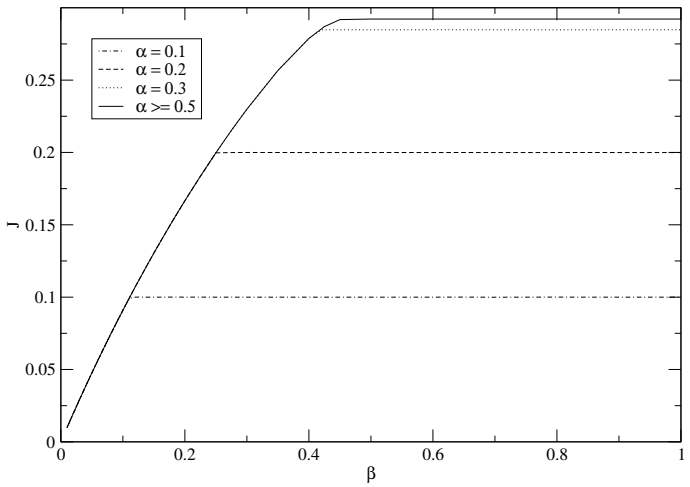

Figure 4.13: System flow vs. outflow rate β. The inflow is set to $\alpha = 0.1, 0.3, 0.5$ and 1. For inflow rates $\alpha > \alpha^*$ the outflow rate regulates the system state, i.e., the system is situated in the maximal current phase for $\beta > \alpha^*$ and in the jammed phase for $\beta < \alpha^*$. Otherwise, for inflow rates $\alpha < \alpha^*$ the system resides in the free flow regime in case of $\beta > \alpha$ and in the jammed regime for $\beta < \alpha$.

4.5.2 Phase Diagram

In fig. 4.14 the phase diagram of the AMOP with open boundary conditions and stochastic movement is depicted in dependence of the buffer size $B = 1, 2$ and 32. Clearly, the influence of the stochastic movement becomes apparent. Expectedly in contrast to the case with deterministic movement a third phase occurs. This maximum current phase C is entered for inflows and outflows larger than the system capacity ($q_{in} \geq J_{max} \leq q_{out}$). Moreover, there is a jammed phase B for $q_{in} > q_{out} < J_{max}$ and a free flow phase A for $J_{max} > q_{in} < q_{out}$.

As in the deterministic case the diverse buffer sizes drastically affect the shape of the phase diagram. One finds that the jammed phase is strongly enlarged for increasing buffer sizes compared to the one of the ASEP ($B = 1$). The free flow phase on the other hand shows only a marginal dependence from varying the buffer size. Here, increasing the buffers leads to a slightly enlarged free flow phase as described in fig. 4.14. Although the maximum current phase shrinks it has to be mentioned that the flow in the maximum current phase itself is strongly increased for an increasing buffer size as a result of the multi-occupation. Even in the jammed and the free flow phase the extension of the buffer size results in a gain of flow compared to systems with smaller buffers for the same set of inflow, outflow and hopping parameter.

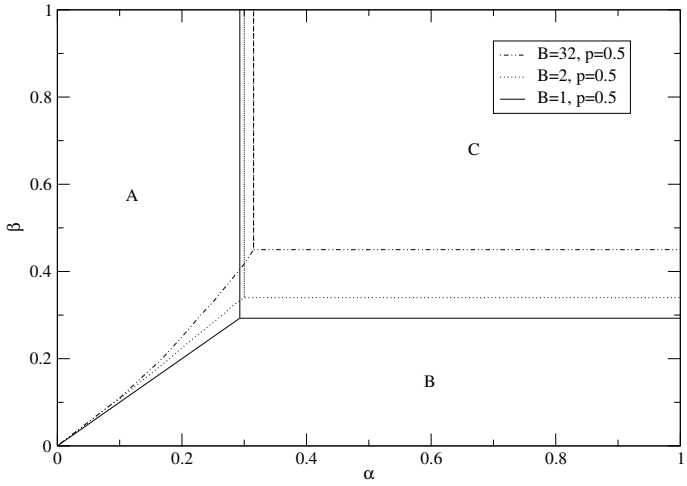

Figure 4.14: Phase diagrams of the stochastic version of the model for buffer size $B = 1$, $B = 2$ and $B = 32$. Three phases can be distinguished. A low density phase in the upper left where the system flow is dominated by the inflow rate α, a jammed phase in the lower right ruled by the outflow rate β and a high flow phase in the top right part of the diagram dominated by the hopping probability p.

In order to show in how far buffer extensions are reasonable methods for obtaining significant higher system flows under open boundary conditions in fig. 4.15 the relative benefit of flow per buffer cell ($\frac{J_B - J_{B=1}}{B}$) is depicted in dependence of the buffer size for a system situated in free flow, jammed and maximum current regime. In the double logarithmic plot in fig. 4.15 clearly an algebraic decay can be identified for increasing buffer sizes which means that the gain of flow rapidly converges to zero. Already for a buffer size of $B = 32$ the relative flow per cell is reduced to approx. 5% in free flow, 10% in jammed and to 20% in the maximum current phase compared to buffer size $B = 2$. This means that despite the fact that extending the buffer size provides higher system flows for identical system parameters α, β and p, distinctive effects are already found for buffer sizes $B < 32$ in all three phases and thus a further extension of the buffer sizes does not provide better or more distinctive results.

4.6 Discussion

In this chapter a one-dimensional cellular automaton model with open boundary conditions is analyzed in the context of boundary induced phase transition behavior. The model can be characterized as a variant of the ASEP with multi-occupation of sites or on the other hand as a discrete mass transport model with finite dimensional single state space and open boundary conditions. It was shown that the maximal current principle holds even for systems with multi-occupation of sites. Moreover, the characteristics of the phase diagrams of the deterministic model were investigated on the basis of analytical investigations whereas the stochastic version was analyzed with the help of numerical simulations.

In case of deterministic system dynamics an analytical approach was introduced to determine the system flow in dependence of the inflow at maximal outflow rates and the outflow at maximal inflow rates. Here, in each case the system was reduced to a single site

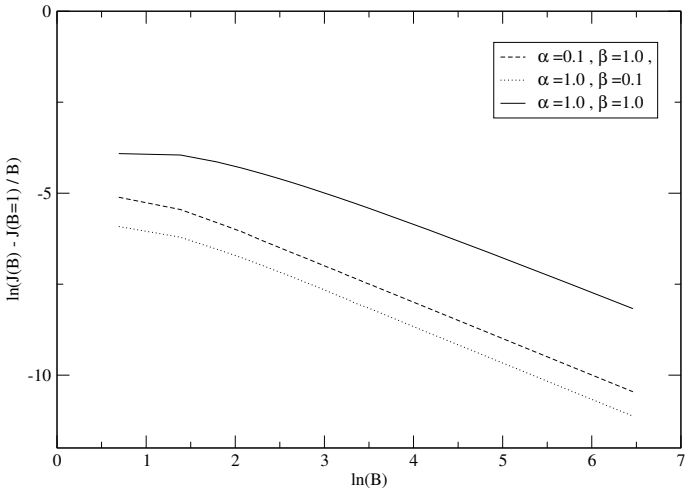

Figure 4.15: Double logarithmic plot of the relative flow per buffer cell in the free flow, jammed and maximum current phase. The system parameters are $L = 100000$ and $p = 0.5$. In all system states an algebraic decay of the gain per buffer cell can be found meaning that the differences found in the FDs are most distinctive regarding small buffer sizes.

problem. Hence, it was possible to derive the complete phase diagram of the deterministic model for arbitrary buffer sizes. Furthermore, it was shown that the multi-occupation of sites exerts an immense influence onto the shape of the phase diagram. It was found that increasing the buffer size results in a highly enlarged jammed phase at the expense of a reduced free flow regime.
With regard to the provided system flows (see fig. 4.4 and fig. 4.5) in dependence of the inflow and outflow rates it becomes apparent that although the jammed phase is highly enlarged the system flow for larger buffers is increased for the same set of parameters α and β. Nevertheless, the individual travel times are not affected by the increase of the buffer size since the system outflow is independent from the buffer sizes as shown in fig. 4.5.

In case of the stochastic model which is characterized by a strongly increased maximal system flow for larger buffer sizes and a shift of the maximal flow to higher densities (see fig. 4.10, 4.11) three phases can be distinguished. Similar to earlier investigations of DLG models turning on stochastic movement a third phase occurs namely a maximum current phase [23]. This phase is characterized by a maximal system inflow providing a maximal particle current throughout the system and an unrestricted outflow. The system is simply overfed because the inflow rate exerts the capacity of the by the moving probability p and the buffer size B provided system flow. For $p \to 1$ the maximal current phase vanishes and the system becomes deterministic. Compared to the ASEP also in the stochastic model larger buffer sizes provide a highly enlarged jammed phase whereas the free flow phase is only slightly increased. As a result the maximum current phase shrinks with larger buffer sizes. However, it has to be mentioned again that the provided bulk flow within all three phases is enlarged for increasing buffer sizes especially in the maximum current phase.

In the context of capacity extensions for Internet routers and gateways the presented results might be used as an indication for a reasonable hardware performance upgrade. For extending the buffer size the gain of flow converges (see fig. 4.15). This means for real world problems that one has to consider if capacity extensions beyond a certain

point do not become disproportionate expensive in relation to the desired performance enhancement. Moreover, the fact that the jammed phase is strongly enlarged compared to systems with smaller buffer sizes at fixed inflow and outflow rates buffer size extensions lead to an increased system flow which means that the performance and therewith the mean travel time of data packets becomes clearly reduced. However, for a fixed demand of particles per time interval reasonable buffer extension are a suitable method to enhance the system flow and therewith the bandwidth. Regarding the response times of Internet connections on the other hand buffer extensions have an antagonized effect. Here, the mean travel times are enlarged. An improve of the response times can therefore only be reached for a reduction of the processing time, i.e., larger moving probability p and an increase of β.

5 AMOP with Interacting Boundaries

In the previous chapter the influence of open boundary conditions was investigated in the context of phase transition phenomena in DLG models. Therefore, an effective and straightforward inflow strategy was chosen providing maximal inflows and therewith allowing to investigate all possible system states. This allows deriving the complete phase diagram of the AMOP with open boundary conditions in case of deterministic as well as in case of stochastic particle movement.

In this chapter now a different more realistic and therewith sophisticated inflow strategy is introduced and investigated in order to include flow control policies that are found to be essential in order to simulate Internet data file transport. Although flow control strategies are disregarded by the inflow strategy used in the original model formulation the features and statistical properties of Ping-experiment data sets could be correctly reproduced. This is plausible because there is no need to control a transmission or receiving rate of a single datagram. Flow control becomes meaningful or necessary only in case of the transmission of a bunch of datagram. An example may be data file transfer where the file that has to be sent is usually larger than a single datagram. Thus, the file is portioned into smaller entities that are broadcast successively. The applied transfer policies are an integral part of the TCP-Protocol and hence essential for the simulation of Internet file transfer.

Here, it has to be stressed again that there is an immense difference between file transfer and the transmission of a single control packet (ICMP packet) as used by the ping command since in case of data file transfer a connection is established between the involved Internet hosts. This means that there is an active information exchange between the two connection partners concerning the transmission rate of the datagram, i.e., segments in which a file is portioned, the acknowledgment of received data packets to guarantee a correct and complete transfer as well as a suitable transfer rate in order to avoid congestions and hence packet losses.

5.1 Introduction

In reality the TCP-Protocol is an essential part for establishing a communication between a source and a destination host. In contrast to the connectionless IP-Protocol responsible for the routing of the data packets which is neglected in the considerations of this work (the investigations are focused on the one-dimensional system), the TCP-Protocol is a so called end-to-end protocol. This means that there is an active information exchange between source and destination host during the file transfer. This information exchange is about various kinds of relevant details that are specified in the header of each single datagram. Since the routing of a datagram is completely ruled by the connectionless IP-protocol, i.e., each datagram is treated individually at each router, flow control has to be part of the TCP-Protocol. Over the years a lot of variants of the TCP-Protocol [3] were derived in order to establish more effective and reliable transfers and thus reduce the appearance of congestions.

Hereby, the heterogeneous hardware and the decentralized structure of the network are enormous difficulties. Regarding the file transfer optimization especially the second point, i.e., the decentralized structure of the network is of prime importance since this means that each connection can only be optimized by an information exchange between sender and receiver. Consequently, the only facility allowing such a flow control is the adjustment of the sending rate by the source host. This means that the transfer rate between the two dedicated hosts can only be evaluated by the connection partners itself and is therewith adjusted with respect of finding the local optimum whereas there is no central entity involved in finding the global system optimum.

Moreover, the decentralized structure of the Internet implies that there exist some more difficulties for optimizing the data file transport. Here, especially the time delay in which the sender and therewith the algorithm implied in the TCP-protocol can react on transmission problems, e.g., packet losses, in order to establish a reliable data transfer has to be mentioned. This delayed reaction time is caused by the fact that the only information the source host can consult is the acknowledgement of the arrival of a datagram at the receiver. This acknowledgement on the other hand has just to be sent back to the source host. Now, the sender can adjust a suitable transmission rate.
Moreover, this means that an optimal inflow can only be reached by increasing the sending rate until some of the sent packages are not acknowledged which indicates that the system has already run into a jammed state. Consequently, in this way neither a stable local optimum nor a global system optimum can be found.

For the sake of completeness in the following a schematic description of the algorithms responsible for the adjustment of the sending rate is given. In particular the method the source hosts react on the absence or delayed arrival of an acknowledgement is determined by the used TCP version known under names like TCP-Tahoe, TCP-Reno, TCP-NewReno TCP-Stack or TCP-Vegas (in chronological order). All these variants of the TCP-protocol follow a general optimization strategy which can roughly be described as follows.

At the beginning of any file transfer, the source host starts with the slowest sending rate that is further increased until some acknowledgement packages do not arrive in a scheduled time interval (window). Simultaneously with the sending rate the window size is also increased. In case of the emergence of a transmission delay or the loss of a datagram the TCP version specific *fall back rule* is applied regulating the adjustment of the new sending rate. This fall back rule implies that the sending rate as well as the window size are reduced depending onto the used version of the TCP-protocol. In case of an established reliable new connection the sending rate and also the window size are increased until packet losses are detected again and the fall back rule is utilized once again. Obviously, the sending rate can also be adjusted via the window size.

As an example in fig. 5.1 the time evolution of the window size is depicted in case of an arising congestion for TCP-Tahoe. Clearly, three different characteristic regions can be distinguished, a *slow start*, a *congestion avoidance* and a *loss recovery, time out* region.
As given in fig. 5.1 the file transfer starts with the slow-start interval where the window size is doubled after every successful acknowledgement until the maximum window size is reached or a packet gets lost.

In case of an existing congestion some packets get lost on their way to the receiver. Since the sender will not get any acknowledgments for these packages no further packet will be broadcast until an internal timer runs to zero. The timer starts whenever a datagram is sent. The initial timer value is estimated by the source host based on the mean and the variance of the RTT (round-trip-time). Thus, whenever a datagram is not acknowledged in the initial slow to start sequence a time out period will arise where no further datagram is sent.

After this time-out period the window size is set back to the initial value of one data packet and the slow-start sequence starts again until half of the window sizes is reached at which the last packet got lost in the congestion before. Here, the congestion avoidance sequence is initialized whereas the increase of the window size is reduced to one packet for each successful acknowledgement. The congestion avoidance sequence ends if the maximal window size is reached or another packet loss is detected. In the later case the cycle of time-out, slow-start and congestion-avoidance sequence starts again.

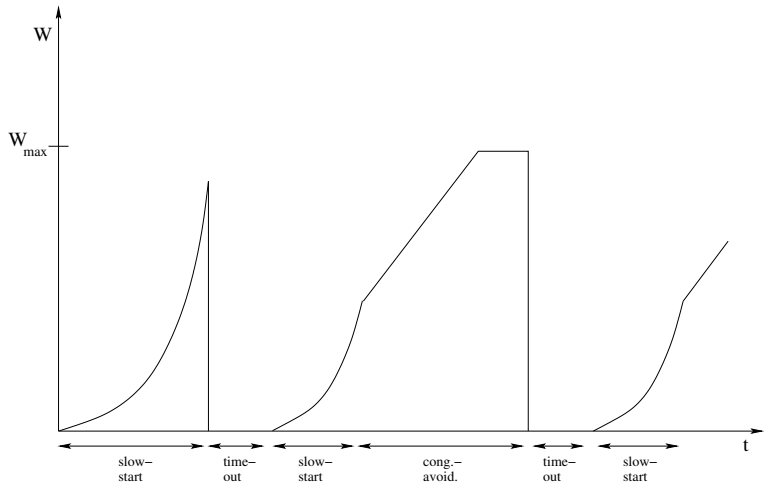

Figure 5.1: Sketch of the adjustment of the window size W in case of an arising congestion given by the fall back rule implied in the TCP-Tahoe protocol.

Detailed specifications of the algorithms implied in the TCP-Protocol in order to prevent the Internet from completely jamming can be found in [3, 74, 91] and references therein.

5.2 AMOP with Fall Back Inflow Strategy

With regard to the inflow strategies integrated in the TCP-Protocol a straightforward policy is introduced where the system inflow is similar to reality determined by the state of the last site of the system. This implies that likewise to the real world strategy the inflow rate is adjusted in dependence of situation of the receiver of a datagram. In case of a delayed arrival the sending rate is reduced that corresponds to a jammed system and therewith to a strongly occupied last site. Otherwise, in a free-flow system the last site is less occupied and the sending rate is consequently increased again.

In order to simulate the influence of a state dependent inflow rate onto the system dynamics a more sophisticated inflow strategy compared to the original model is introduced and investigated. Therefore, the inflow into the system is verified in the sense that particles

are inserted into the buffer of the first site depending on the state of the last site. This is realized by inserting particles with probability α as long as occupation number of the buffer of the last site is not beyond a certain threshold T_B. In case of an occupation number of the last site L of $\tau_L > T_B$ the inflow rate is reduced to an inflow rate $\alpha_- < \alpha$. This reduced inflow rate provides that possible congestions induced by the last site could resolve for a suitable choice of parameters in order to prevent the system from a complete jamming. Upon the congestion of the last site has resolved the inflow rate is set back to the initial inflow rate α. A sketch of the fall back inflow strategy is depicted in fig. 5.2.

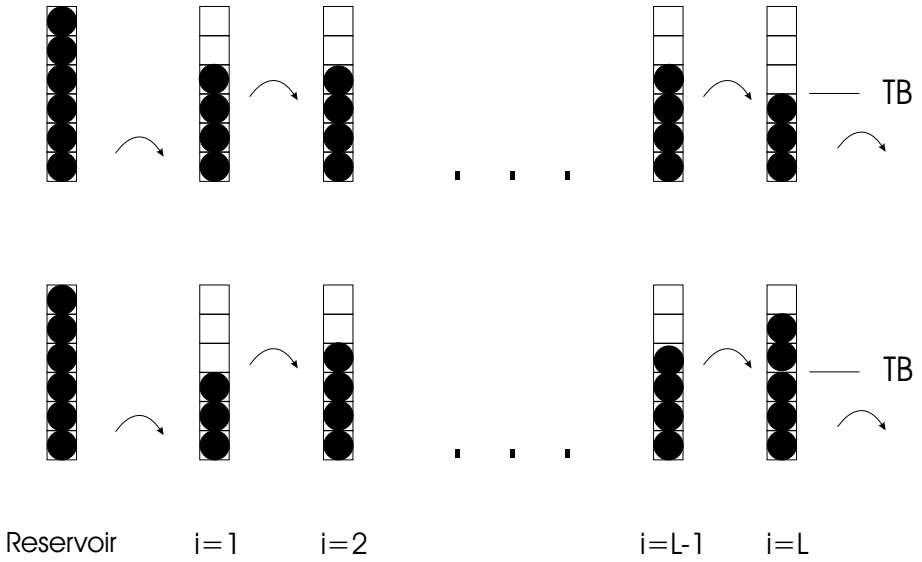

Figure 5.2: Schematic representation of the AMOP with fall back inflow rule. Particles are inserted at the left boundary according to the state of the last site L of the system. In case of an occupation number less than a given threshold T_B particles are inserted with probability α while for a occupation number larger than this threshold the inflow probability is reduced to $\alpha_- < \alpha$.

The definition of the model with reduced inflow is then as described in the following:

Particles are inserted form a reservoir, for convenience reasons positioned at the left side of the system, into the buffer of the first of L sites with a given inflow rate α as long as the number of particles in the buffer of last site of the system L is less than T_B, meaning $\tau_L \leq T_B$. Otherwise, for $\tau_L > T_B$ particles are inserted with a reduced inflow rate $\alpha_- < \alpha$ into the first site. This means that the inflow is determined by the actual occupation number of the last site. From here the particles move with a dedicated probability p into the next succeeding site towards the other end of the system as long as the buffer of the succeeding site is not completely filled. Then, at the right end of the chain the particles are removed with probability β.

Thus, the dynamics within the system are identically to the dynamics known from the AMOP. The only differences are based upon the different inflow strategies. Remind that conform to the previous model definitions the particles obey parallel dynamics and move with maximal velocity $v = 1$, i.e., one site at each time-step. Moreover, all buffers in the system are of identical size B and equipped with an identical hopping probability p. Note that in the following investigations only the case with $\alpha_- < \alpha$ will be considered.

Here, it has to be mentioned again that the applied inflow rate is determined at each time step by the actual state of the last site.

5.3 Numerical Investigations

In the following the most relevant results of the introduced fall back inflow strategy onto the system dynamics are investigated and discussed on the basis of numerical simulations. Therefore, especially the influence of the new system parameters α_- and T_B onto the system flow and the system density are of special interest. Moreover, the phase transition behavior induced by the new inflow strategy is roughly investigated.

In order to get a first impression of the system properties induced by the fall back inflow strategy in fig. 5.3 exemplarily a typical FD of the model with fall back inflow strategy is opposed the FD of the model with generic inflow strategy at identical parameters of α and β. Remind that the fall-back rule is a special inflow strategy and thus only systems with open boundary conditions are compared. Clearly, the outstanding differences introduced by the fall back rule can be identified.

A striking point is hereby that in a dedicated area between the two densities ρ_1 and ρ_3 for outflows less than the given inflow the system does not follow the jammed system branch as expected but *falls back* onto the free-flow branch until a density of $\rho_2 < \rho_1$ is reached. From here the FD is not further affected by the introduced fall back rule and the FD becomes identical to the one of the generic inflow strategy. Regarding the free-flow regime clearly it can be noticed that even the free-flow branch is affected by the new inflow strategy. In contrast to the deterministic model here the maxima system flow of the periodic AMOP is not reached.

Considering fig. 5.3 one would first expect to find meta-stable system states since the shape of the FD seems to be rather similar to the FD of the velocity dependent randomization (VDR) model introduced by Barlović et al. in [16]. In the field of traffic theory meta-stable system states are a well known and therefore well understood phenomena and a required model attribute since investigations of highway traffic revealed explicitly the existence of such meta-stable high flow states. With regard to this effect the original formulation of the NaSch model was enhanced by the introduction of a velocity dependent randomization as described in [16]. Here, explicitly the slow to start rule, i.e., standing vehicles or particles ($v = 0$) accelerate with a time delay or in the notation of stochastic CA model with a reduced probability, induces phase separated wide jams and meta-stable high flow states [16, 18].
Moreover, it was shown in the context of boundary induced phase transition phenomena that the VDR model with its intrinsic meta-stability exhibits a new so called jam outflow phase (JO-phase) representing a meta-stable high flow state. For further details see [15].
However, the fall back rule exhibits some similarities to the VDR rule set, e.g., the reduced inflow probability can be seen as a pendant to the reduced acceleration probability for standing particles and a similar shape of the FD, but it has to be explicitly stated here that meta-stable system states do not exist.

With regard to the diagrams in fig. 5.3 the FDs of the AMOP for both inflow strategies are compared. Here, clearly the influence of the fall back rule can be recognized. Until

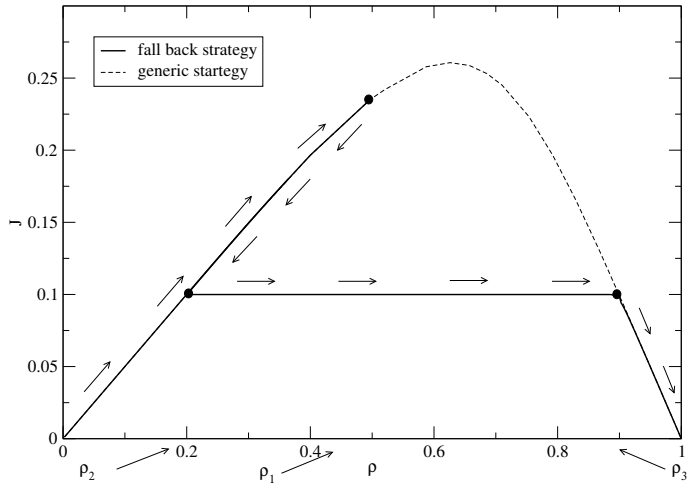

Figure 5.3: FDs of the model with fall back inflow strategy and stochastic movement ($p = 0.5$) in comparison to the model with generic inflow strategy. Clearly, the influence of the reduced inflow rate of $\alpha_- = 0.1$ at a threshold value of $T_B = 1$ can be identified. The system parameters are $L = 1000$ and $B = 5$ respectively.

$J(\rho_1)$ is reached the system resides in the free-flow regime and the shape of the diagrams is identically. The flow rises with increasing density. In case of low values of T_B and α_- the fall back rule is applied even in the free-flow regime and thus the maximal system flow of the model with generic inflow strategy might not be reached for maximal inflow rates of $\alpha = 1$. Conform to the previous investigations the free-flow branch is scanned by keeping the outflow rate fixed at $\beta = 1$ while the inflow rate α is used to adjust the system inflow.

The jammed system branch is scanned by setting the inflow rate to $\alpha = 1$ in order to obtain maximal inflows. The outflow rate is then applied to regulate the system flow and density. Also in this case the two diagrams diverge. While in case of the original model the flow decreases with increasing densities in the model with fall back strategy the flow decreases with decreasing density until the system density becomes ρ_2. From here the system flow becomes approximately constant to $J \approx q_{in}(\alpha_-)$ until the jammed branch of the model with generic inflow strategy is reached. This means that it is possible to get two different stationary system flows at identical system densities in dependence of the chosen combination of inflow and outflow rate. In the jammed regime at densities $\rho > \rho_3$ the two diagrams coincide again. As a consequence the jammed branch is strongly reduced compared to the model with generic inflow strategy and the corresponding densities are *falling back* onto the free flow branch.

In order to reveal the influence of the threshold value T_B onto the model dynamics in the following investigations the flow density relation is investigated. It is important to mention here that the flow density relation is not a FD in the sense that a given system density provides a defined system flow. In fact the boundary conditions and the internal interactions determine the system state and therewith the system flow and density. For the sake of simplicity the free-flow system is scanned by adjusting the inflow rate α and keeping the outflow rate fixed to $\beta = 1$. On the other hand the jammed system is scanned by choosing a fixed inflow rate $\alpha = 1$ and varying β.

Moreover, it has to be mentioned that the inflow in both cases is reduced to α_- whenever

the threshold value is exceeded in the last site $i = L$. Furthermore it is to mention that because of the fact that the investigated model exhibits open boundary conditions and so the number of particles is not conserved the system flow and density are averaged values measured after relaxation into the *steady state* or to be more exact after the variance of flow and density do not change significantly. This is of prime importance because of the inhomogeneous character of some new system states as shown in the following investigations.

Here, it is to mention that the found features are induced by the modified inflow strategy with reduced inflow rate α_- in combination with the chosen parameter set for inflow rate α, outflow rate β and the threshold value T_B.
In the following the system dynamics are investigated on the basis of numerical simulations to get a clear impression of the system properties. Similar to the investigations of the previous chapter in particular the phase diagram depending on the interplay between inflow, outflow, reduced inflow rates as well as on the threshold value T_B and the moving probability p is of special interest.

5.4 Deterministic Model Dynamics, $p = 1$

First the AMOP with deterministic particle movement and fall back inflow strategy is investigated. In comparison to the original formulation of the model there are two distinctive new model parameters T_B and α_- that are responsible for the new dynamics. Consequently, the influence of these two model parameters is investigated first.
As a starting point in the following vanishing reduced inflow rates, meaning $\alpha_- = 0$ are considered. This system configuration is of prime interest since in this case the pure influence of the fall back rule can be investigated.

5.4.1 Vanishing Reduced Inflow Rate, $\alpha_- = 0$

Here, vanishing reduced inflow rate means that the inflow into the system is reduced to $\alpha_- = 0$ whenever the threshold value T_B at the last site is exceeded. Remind that this threshold represents the state of the last site of the system τ_L and therewith introduces strong correlations in the system dynamics. This is because of the fact that the inflow rate into the first site is either given by α or α_- depending directly on the state of the last site.
Considering FDs in fig. 5.4 clearly one finds that the free-flow regime is not affected at all and the maximal system flow $J = 1/2$ is reached for any chosen value of T_B. There is a linear increase of the system flow with increasing densities provided by the increase of the inflow rate α.
For threshold values $T_B \geq B - 1$ the jammed branch is not affected by the fall back rule and thus by the reduced inflow rate α_-. The complete FD becomes identical to the one of the ASEP or the model without fall back rule since $T_B \geq B - 1$ means that the inflow is reduced only if exactly B particles are present in the last site.
Therefore, the influence of the new fall back inflow strategy becomes apparent first when the threshold T_B becomes less than $B - 1$. In this case the model dynamics are strongly modified and the complete density range can not be examined due to the appliance of the fall back rule. Moreover one finds that for threshold values $T_B < B/2$ densities of $\rho > 1/2$ can not be adjusted.

In order to get a deeper insight into the system dynamics modified by the fall back rule,

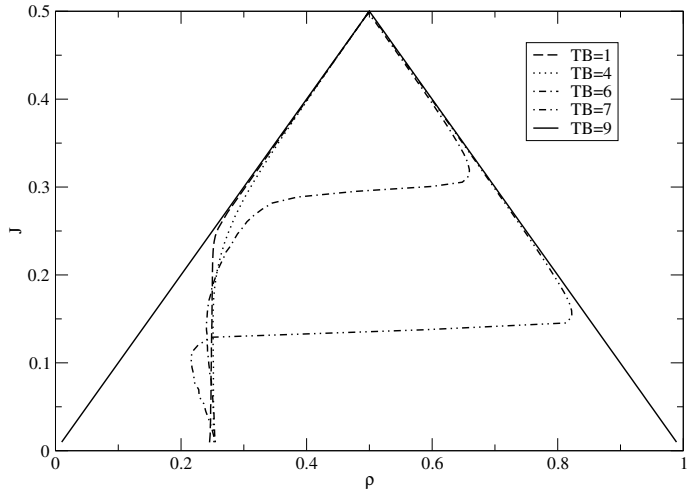

Figure 5.4: FDs for different values of T_B in case of a reduced inflow rate of $\alpha_- = 0$. In the free-flow regime the fall back rule does not have any effect onto the shape of the FD compared to the model without fall back rule. Contrary, the high density regime is strongly affected. In case of threshold values $T_B < 5$ the system does not enter the jammed regime for all combinations of α and β, while for $5 < T_B < 10$ densities $\rho > 1/2$ are exceeded. The system parameters are $L = 100$, $B = 10$ and $p = 1$.

in the following the corresponding space-time plots for the relevant parameter sets are investigated to obtain a detailed description of the course of events resulting in the unusual shape depicted in fig. 5.4.

In fig. 5.5 and 5.6 typical space-time plots of the free-flow and the jammed regime are depicted. Here, it is shown that the fall back rule strongly affects both regimes since a striped pattern can be found in the free-flow as well as in the jammed regime.

In the left and the right diagram of fig. 5.5 typical space-time plots of the free-flow branch are given, characterized by an unrestricted outflow ($\beta = 1$) whereas the system flow and therewith the mean density are controlled by the interplay of the inflow rates α and α_-. The particles inserted with probability α move completely deterministic throughout the entire system and no disturbances occur because of the unbound outflow. Consequently, the shape of space-time plot in the free-flow regime is given by the combination of the system inflow and thus by the appliance of the fall back rule.

The system flow can be approximated by regarding the probability $P_{\alpha_-}(\alpha)$ that the inflow α provides more than T_B particles resulting in the utilization of the fall back rule.
Here, $P_{\alpha_-}(\alpha)$ becomes:

$$P_{\alpha_-}(\alpha) = \sum_{n=T_B+1}^{B} P_n, \tag{5.1}$$

whereas P_n is given by eq. (4.6) and represents the probability that exactly n particles are inserted into the first site with inflow rate α and for a buffer of size B. Therewith, the inflow respectively the system flow in the homogeneous free-flow state can be approximated by:

$$q_{in} = (1 - P_{\alpha_-}(\alpha))q_{in}(\alpha). \tag{5.2}$$

Note that this approximation becomes valid only for deterministic outflows, i.e., $\beta = 1$. In case of inflow rates α providing less than T_B particles into the system, i.e., very low inflow rates, one finds a rather homogeneous pattern, while for inflow rates α providing more than T_B particles even in the free-flow regime a striped pattern arises.

Regarding the space-time plots of the free-flow regime in fig. 5.5 the two different patterns can be explained as follows. Consider the left space-time plot with $\alpha = 0.1$. In case of a buffer size of $B = 10$, statistically one single particle is inserted at each time step. Since α is relatively small there is a finite probability that no particle is inserted and this on the other hand means that the probability for inserting a sequence of particles becomes very small. Consequently there is no definite segregation between intervals with and without system inflow.
On the other hand for rising inflow rates α the probability that no particle is inserted becomes smaller and smaller. This means that the probability for inserting a sequence of particles in the number of the system size L is increased as well. As a result one finds a clear separation between intervals of inflow α and α_- respectively.

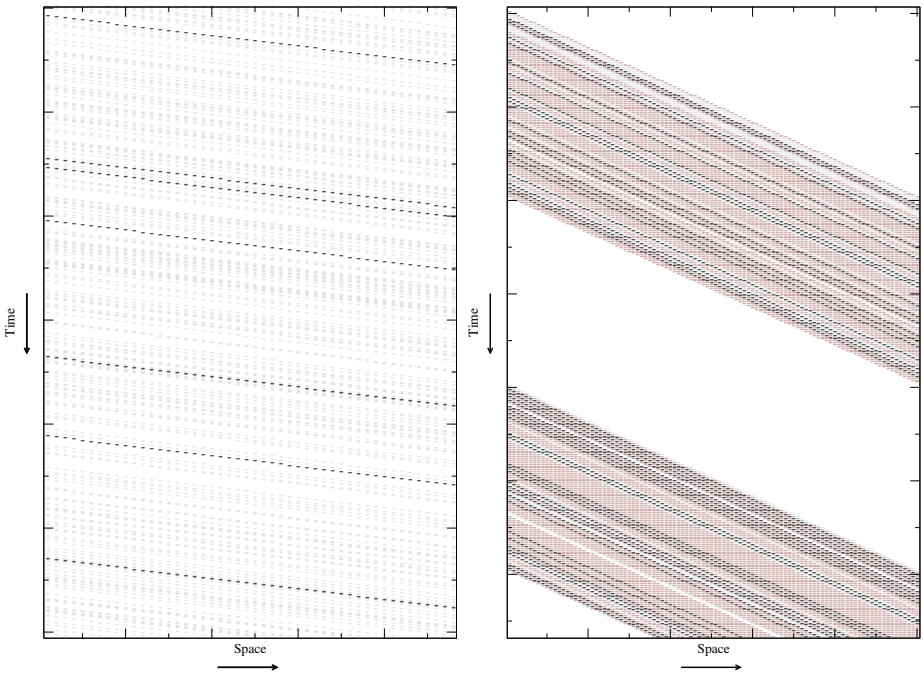

Figure 5.5: Space-time plot of the AMOP with fall back inflow rate $\alpha_- = 0$, $T_B = 0$, $B = 10$ and $L = 100$. **Left:** System in the free-flow regime with $\alpha = 0.1$ and $\beta = 1$. The fall back rule is hardly applied and one finds no differences compared to the model with the generic inflow strategy. **Right:** System situated in the free-flow regime as well for $\alpha = 0.8$ and $\beta = 1$. There is no jam existing in the system. Nevertheless, the fall back rule is applied and a striped pattern arises.

Turning to the jammed system state (see fig. 5.6) in contrast to the free-flow system in the right diagram clearly jam formation in front of the right boundary can be identified as well as the arising of a striped pattern. The system resides in the jammed regime since

$q_{in} > q_{out}$.
Here, two alternating system states with characteristic life times T_1 and T_2 can be distinguished representing the alternation of a free-flow and a jammed system state. In the free-flow state, given by the time interval T_1, bunches of B particles induced at the left boundary by the maximal inflow rate $\alpha = 1$ are moving undisturbed throughout the entire system until the first one reaches the right end of the chain. Under consideration of deterministic movement it takes exactly $T_1 = L - 1$ time steps until the first bunch arrives at the last site L. For a threshold value of $T_B < B - 1$ the inflow into the system is reduced to $\alpha_- = 0$ respectively vanishes. In case of an reduced outflow $q_{out} < q_{in}$ the induced bunches accumulate in front of the right boundary and a jam emerges. Here, $q_{in}(\alpha)$ and $q_{out}(\beta)$ can simply be calculated with (4.7) and (4.11).

For the time interval T_2 the system inflow vanishes until the jam at the right boundary dissolves completely and no more particles are present in the system. Now the inflow rate is set back to $\alpha = 1$.
The time interval T_2 can simply be approximated by considering that at the end of the interval T_1 in case of an even system size L the amount of $LB/2$ particles is present in the system while in case of an odd system size $(L+1)B/2$ particles are situated in the system. Because of $T_B = 0$ no more particles will be inserted until the jam at the right end of the system has dissolved and the system runs completely empty. The width of the jammed cluster at the right boundary follows a biased random walk and T_2 can be approximated in case of even values of L by:

$$T_2 = \frac{L/2 - q_{out}}{q_{out}}. \tag{5.3}$$

The numerator in eq. (5.3) represents the loss of particles depending on the outflow and of course the number of particles present in the system at the beginning of T_2. The denominator denotes the outflow per time step responsible for the dissolution of the jamming. In case of odd values of L the numerator is given by $(L + 1)/2 - q_{out}$ respectively.

With the help of eq. (5.1) and eq. (5.3) the mean system flow in the striped phase can be easily approximated by regarding the system outflow in a complete cycle from free-flow to jammed and back to the free-flow regime. The bulk flow is then given by:

$$J_{stripe} = \frac{T_2 q_{out}}{T_1 + T_2}, \tag{5.4}$$

while the mean density can be approximated as:

$$\rho_{stripe} = \frac{T_2(1 - q_{out})}{T_1 + T_2}. \tag{5.5}$$

Coming back to the FDs in fig. 5.4 the shape of the jammed branch can be explained as follows. Considering threshold values of $T_B < 5$ the FDs do not merge into the jammed branch of the model with generic inflow strategy or periodic boundary conditions. This is due to the fact that the maximal system outflow is given in case of $\alpha = 1$ by eq. (4.11) as $\frac{\beta}{\beta+1}$.

With decreasing outflow rate $\beta < 1$ the amount of particles resting in the last site statistically increases and the fall back rule is applied for more than one time step and a striped pattern arises. Considering a cycle of maximal and reduced inflow, densities of $\rho > 1/2$

can only be reached for rising values of T_B. This is due to the fact, that a sequence of vanishing inflows has to be broken up as depicted in the right space-time plot of fig. 5.6. This is only possible for system outflows providing that less than T_B particles are present in the last site. And this again means that for a buffer size of $B = 10$ a threshold value of $T_B = 7$ is statistically exceeded for outflow rates of $\beta > 0.43$. Choosing $T_B < B/2$, the probability converges to zero. A typical space-time plot of this scenario is depicted for $T_B = 7$ in the left part of fig. 5.6. Here, a mean density of $\rho > 1/2$ can not be adjusted for any combination of inflow and outflow rates.

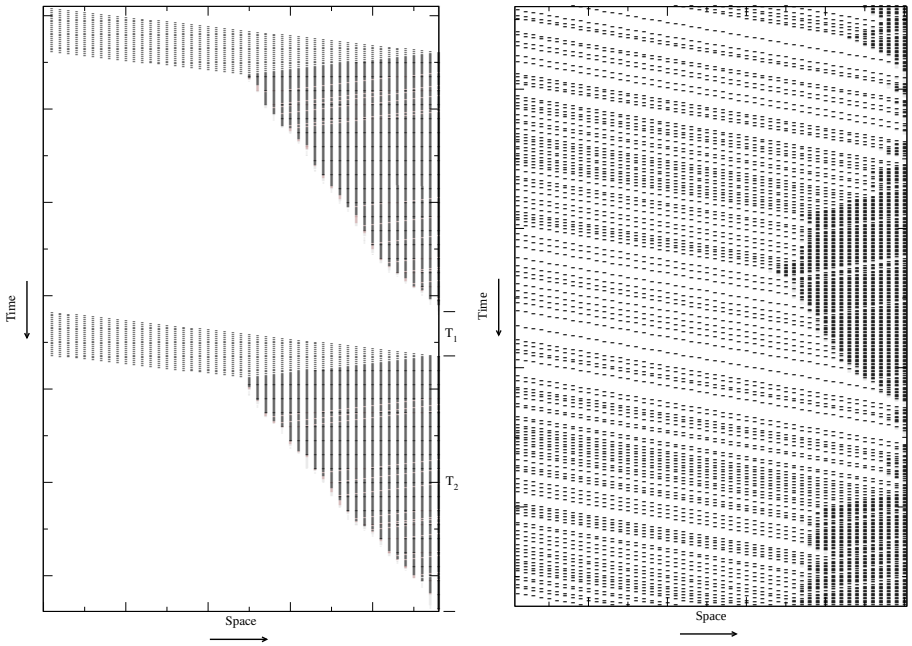

Figure 5.6: Space-time plot of the AMOP with fall back inflow rate $\alpha_- = 0$, $B = 10$ and $L = 100$. **Left:** System in the jammed state. Clearly, the striped pattern induced by the fall back rule with $T_B = 7$ can be recognized. High density regions alternate with empty system regions. The system parameters are $\alpha = 1$ and $\beta = 0.1$. **Right:** System in the striped high density regime for $T_B > B/2$, i.e., $T_B = 7$. Here, the interval with reduced inflows is interrupted and particles are inserted with the maximal inflow rate $\alpha = 1$ while the outflow rate is set to $\beta = 0.3$

Note that these approximations are only valid in case of a threshold value of $T_B = 0$ since otherwise outflows provided by β may affect the system inflow in so far that statistically less than $T_B \neq 0$ particles are present in that last router after one update step in the jammed regime and therefore the inflow rate is set back to α. This probability is obviously given by eq. (5.1) and eq. (5.2) meaning that even in the time interval T_1 bunches of B particles might arrive at the right boundary. Moreover, it has to be mentioned that the striped pattern becomes less distinctive for larger threshold values T_B since the fall back rule then is applied for larger inflow rates.

5.4.2 Reduced Inflow Rates, $\alpha_- \neq 0$

In the previous section it was shown that in case of vanishing reduced inflow rates $\alpha_- = 0$ the complete density range can only be scanned for $T_B > B - 1$. This means that the the fall back rule is not applied. Otherwise, the system inflow is reduced to zero due to the fall back rule and no particles are inserted.

Now, in the following investigations the influence of the fall back rule and in particular the impact of T_B at reduced inflow rates of $\alpha_- \neq 0$ is investigated. Therefore, in fig. 5.7 typical FDs for different values of T_B and $\alpha_- = 0.1$ are depicted. Furthermore, in fig 5.8 the FDs for different α_- are given for a fixed value of $T_B = 1$.

At this point it has to be recalled that α_- is set to α for a chosen $\alpha < \alpha_-$ as described in the model definition. This is important in order to tune densities less than by α_- provided. This method prevents from obtaining an artificial shape of the FD at these small densities.

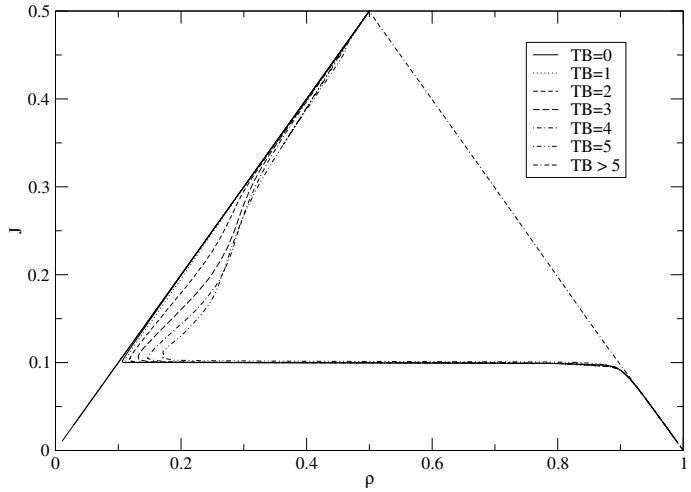

Figure 5.7: FDs of an open system with fall back rule and deterministic movement for different values of T_B. The system parameters are $L = 1000$, $B = 10$ and $\alpha_- = 0.1$. Clearly, the influence of the different chosen threshold values for the use of the fall back rule can be recognized. For $T_B > 5$ the fall back rule does not have any influence and the shape of the FD becomes regular or more precisely identical to the one of the AMOP without fall back inflow strategy.

Starting with fig. 5.7 clearly one finds that the free-flow regime is not affected by the fall back rule for any value of T_B. Here, similar to the investigations of the case with $\alpha_- = 0$ the outflow is unbound and the system flow and density are adjusted by the inflow given by the interplay of α and α_-. Clearly, one finds a linear increase of the system flow with rising densities until the maximum flow of $J^* = 1/2$ is reached at the density $\rho^* = 1/2$.

Regarding maximal inflow rates $\alpha = 1$ and varying β in order to tune densities $\rho > 1/2$ one clearly finds that for $T_B < B/2$ density and also system flow are affected due to the application of the fall back rule. Otherwise, for values of $T_B > B/2$ the jammed branch is not affected by the reduced inflow rate α_- as well and the FD becomes again identical to the one of the ASEP respectively the model without fall back rule.

Considering $T_B < B/2$ similar to the case of vanishing reduced inflow rates the system flow as well as the system density are reduced with decreasing outflow rates until the system flow becomes approximately q_{in-}. Here, q_{in-} represents the system flow given by the reduced inflow rate α_-. A further decrease of the system outflow results in the formation of a plateau for a wide range of densities. The system flow is kept constant at $\approx q_{in-}$. The jammed branch is entered first for $q_{out} < q_{in-}$. Here, the typical linear decrease of the system flow with increasing densities can be recognized.

The influence of different values of the fall back inflow rate α_- onto the FD and therewith onto the system dynamics is depicted fig. 5.8. The buffer size is again set to $B = 10$ and the threshold for applying the fall back rule is set to $T_B = 1$ in order to get prominent effects as shown above.
Similar to the previous investigations the typical modified FDs with fall back characteristics and plateau formation becomes arises whereas the plateau value rises with increasing α_- until the FD merges into the one of the model with generic inflow strategy.

With regard to the FDs from fig. 5.7 and fig.5.8 where the choice of the threshold T_B and α_- exerts an immense influence onto the system flow the influence of the fall back rule can clearly be identified. The effect becomes more distinctive for low values of the reduced inflow rate α_- and low values of the threshold T_B. Moreover, it has to be mentioned here that with respect to the density one clearly finds threefold degenerated system states as depicted in fig. 5.8 for $\alpha_- = 0.1$ or more articulately in fig. 5.7 for $T_B = 5$ at densities of $\rho \approx 0.2$.

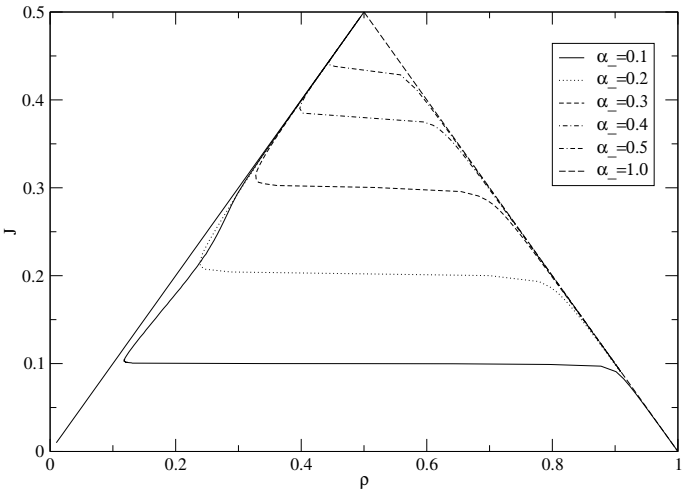

Figure 5.8: FDs for different values of α_-. The system size is set to $L = 1000$ and the buffers are restricted to $B = 10$. The threshold is set to $T_B = 1$ in order to get distinctive effects on the FDs. Clearly, the influence of the fall back rule can be noticed in the region of medium and high densities until the system enters the jammed regime for $q_{out} < q_{in}$. The outflow dominates the system dynamics. In the free-flow regime the fall back rule does not have any effect an the FDs for both inflow strategies become identical.

5.4.3 Space-time Plots

As considered before a useful method to get a clearer impression of the system dynamics involved in the appearance of different system states is the investigation of typical space-time plots. Here, especially the two free-flow and the two jammed states are of prime interest. Thus, in order to characterize the different system properties, space-time plots of exactly these system states are considered.

In fig. 5.9 space-time plots of the two different free-flow regimes are depicted for a system of $L = 100$ sites equipped with buffers of size $B = 10$ and a threshold $T_B = 5$ for applying the reduced inflow rate of $\alpha_- = 0.1$.
Here, the inflow rate dominates the system dynamics since all inserted particles move deterministically throughout the entire system. No jams will appear because of the deterministic outflow given by $\beta = 1$. Remind that the inflow is reduced to α_- whenever more than T_B particles induced by the inflow rates α or α_- arrive at the last site.

In the left diagram of fig. 5.9 the inflow probability is chosen to $\alpha = 0.1$ and thus the probability that more than T_B particles are inserted becomes very small. This means that the fall back rule is hardly applied and the space-time plot is characterized by a rather homogeneous pattern.
Considering the right diagram of fig. 5.9 the inflow rate is set to $\alpha = 0.7$. Now statistically more than T_B particles are inserted and the fall back rule is applied. As a result one finds that the space-time plot exhibits a rather striped than a homogeneous shape.

Nevertheless, it is to mention that because of the parallel dynamics anyway the inflow alternates between effective inflow rates of $\alpha = 0.7$ and $1 - q_{in}(\alpha = 0.7)$. Thus, in case of $T_B = 5$ the influence of the fall back rule is reduced. This is due to the fact that fall back rule is statistically applied every second time step meaning that the inflow alternates between $q_{in}(\alpha = 0.7)$ and $q_{in-}(\alpha_- = 0.1)$. Obviously the differences between $q_{in-}(\alpha_- = 0.1)$ and $1 - q_{in}(\alpha = 0.7)$ are very small and thus the impact of the fall back rule can hardly be noticed.
For the sake of simplicity in the following investigations the inflow rate respectively the corresponding mean inflow providing more than T_B particles into the first site will be denoted by α_T resp. q_{in}^T.

With the help of this notation a schematic representation of the free-flow phases induced by the fall back inflow strategy is given:

- $q_{in} > q_{in}^T \wedge q_{in-} > q_{in}^T$
  The system inflow is given by q_{in-}. The fall back rule is applied all the time.

- $q_{in} > q_{in}^T \wedge q_{in-} < q_{in}^T$
  The inflow rate alternates between α and α_-, depending on the probability that more or less than T_B particles are inserted respectively present in the last site.

- $q_{in} < q_{in}^T \wedge q_{in-} < q_{in}^T$
  The system flow is mostly given by q_{in} and the fall back rule is hardly applied.

Note that the first and the second case show identical system dynamics. The only existing difference is the applied inflow rate and thus in both cases the system resides in homogeneous free-flow regime.

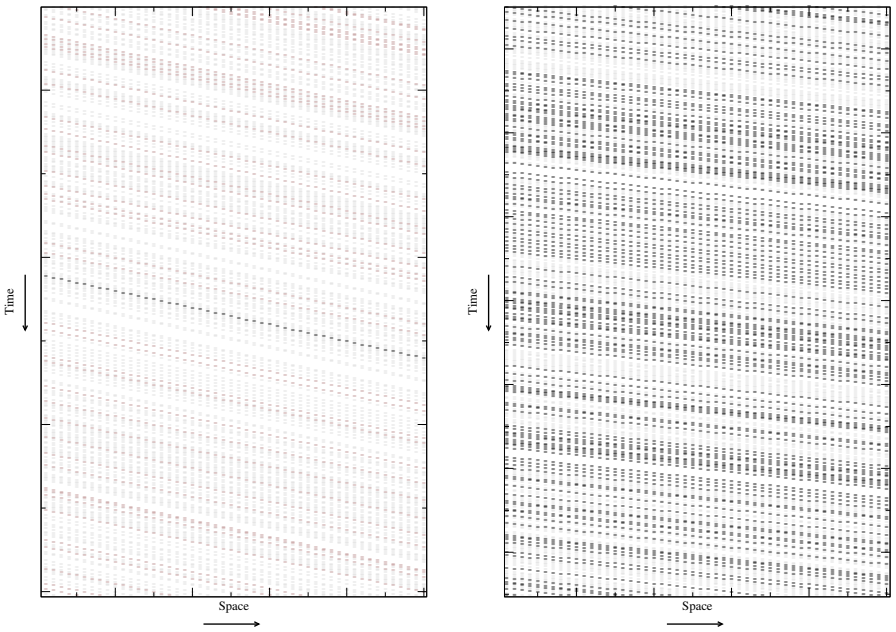

Figure 5.9: Space-time plots of the AMOP with fall back inflow strategy and deterministic bulk movement. The system parameters are $L = 100$, $B = 10$, $\alpha_{-} = 0.1$ and $T_B = 5$. **Left:** Space-time plot of the free-flow regime. For $\alpha = 0.3$ and $\beta = 1$ the particles move nearly undisturbed throughout the system and no jams exist. **Right:** Space-time plot of the second free-flow regime. Here, for $\alpha = 0.7$ and $\beta = 1$ in contrast to the rather homogenous system a striped pattern can clearly be identified. Even here no jams exist.

Regarding fig. 5.10 the two different jammed system states are depicted. In this case the density and therewith the system flow is tuned by the outflow rate β since maximal inflows are provided by $\alpha = 1$.

In general the jammed state is entered for inflows larger than the maximal system outflow q_{out}. Regarding the space-time plots in fig. 5.10 clearly the jammed system states can be identified. Starting with the left plot it is shown that the system is complete jammed. The outflow given by eq. (4.11) determines the flow and the fall back rule has no influence onto the system dynamics.
Otherwise, in the right diagram the jammed phase with its characteristic striped pattern can be identified and the efficiency of the fall back rule becomes apparent since the evolving jams dissolve and the system is prevented from complete jamming. Hereby, the inflow alternates between time intervals with reduced inflow rates and intervals where the maximal system inflow is provided.

This means that compact density clusters, induced at the left boundary by the maximal inflow are moving throughout the entire system until they reach the right end. Here, jams evolve for $q_{in} > q_{out}$. Provided that the threshold T_B is less than $B/2$ the inflow rate is

reduced to α_- due to the fall back rule and the jam dissolves for $q_{in-} < q_{out}$. After that the inflow rate is set back to α and the cycle starts again resulting in the alternation of high density and low density regions.

Even here one has to distinguish different relations between inflow, outflow and reduced outflow since the reduced system inflow is determined by the interplay of β and T_B. Similar to the case with $\alpha_- = 0$ the system inflow in the reduced inflow regime is given by the probability that the amount of particles at the right boundary becomes $\tau_L > T_B$ or $\tau_L \leq T_B$. This probability determines the alternation rate between maximal and reduced inflow rates and therewith the mean system inflow.

A schematic representation of the two different jammed states is given next:

- $q_{in} > q_{out} \wedge q_{in-} > q_{out}$
  The reduced inflow q_{in-} given by α_- becomes larger than the maximal system outflow q_{out} provided by β and the system runs into the completely jammed state.

- $q_{in} > q_{out} \wedge q_{in-} < q_{out}$
  The fall back rule is applied whenever a jam emerges at the right boundary and the typical striped pattern arises.

Summarizing this with respect to the space-time plots and the corresponding FDs the most important fact is that in a wide density range the fall back rule prevents the system from a complete jamming. Moreover, compared to the model with generic inflow strategy for a suitable choice of parameters a *striped pattern* can be identified in the free-flow as well as in the jammed regime. As mentioned before the striped pattern becomes more prominent for small values of T_B since in this case the alternation between high density and low density patterns becomes more conspicuous. This is also valid for low reduced inflow rates α_- compared to α.

5.4.4 Phase Diagram

In the previous sections it was shown that even in case of deterministic movement the FDs and the space-time plots exhibit distinctive new system properties in case of the fall back inflow strategy. The most important features compared to the rather elementary dynamics provided by the generic model definition are hereby the appearance two new system states. These are characterized by a striped pattern in the corresponding space-time plots.

In this section now the influence of the fall back inflow strategy on the phase diagram is investigated in case of deterministic particle movement. Obviously in the two special cases where $\alpha_- = \alpha$ or $T_B > B/2$ the fall back rule does not affect the system dynamics and the FDs and consequently the phase diagrams of the AMOP with both inflow strategies, i.e., generic and fall back, are identical and obviously both correspond to the FD of the model with periodic boundary conditions.

In order to point out in how far the fall back inflow strategy affects the shape of the phase diagram the impact of the inflow rate α and the outflow rate β on the system flow

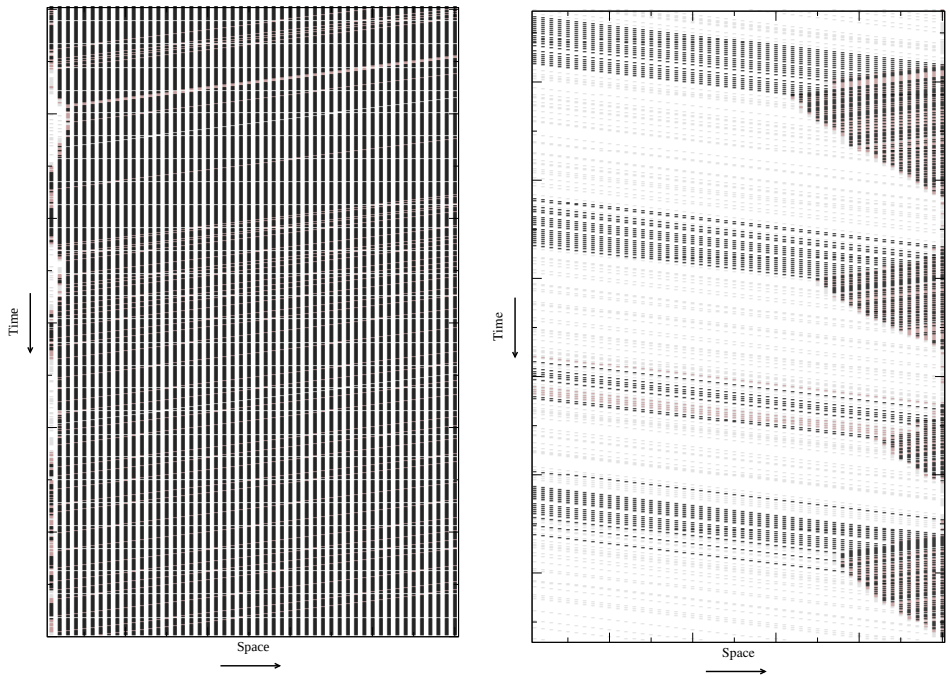

Figure 5.10: Space-time plots of the AMOP with fall back rule for deterministic movement. The system parameters are again $L = 100$, $B = 10$, $\alpha_- = 0.1$ and $T_B = 5$. **Left:** Space-time plot of the completely jammed system. Here, for $\alpha = 1$ and $\beta = 0.05$ the fall back rule exhibits no influence onto the system dynamics. The system flow is given by the outflow. **Right:** Space-time plot of the second jammed system state. In contrast to the completely jammed state here the fall back rule strongly affects the dynamics and a striped pattern can clearly be identified for $\alpha = 1$ and $\beta = 0.4$.

is depicted for different fixed outflow and inflow rates respectively and in particular in dependence of T_B and α_-. Consequently, the simplest case with $\alpha_- = 0$ and $T_B = 0$ is investigated first.

Case $\alpha_- = 0$

In fig. 5.11 and fig 5.12 the system flow is depicted in dependence of the inflow rate and the outflow rate respectively. The system parameters are chosen in both cases to $L = 1000$, $B = 10$, $T_B = 0$, $\alpha_- = 0$ and $p = 1$.

Remind that $T_B = 0$ implies as described in the previous investigations that the fall back rule is applied whenever a particle is present in the last site and consequently the system flow is in general drastically reduced compared to the model with generic inflow strategy and deterministic movement.

Regarding fig. 5.11 one finds that for inflows less than the maximal outflow provided by β the system is situated in the free-flow regime. There are only a few small disturbances at the right boundary but no large jams exist. Note that the fall back rule is actually applied for any chosen inflow rate α since $T_B = 0$. Thus, the free-flow regime is characterized by a striped pattern with periods of inflows $q_{in} < q_{out}$ and regions where the inflow rate is

ruled by α_-, i.e., $q_{in-} = 0$.

A further increase of the inflow rate α results in higher inflows and in case of $q_{in} > q_{out}$ the jammed regime is entered for any regarded outflow rate $\beta < 1$. Even here a striped pattern can be identified. However, the system is characterized by the appearance of jams evolving at the right end of the system.

In case of deterministic outflows given by $\beta = 1$ the maximal system flow is reached and the system turns back into the free-flow regime. This is due to the fact that the fall back rule does not have any effect in case of the maximal inflow rate $\alpha = 1$. Here, a completely filled buffer alternates with an empty one and thus the fall back rule is applied every second time step. This means that the maximal system flow is provided in case of an odd system length L. Otherwise, in case of even values of the system length the insertion is suspended every L-th time step .

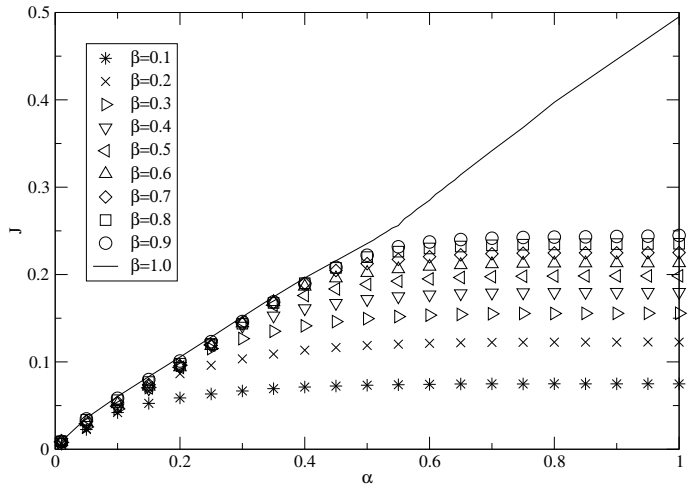

Figure 5.11: System flow J in dependence of the inflow rate α for fixed outflow rates β. The system parameters are $L = 100$, $B = 10$, $\alpha_- = 0$ and $T_B = 0$. Note that the maximal deterministic system flow is only reached for $\beta = 1$. Otherwise, there is a capacity drop meaning that the fall back rule reduces the maximal system inflow.

With regard to the diagram in fig. 5.12 one clearly finds that similar to the previous considerations the system flow is reduced strongly. Even here in case of outflows less than the system inflow ($q_{in} > q_{out}$) the jammed regime is entered meaning that the bunches of particles induced by α accumulate in front of the right boundary. Because of the fall back rule and $T_B = 0$ the inflow is reduced to $q_{in} = 0$ as long as particles are present in the last site. The inflow rate is set back to α not until the system runs empty. Considering inflow rates providing fewer particles than the capacity of the right boundary no jams exist and the system enters the free-flow regime. Similar to the jammed case a striped pattern arises. The system inflow vanishes due to the fall back rule with $T_B = 0$ for L time steps. Again for maximal inflow and outflow rates the maximal system flow of $J = 1/2$ is reached and the free-flow regime is entered again. Moreover, as described before for deterministic outflows $\beta = 1$, for any chosen inflow rate α there is a strong capacity increase compared to the striped free-flow regime.

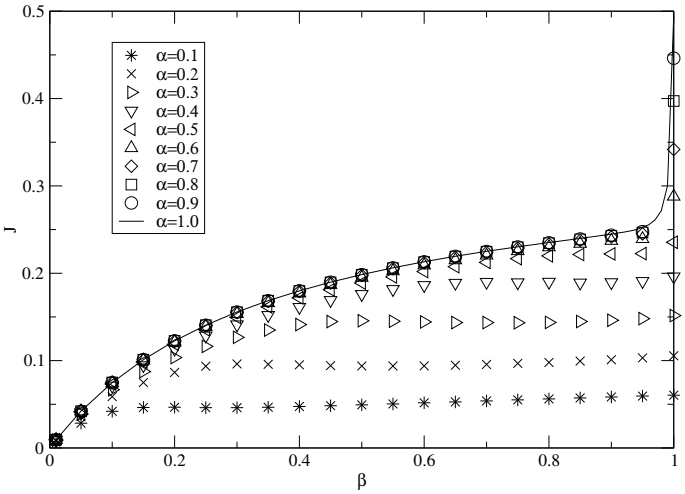

Figure 5.12: System flow J vs. β for fixed inflow rates α. The system parameters are identical to the considerations of J vs. α given by $L = 100$, $B = 10$, $\alpha_- = 0$ and $T_B = 0$.

With regard to the diagrams in fig 5.11 and fig. 5.12 two system states can be identified. There is a free-flow state for $q_{in} < q_{out}$ and jammed state for $q_{in} > q_{out}$. Nevertheless, the results for this special case with $\alpha_- = 0$ and $T_B = 0$ have to be considered in more detail since the free-flow as well as the jammed state exhibit a striped pattern induced by the fall back rule whereas neither a pure free-flow nor a completely jammed system state exists.

Case $\alpha_- \neq 0$

In contrast to the investigations of vanishing reduced inflow rate in the following $\alpha_- = 0.1$ is regarded exemplarily. The corresponding plots $J(\alpha)$ and $J(\beta)$ are depicted in fig. 5.13 and fig. 5.14 for a threshold value of $T_B = 5$.
In contrast to the case with $\alpha_- = 0$ the complete density range can be scanned as shown in the FDs in fig. 5.8 and in fig. 5.7. This is due to the fact that now for $q_{in-} > 0$ it is possible to provide reduced inflows of $q_{in-} > q_{out}$.

Starting with the consideration of $J(\alpha)$ in fig. 5.13 one finds completely different system dynamics compared to the case with vanishing reduced inflow rates.
Here, for inflows $q_{in} < q_{out}$ the system resides in the free-flow regime. Nevertheless, one has to distinguish two different cases. For inflow rates α providing less than T_B particles, i.e., $q_{in} < q_{in}^T$, the system shows a homogeneous pattern known from the model with generic inflow strategy as depicted in the left space-time plot of fig. 5.9. Otherwise, for rising inflow rates α the probability that q_{in} provides more than T_B particles is increased as well and thus the fall back rule is applied more often. Consequently a striped pattern can be identified (see right part of fig. 5.9).

As a result, for $q_{in} < q_{in}^T$ one finds that the system flow increases with rising inflow rates α given by eq. (4.7) whereas the fall back rule is applied marginal. For increasing inflow rates α the probability to insert more than T_B particles rises and consequently the system inflow is reduced more often resulting in a descending slope of the current. The fall back rule counteracts the increase of α and the system flow is increased only marginally.

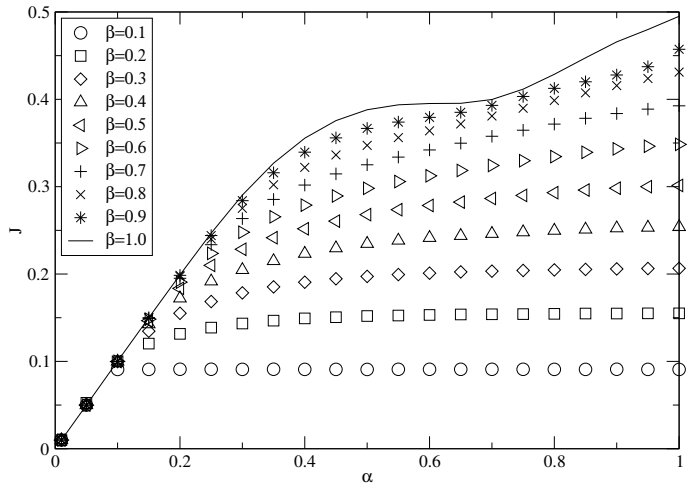

Figure 5.13: System flow J in dependence of the inflow rate α for for fixed outflow rates β and deterministic bulk movement. The system parameters are $L = 100$, $B = 10$, $\alpha_- = 0.1$ and $T_B = 5$.

In case of an unrestricted outflow with $\beta = 1$ even a small plateau arises for $q_{in} \approx q_{in}^T$. Nevertheless, conform to the previous investigations the system flow is increased for increasing inflow rates α until the maximal deterministic system flow is reached at maximal in- and outflows. Here, again the alternation of maximal inflow and zero inflow provides the maximal deterministic current.

Contrary, for outflows less than the given inflow ($q_{in} > q_{out}$) the jammed system state is entered. Similar to the previous investigations one has to distinguish the following two cases.
Provided that more than T_B particles are present in the last site, the fall back rule is applied whenever a jam exists at the right boundary. Thus, for $q_{in-} < q_{out}$ the system is prevented from a complete jamming. Here, the jams evolving at the right boundary dissolve and the system outflow dominates the system flow. The striped pattern arises as depicted in the right space-time plot of fig. 5.10 and consequently one finds a slightly rising plateau in the diagrams in fig. 5.13. This is due to the fact that in the free-flow cycle an increasing inflow rate α provides a larger number of particles and thus the time interval where the fixed outflow rate β determines the constant outflow is enlarged.
Otherwise, for $q_{in-} > q_{out}$ the system is completely jammed as depicted in the left part of fig. 5.10 since the system is overfed even by the reduced inflow and the fall back rule has no effect.

With respect to the diagrams in fig. 5.14 the results from the previous considerations are confirmed. For outflows less than the reduced inflow $q_{out} < q_{in-}$ the system enters the jammed phase and the flow can be calculated with eq. (4.11). Increasing of the outflow rate β further more with $q_{in} > q_{out} > q_{in-}$ the striped pattern arises provided that the fall back rule is applied for suitable chosen values of T_B.
Finally, for $q_{in} < q_{out}$ the system enters the free-flow regime. Again two free-flow states can be distinguished by considering whether q_{in} provides less or more than T_B particles into the system. Consequently, $P_{\alpha_-}(\alpha)$ given by eq. (5.1) can be accounted to characterize the nature of the free-flow phases, i.e., striped or homogeneous, as described before.

In case of inflows providing less than T_B particles ($q_{in} \leq q_{in}^T$) the free-flow regime is characterized by a homogeneous pattern and a plateau arises. Otherwise, for inflows providing more than T_B particles ($q_{in} < q_{in}^T$) the fall back rule is applied and the striped free-flow regime is entered. Here, the slope decreases since the fall back rule is applied more often for increasing inflow rates α. Thus, the probability for applying the fall back rule $P_{\alpha_-}(\alpha)$ rises as well. Finally, it is shown again that in case of $\beta = 1$ the system does not enter the jammed system state for any inflow rate α.

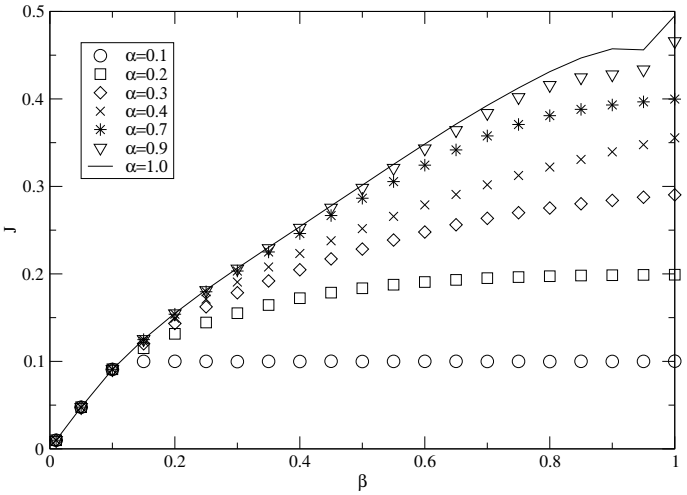

Figure 5.14: System flow J in dependence of the outflow rate β for for fixed in flow rates α. The system parameters are $L = 100$, $B = 10$, $\alpha_- = 0.1$ and $T_B = 5$. Here, for very small outflow rates the system enters the homogeneous jammed regime. Otherwise, the fall back rule prevents the system from a complete jamming.

It has to mentioned here that for large inflow rates $\alpha \to 1$ there is a strong increase of the system flow for deterministic outflows compared to slightly smaller vales. This is caused by the fact that there is a finite probability, that in case of $\beta \neq 1$ more than T_B particles rest in the last site after the update of a completely filled buffer. Thus, the fall back rule is applied consecutively for more than one time step resulting in a strongly reduced system inflow.
Contrary, in case of $\beta = 1$ this probability vanishes and the fall back rule is not applied consecutively for more than one update step. This effect is more distinctive for low values of T_B and large inflow rates α since large inflow rates provide a large amount of inserted particles and this means that the system inflow alternates due to the parallel dynamics between large and small bunches of particles. As a consequence the probability for exceeding T_B alternates every second time step.

In fig. 5.15 a schematic phase diagram of the deterministic model with fall back inflow strategy is depicted. The transition lines are derived by numerical simulations. Clearly, one finds that the free-flow as well as the jammed regime known from the AMOP with deterministic particle movement and generic inflow strategy are both separated by additional transition lines. These lines are given by the reduce inflow rate α_- and the inflow rate α_T indicating the inflow rate at which more than T_B particles are inserted into the chain.

The two free-flow regimes are denoted AI and AII. In both regimes the system inflow

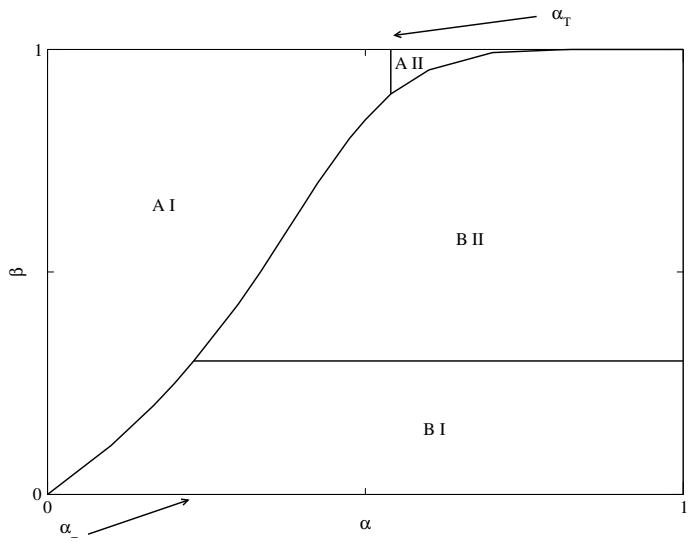

Figure 5.15: Phase diagram of the deterministic AMOP with fall back inflow strategy. Four different phases can be distinguished. Two free-flow phases AI and AII in the upper left and two jammed phases BI and BII down right part of the diagram.

provided by α is less than the maximal system outflow given by β, i.e., $q_{in} < q_{out}$. Thus, no wide jams exist. There are only a few density fluctuations in front of the right boundary which dissolve quickly.
The phase denoted to as AI represents the homogeneous free-flow regime, where the fall back rule is hardly applied since the system inflow is less than the inflow needed to exceed T_B, i.e., $q_{in} < q_{in}^T < q_{out}$. The second free-flow regime denoted as AII is characterized by a widely use of the fall back rule. In this case similar to the AI regime no wide jams exist since the system outflow is larger than the system inflow. Nevertheless, the use of the fall back rule implies a different structure of this free-flow phase and as depicted in the space-time plots in fig. 5.9 one finds a striped pattern with oscillating high flow and low flow areas induced by the alternation of the inflow rates α_- and α.

Regarding the jammed phase two different regimes, BI and BII can be distinguished as well. In general the jammed regime is characterized by system inflows providing more particles into the chain than the right boundary can deal with, i.e., $q_{out} < q_{in}$. Consequently, a jam emerges at the right end of the system. In case of $q_{in-} < q_{out}$ the fall back rule is applied and the jams emerging at the right boundary dissolve. The typical striped pattern arises. This regime is denoted to as BII. For reduced inflows larger than the capacity of the right boundary the application of the the fall back rule does not have any influence and the system is completely jammed. This state is labeled here as BI.

Note that for vanishing reduced inflow rates $\alpha_- = 0$ the jammed system state BI is not entered. This is only valid for $T_B < B - 1$ since otherwise the fall back rule is not applied. Remind that the case of $\alpha_- > \alpha$ is excluded in the model definition and thus not regarded. On the other hand the free-flow regime AI vanishes for $T_B = 0$ since now the fall back rule is applied whenever a particle is present in the last site. Contrary, for $T_B > B - 1$ the fall back rule hardly affects the system dynamics and the free-flow regime AII can not be entered.

Moreover, it is to mention that for $\alpha_T < \alpha_-$ the fall back rule is applied all the time and the system dynamics are governed by α_-. However, the characteristics of the two phases AI and AII are retained.

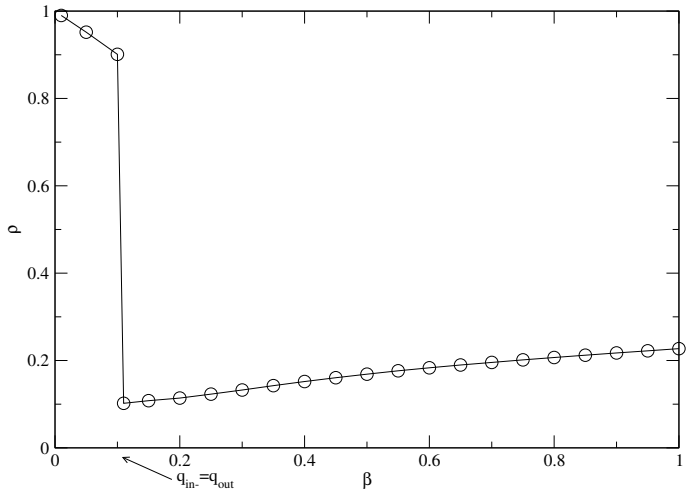

Figure 5.16: ρ vs. β at the transition line from the jammed phases BI to BII. Clearly, a discontinuity can be recognized at $q_{in-} = q_{out}$. The system parameters are $\alpha_- = 0.1$, $T_B = 1$, $B = 10$, $L = 1000$ and $\alpha = 0.2$

In order to evaluate if and in how far phase transitions arise in fig. 5.16 the mean system density ρ is depicted in dependence of the outflow rate β. Clearly a discontinuity in the density can be identified for the transition from BI to BII indicating the existence of a first order phase transition at reduced inflow rates α_- providing $q_{in-} = q_{out}$. This is not further surprising since for $q_{in-} > q_{out}$ the inflow strategy does not have any effect onto the dynamics while otherwise for $q_{in-} < q_{out}$ the arising jams dissolve immediately.

To evaluate the case AI to AII in fig. 5.17 the mean density is depicted in dependence of the inflow rate α for a suitable large outflow rate β. In contrast to the previous case here one finds that there is a smooth transition at α_T. The increase of the inflow rate vanishes and a small plateau is formed. This may indicate a second order or cross over phase transition.

However, the transitions have to be analyzed more detailed in further investigations.

5.5 Stochastic Model Dynamics, $p \neq 1$

In this section the influence of the fall back inflow strategy is investigated by means of numerical simulations in case of stochastic model dynamics. As shown in the previous sections the introduced fall back rule exerts an immense influence onto the system behavior even in case of deterministic particle movement. An important feature is hereby the inflow reduction in case of an arising congestion in order to prevented the system form a complete jamming.

Similar to the previous analysis the influence of the model parameters α_- and T_B responsible for the application of the fall back is investigated first. Thus, in fig. 5.18 FDs are

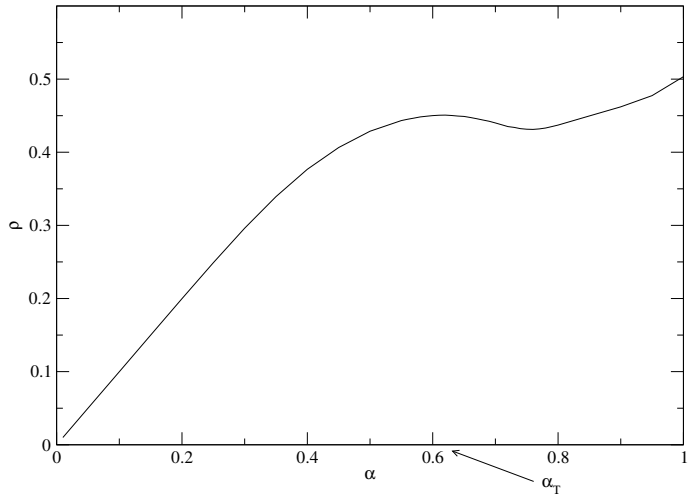

Figure 5.17: ρ vs. α at $\beta = 0.975$. The system parameters are $\alpha_- = 0.1$, $T_B = 5$, $B = 10$ and $L = 1000$. At α_T a region can be identified where a further increase of α does not have major effects onto the system density ρ.

depicted for $T_B = 1$ and $T_B = 3$ in case of stochastic system dynamics given by the moving probability $p = 0.5$. As before the free-flow branch is derived by considering deterministic outflows at dedicated inflow rates α while the jammed branch is scanned by providing maximal inflows and varying the outflow rate β.

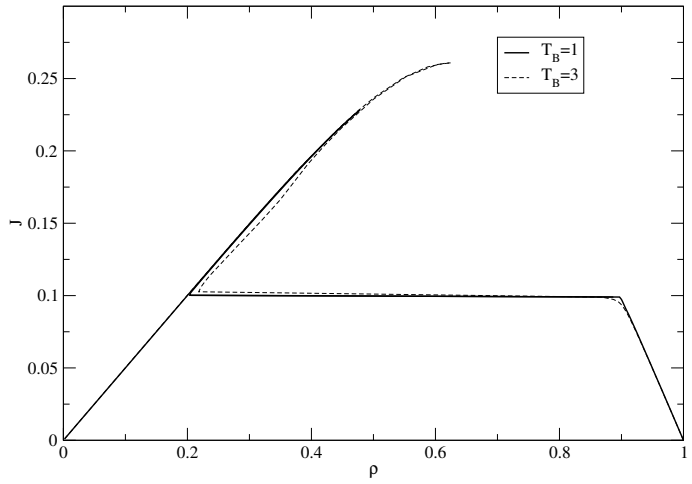

Figure 5.18: FDs of the model with fall back inflow strategy and stochastic movement ($p = 0.5$) for $T_B = 1$ and $T_B = 3$. Clearly, the influence of the reduced inflow rate of $\alpha_- = 0.1$ at a threshold value of $T_B = 1$ can be recognized in the jammed and even in the free-flow branch whereas in case of $T_B = 3$ only the jammed branch is affected. The system parameters are $L = 1000$ and $B = 10$.

Regarding the FDs in fig. 5.18 in contrast to the deterministic model even the free-flow branch ($q_{in} \leq q_{out}$) is affected by the fall back strategy. Here, in case of small values of α_- and T_B the maximal stochastic system flow of the AMOP with periodic boundary conditions can not be reached (straight line) due to the application of the fall back rule ($q_{in} > q_{in}^T$). Otherwise, for larger threshold values and reduced inflow rates q_{max} can be

adjusted (dashed line).
Considering the jammed branch ($q_{in} > q_{out}$) in both cases the FD shows the typical S-shape. For decreasing outflow rates the density as well as the system flow are decreased until the outflow becomes equal to the reduced inflow ($q_{out} \geq q_{in-}$). In this case the fall back rule is applied and the system is not completely jammed. In case of a further decrease of the outflow rates the system runs into a complete jamming ($q_{out} < q_{in-}$). Here, the system density is increased drastically and the FD merges into the jammed branch of the model with periodic boundary conditions.

Although the FDs for deterministic and stochastic bulk dynamics show similar characteristics there are apparent differences. Especially the fact that the maximal system flow of the periodic model can not be reached for some parameter sets of α_- and T_B is of prime importance. In this case the fall back rule obviously prevents the system from entering the maximum current phase and this means that the full capacity of the system is not reached.

In order to get a deeper insight into the model dynamics in the following typical space-time plots are investigated for meaningful parameter sets of α_- and T_B.

5.5.1 Space-Time Plots

Regarding the space-time plots in fig. 5.19 and fig. 5.20 the influence of the randomized particle movement becomes visible. As in the investigations of the AMOP with generic inflow strategy particles rest at their current position with probability $1 - p$ and thus density fluctuations arise within the system due to the internal dynamics. With regard to the fall back inflow strategy this is of prime importance. In contrast to deterministic particle movement, where inflow fluctuations induced by the fall back rule could be directly mapped to the last site, the inflow is strongly affected by the noise induced by the moving probability p. Thus, in case of stochastic bulk motion the inflow can not directly be mapped to the end of the chain and fluctuations induced by the fall back rule are smoothed.

In fig. 5.19 space-time plots of the free-flow regime are depicted for identical inflow rates α and α_-. In the left diagram the system inflow rate α mostly provides less than T_B particles, i.e., $q_{in} < q_{in}^T$ and thus the fall back rule is hardly applied. There are some fluctuations due to the stochastic dynamics but no large jams exist.
In contrast thereto in the right diagram for a suitable small value of T_B, α provides more than T_B particles and thus the fall back rule is utilized. However, the system density is reduced and a striped pattern can slightly be recognized despite the fact that the alternation of the inflow is strongly affected by probabilistic bulk movement.

In fig. 5.20 typical space-time plots of the jammed system state are shown. Considering the left plot a complete jamming of the system is depicted. For $q_{in-} > q_{out}$, meaning that even the reduced inflow rate provides a larger inflow than the right boundary can deal with a jam emerges at the right end of the system. The domain wall of free flowing and jammed particles is moving, depending on the ratio of q_{in} and q_{out}, in opposite direction of the particle motion until the left boundary is reached. The system gets completely jammed.
Contrary, in the right diagram the fall back rule is successfully applied and the emerging jams induced by the inflows larger than the capacity of the right boundary dissolve for $q_{in} > q_{out} \wedge q_{in-} < q_{out}$.

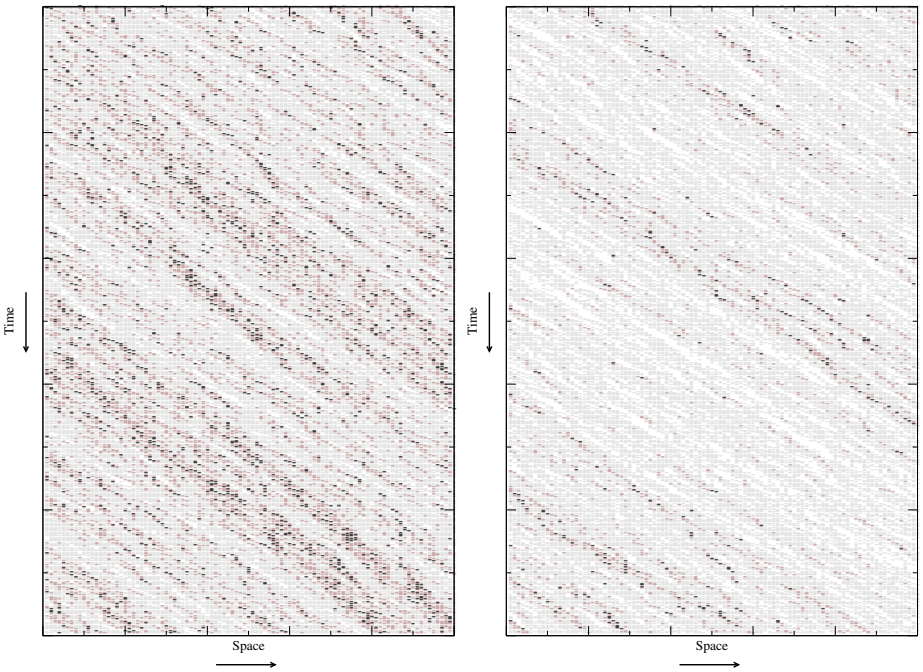

Figure 5.19: Typical space-time plots of the free-flow system. In both cases the system parameters are $\alpha = 0.3$, $\beta = 0.7$, $p = 0.5$ and $\alpha_- = 0.1$. **Left:** System in the free-flow state. The fall back rule is hardly applied since the mean system inflow provides less than $T_B = 4$ particles. **Right:** System in the free-flow state as well. The system density is strongly reduced due to the application of the fall back rule provided by $T_B = 2$.

With regard to the maximum current phase it is to mention here that the corresponding space-time plot provides the same characteristics as depicted in the left diagram of fig. 5.19. The main points are that no large jams exist and moreover, the mean inflow and outflow are higher than the maximal system flow q_{max}. It has to be mentioned again that due to the stochastic movement within the system one has to consider that the cumulative inflow is given by the combination of α and α_- and thus depending on the threshold value T_B.

With regard to the diagrams in 5.19 and 5.20 clearly the influence of stochastic model dynamics can be identified. The most important point is hereby that the system current arriving at the last site of the system is determined by the overlaid noise induced by the hopping probability p. Thus, especially in case of the free-flow and maximum current regime one has to consider the mean particle current within the system in order to evaluate in how far T_B is exceeded or not.

5.5.2 Phase Diagram

In the following the influence of the fall back strategy onto the phase diagram of the stochastic model is investigated. Therefore, the system flow is analyzed in dependence of the inflow and outflow rates at fixed values of T_B and α_-. Note, that if not stated otherwise the moving probability is set to $p = 0.5$ and the reduced inflow rate to $\alpha_- = 0.1$. More-

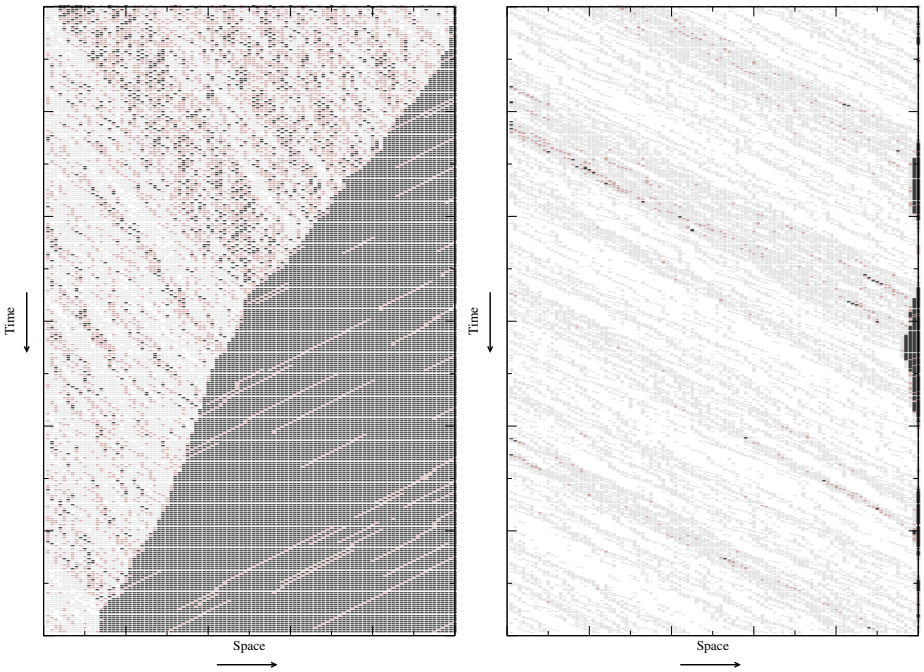

Figure 5.20: Typical space-time plots of the jammed system. **Left:** System in the jammed state. The fall back rule does not have any effect since $q_{in-} > q_{out}$. The domain wall between jammed and free flowing particles is moving to the left boundary. **Right:** System in the striped jammed state. Here, the jams induced in front of the right boundary dissolve due to the application of the fall back rule. The inflow is reduced in case of an emerging jam.

over the maximal system flow provided by the moving probability p and the buffer size B is referred to as q_{max} and thus represents the inflow respectively outflow that has to be exceeded in order to enter the maximum current phase.

Similar to the investigations of the deterministic model in fig. 5.21 and in fig. 5.22 $J(\alpha)$ and $J(\beta)$ are depicted for $T_B = 0$ and $\alpha_- = 0.1$.
Starting with the diagrams in fig. 5.21 for inflows less than the maximal outflow and less than the maximal system flow ($q_{in} < q_{out} \wedge q_{in} < q_{max}$) the system resides in the free-flow regime and the fall back rule is applied whenever a particle is situated in the last site of the system. Remind that the threshold is set to $T_B = 0$. However, for inflow rates $\alpha < \alpha_-$ the fall back rule does not have any effect since here α_- is set to α and thus for $\alpha \leq 0.1$ the system resides in the homogeneous free-flow regime known from the model with generic inflow strategy. A typical space-time plot of this scenario is depicted in the left part of fig. 5.19. For rising inflow rates $\alpha > 0.1$ the fall back rule is applied and the current is increased slightly.

In case of $q_{in} > q_{out} \wedge q_{out} < q_{max}$ the jammed system is entered and again two distinctive system states can be distinguished.
Considering the case with $\beta = 0.1$ in fig. 5.21 for inflows rates larger than $\alpha = 0.1$ the system inflow becomes larger than the system outflow and thus the fall back rule providing a reduced inflow of $\alpha_- = 0.1$ does not have any effect. Here, $q_{in-} > q_{out} \wedge q_{out} < q_{max}$ and thus the completely jammed system state is entered. This can also be found in fig. 5.22 for any chosen $\beta < 0.1$. In this case q_{out} determines the system flow and thus the current

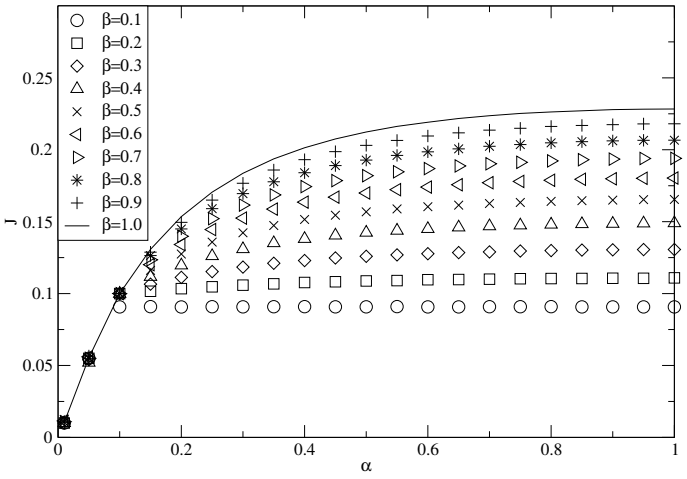

Figure 5.21: System flow vs. inflow rate at stochastic particle movement with $L = 1000$, $B = 10$, $p = 0.5$, $T_B = 0$ and $\alpha\_0.1$ for fixed values of β. Note that for $\alpha = 1$ the system flow decreases with decreasing outflow rates. Moreover the maximal system flow of the periodic AMOP is not reached for any chosen combination of α and β, indicating that the maximum current phase is not entered.

is increased with increasing β. A corresponding space-time plot is depicted in the left diagram of fig 5.20.
Regarding $q_{in-} < q_{out} \wedge q_{in} > q_{out} \wedge q_{out} < q_{max}$ the induced jams at the right boundary dissolve and the system is prevented from a complete jamming. A typical space-time plot of this scenario is depicted in right diagram of fig. 5.20.

With respect to the maximum current phase known from the investigations of the model with generic inflow strategy in case of $T_B = 0$ there is a constant rise of the system flow with increasing inflow and outflow rates whereas the maximal system flow of the periodic model is not reached. Thus, the maximum current phase is not entered. This is obviously induced by the fall back rule, preventing to provide inflows of $q_{in} > q_{max}$. This is also confirmed in the FDs in fig. 5.18 where the maximum system flow is not reached (see full lines).

In fig. 5.23 and fig. 5.24 $J(\alpha)$ respectively $J(\beta)$ are depicted for a threshold value of $T_B = 3$. The increased threshold implies that the sensitivity for applying the reduced inflow rate is reduced and thus it should be possible to enter the maximum current phase. This is confirmed by regarding the FDs in fig. 5.18. Here, obviously the maximal system flow of the model with generic inflow strategy and therefore of the AMOP with periodic boundary conditions is reached.

Considering fig. 5.23 in contrast to the case with $T_B = 0$ a plateau is formed for large inflow and outflow rates. Here, the flow becomes independent from α and β meaning that q_{max} is reached and the maximum current phase is entered for $q_{in} > q_{max} \wedge q_{out} > q_{max}$. This is also approved in fig. 5.24 where a plateau arises for outflow rates $\beta > 0.8$ and inflow rates $\alpha > 0.7$.

For inflow rates providing a system inflow larger than q_{out} and q_{out-} the system is completely jammed and thus the system flow is increased with rising outflow rates until

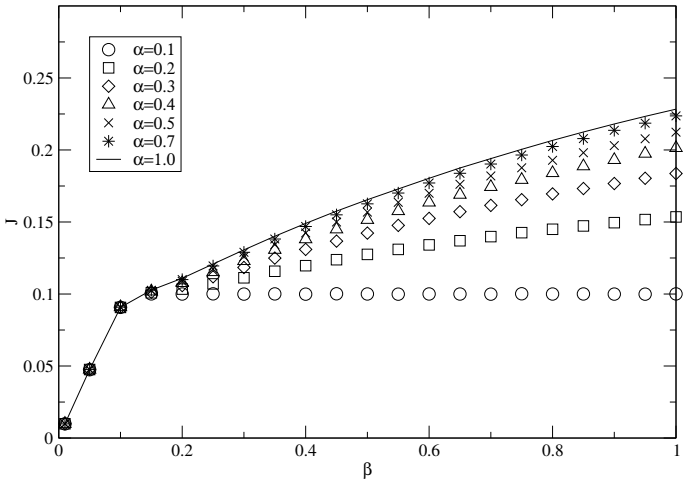

Figure 5.22: J vs.β for fixed inflow rates α and stochastic bulk movement. The system parameters are $L = 1000$, $B = 10$, $p = 0.5$, $T_B = 0$ and $\alpha_- = 0.1$. Even here the maximal system flow of the periodic AMOP is not reached and thus the maximum current phase can not be entered for the considered value of α_- and T_B.

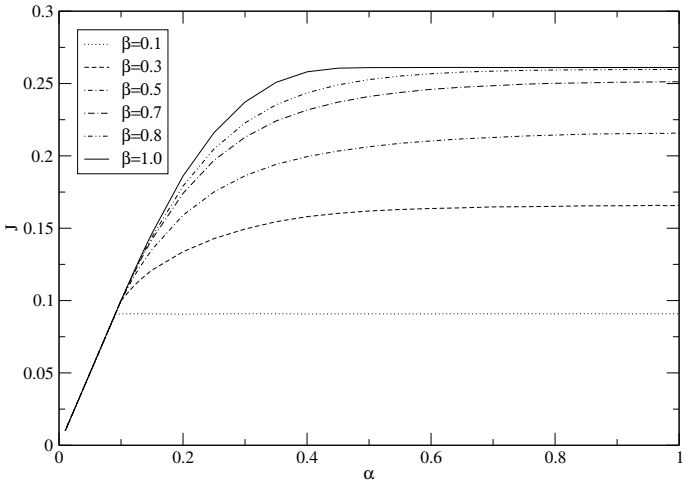

Figure 5.23: J vs. α in case of stochastic particle motion. Here, $T_B = 3$ while the remaining system parameters are again chosen to $L = 1000$, $B = 10$, $p = 0.5$, $T_B = 0$ and $\alpha_- = 0.1$. The maximal system flow of the AMOP is reached for some combinations of in and outflow rates. As a result the maximum current phase is entered.

$q_{in-} < q_{out} \wedge q_{out} < q_{in}$. Now the fall back rule is applied and prevents the system from a complete jamming. Nevertheless, some small jams arise in front of the right boundary. Here, the system flow is only slightly increased with increasing inflow rates α.

Regarding the free-flow regime even here two characteristic states known from the previous investigations can be identified. For $q_{in} < q_{out} \wedge q_{out} < q_{max}$ the system resides in the homogeneous free-flow regime and the fall back rule does not have any influence on the model dynamics. The flow is increased with rising α until more than T_B particles are inserted into the system ($q_{in}^T < q_{in} < q_{out} < q_{max}$). Now, the fall back rule is applied and

the system flow increases slowly with increasing inflow rates α.

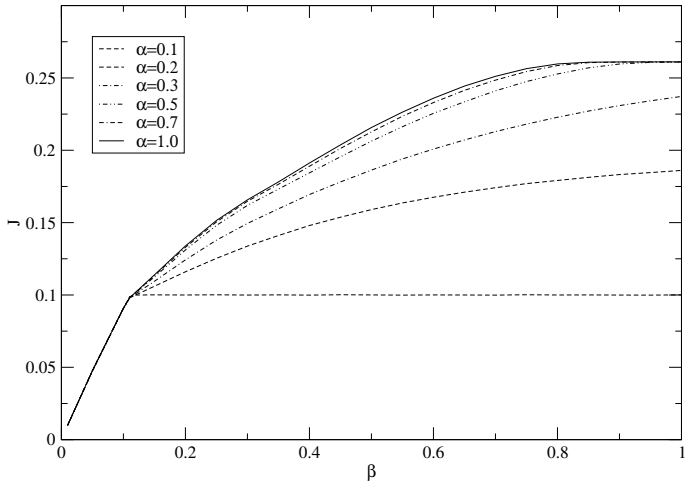

Figure 5.24: System flow J vs. β for $L = 1000$, $B = 10$, $p = 0.5$, $T_B = 0$, $\alpha_- = 0.1$ and $T_B = 3$. In contrast to the case with $T_B = 0$ here a plateau is formed at q_{max} for large values of α and β indicating that the maximal current phase is entered.

Considering the diagrams from fig. 5.21 to fig. 5.24 as expected the fall back rule strongly influences the system dynamics. Especially the maximum current regime is strongly affected. Here, the mean inflow given by α and α_- has to provide the maximal system flow q_{max}. As shown, this is only possible for a suitable choice of the threshold T_B and the reduced inflow rate α_-. An important point is hereby that as depicted in the diagrams for thresholds $T_B = 3$ the maximum current phase is entered. Compared to the AMOP with generic inflow strategy the combinations of α and β providing maximal system flows are strongly increased.

As a result the phase diagram of the AMOP with stochastic particle movement and fall back inflow strategy shows some yielding new features compared to the model with generic inflow strategy. Especially the maximum current phase is strongly affected by the interacting boundaries. A schematic representation of the phase diagram is depicted in fig. 5.25. Conform to the previous investigations the free-flow phases are denoted as AI and AII while the two jammed phases are referred to as BI and BII. Finally, the maximum current phase is denoted as C.

Similar to the phase diagram of the deterministic AMOP there are two jammed phases BI and BII. Here, BI represents the completely jammed system state. The fall back rule does not affect the system dynamics since α_- provides more particles than the right boundary can deal with. In contrast thereto in the phase denoted as BII the fall back rule is effectively applied. Emerging jams induced in front of the right boundary dissolve due to the reduction of the inflow rate and the jam vanishes. The inflow rate is set back to the initial value. Here, the typical striped pattern arises with the cycle of jammed - free-flow - jammed ... system states.

Regarding the free-flow states two special cases have to be distinguished.
For $\alpha_T \geq \alpha^*$, whereas α^* represents the inflow rate that has to be exceeded in order to

enter the maximum current regime, the free-flow as well as the maximum current phase are not affected and the phase diagram of these two phases becomes identical to the one known from the model with generic inflow strategy. In this case that the fall back rule is not applied in the free-flow as well as in the maximum current phase.

Otherwise, for $\alpha_T < \alpha^*$ the free-flow as well as the maximum current phase are strongly influenced. Regarding the free-flow regime now two phases can be distinguished referred to as AI and AII. In the AI phase given by $\alpha \leq \alpha_T$ the inflow rate is hardly reduced to α_- and thus the dynamics are not affected by the fall back rule. In contrast thereto for $\alpha > \alpha_T \wedge \alpha_T < \alpha_-$ the fall back rule is applied and the AII phase is entered. In this case striped characteristics can be identified in the space-time plot. Similar to the case with deterministic dynamics for $\alpha_- > \alpha_T$ the fall back rule is applied almost continuously and the homogeneous free-flow phase AI is entered.

Finally, the maximum current regime denoted as C is given by $q_{in}^{max} > q_{max} \wedge q_{max} < q_{out}$. Here, q_{in}^{max} represents the maximal system inflow in case of $\alpha_T < \alpha^*$. This means that the fall back rule is frequently applied. As shown in fig. 5.21 and fig. 5.22 this is of prime importance since for $q_{in}^{max} < q_{max}$ the maximum current phase is not entered. In this case the flow is restricted to q_{in}^{max} given by $\alpha = \beta = 1$.
As a result, in order to provide $q_{in}^{max} > q_{max}$ for low reduced inflow rates the threshold has to be increased. Thus, the application of the fall back rule is reduced while the system flow is increased.

Consequently the maximum current phase is strongly reduced or actually vanishes for low reduced inflow rates and small values of T_B. The corresponding inflow rate at which the maximum current phase is entered is denoted as α_{in}^{max}. Moreover it is to mention that as depicted in fig. 5.25 the phase boundaries of AII - C and BII - C are increased for increasing outflow respectively inflow rates.

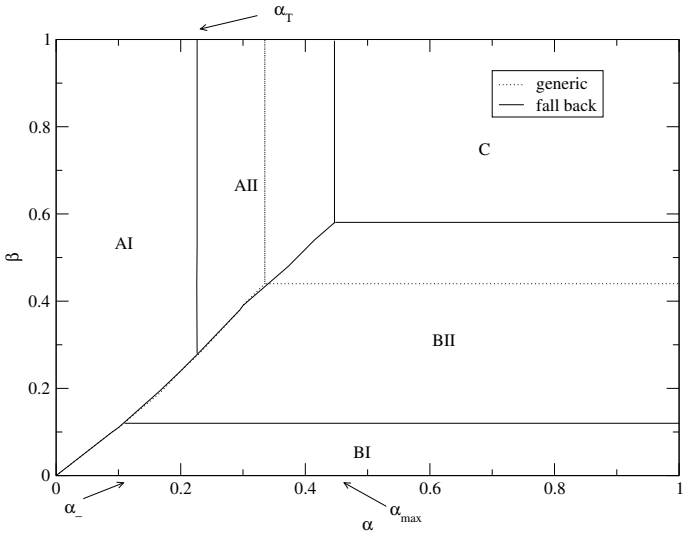

Figure 5.25: Phase diagram of the stochastic AMOP with fall back inflow strategy. Here, five different phases can be distinguished for $\alpha_T < \alpha^*$. Two free-flow phases AI and AII, two jammed phases referred to as BI and BII and a maximum current phase denoted as C.

Summarizing this, the most important fact is that the BI-phase is drastically reduced compared to the AMOP with generic inflow strategy. Here, in a wide area the fall back rule prevents the system from a complete jamming. Moreover it is to mention that for a suitable large value of T_B neither the free-flow nor the maximum current phase is affected by the fall back rule. Otherwise, for very small values of T_B and α_- the maximal system flow is reduced and thus the maximal current phase is not entered. The corresponding inflow rate in the phase diagram is referred to as α_{max}.

5.5.3 Discussion

In this chapter the influence of interacting boundaries on the system dynamics was investigated. Hereby, the focus lies on the analyze of flow control strategies known from the Internet. Therefore, a rather simple inflow rule was introduced with respect to the complex strategy implemented in TCP. A peculiarity of this strategy is the interaction of the boundaries meaning that the system inflow is determined by the state of the last site. Therefore, two new system parameters were introduced: A reduced inflow rate $\alpha_- < \alpha$ and a threshold value T_B determining that α_- is applied whenever the buffer of the last site is occupied with more than T_B particles.
It was shown that the modified inflow dynamics denoted as fall back strategy drastically affects the FDs as well as the phase diagrams in case of stochastic and deterministic particle movement.

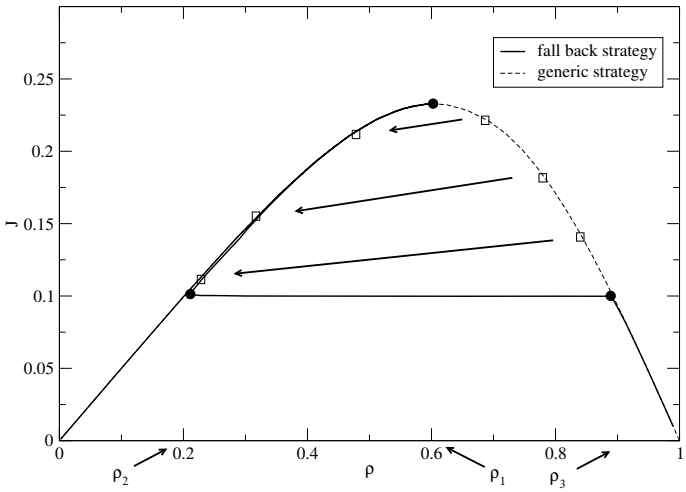

Figure 5.26: FDs of the AMOP with generic and fall back strategy. The marked points represent sets of identical in and outflow rates α and β. In case of the AMOP with fall back rule the jammed branch falls back to the free-flow branch for densities between ρ_1 and ρ_2.

With respect to the phase diagrams in case of both dynamics, i.e., deterministic and stochastic, two new phases could be identified. These new phases are characterized by a microscopic striped structure of alternating high and low density regimes migrating throughout the entire system. Here, especially the new striped jammed state is of special interest since jams arising at the right boundary dissolve due to the application of the fall back rule and thus the system is prevented from a complete jamming.

From the practical point obviously the survey of the stochastic model is of special interest

in order to figure out in how far the fall back strategy influences the global properties. With regard to the investigations of the phase diagram T_B should be chosen not to affect the free-flow as well as the maximum current phase, i.e., $\alpha_T > \alpha^*$. Thus, it is granted that the maximal system flow can be achieved. On the other hand the threshold has to be adjusted sufficiently small in order to prevent the system from a complete jamming.
Hence, in fig. 5.26 two FDs of the AMOP with generic and fall back inflow strategy are compared for characteristic values of α_- and T_B. Obviously the fall back rule does not affect the free-flow branch since the maximal system flow is reached. Considering the jammed branch exemplarily system flow and density of corresponding outflow rates β are marked by squares. Remind that the inflow rate is set to $\alpha = 1$. It can clearly be recognized that for a wide area of jammed system states between ρ_1 and ρ_3 the density falls back to the free-flow branch whereas the flow is slightly reduced compared to the corresponding parameter set of α and β of the generic inflow strategy. Obviously for smaller values of T_B the corresponding flow is reduced due to the more frequent application of the fall back rule. Considering the plateau it is shown that the corresponding boundary rates emerge from a small range of outflow rates given by $q_{out} \approx q_{in-}$.

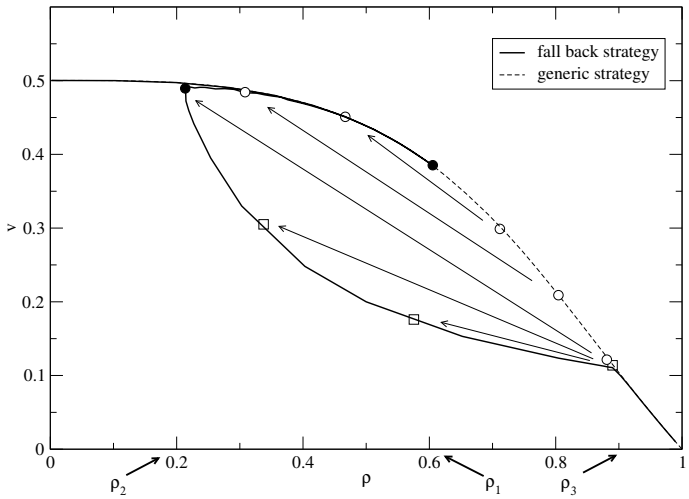

Figure 5.27: Mean velocity vs. density for the AMOP with generic and fall back inflow strategy. Identical sets of in and outflow rates for both strategies are opposed. One finds that a wide range of jammed system densities is not reached. Here, the fall back rule prevents the system from entering a complete jamming.

With respect to the travel times of data packets a more sophisticated representation of the influence of the fall back rule is given in fig. 5.27. Here, the mean velocity is depicted in dependence of the system density. As in the considerations of the FDs densities of $\rho \leq \rho^*$ are adjusted by considering deterministic outflows and varying the inflow rate α while densities of $\rho > \rho^*$ are scanned by setting $\alpha = 1$ and varying β. Similar to the previous investigations identical sets of inflow and outflow rates for both strategies are compared.

Regarding fig 5.27 one finds that the mean velocity of the model with fall back inflow strategy is strongly increased for a wide area compared to the case with generic inflow strategy. Thus, the mean travel times are drastically decreased. This is essential for real data transport.
With respect to reality this means that for a suitable choice of the threshold value the

free-flow phase is not affected. However, in case of an emerging jamming the fall back is effectively applied and thus the reduction of the inflow rate prevents the system from a complete jamming. Obviously the window size can be regarded as the equivalent to the threshold T_B while the reduced inflow would be the initial inflow rate at the beginning of a transmission that is increased until the threshold is exceeded.

6 Summary and Outlook

The intention of this work is to provide insight into the model dynamics of the asymmetric multi occupation process (AMOP), especially with open boundary conditions, first introduced to simulate Internet data transport.

This model is related to the class of driven lattice gas (DLG) automata models. In particular, the AMOP can be characterized as a discrete mass transport model with finite state space since each cell is equipped with a buffer of finite size. The local dynamics is realized by the totally asymmetric shift of discrete masses or particles under consideration of hard-core repulsion. Hereby, the update is considered to obey parallel dynamics.

In the *first chapter* of this thesis an introduction into the topic Internet is given. Thereon, in the *second chapter* the most important empirical results of Internet data transport are discussed in the context of statistical data analysis. Therefore, the fundamental techniques of time series analysis are recalled. After this, basic simulation models for Internet data transport are introduced and finally the most relevant cellular automaton (CA) model approaches and their analytical results are presented.

In the *third chapter* the AMOP with periodic boundary conditions is investigated in detail. A generic Mean-Field (MF) approach is applied in order to calculate the fundamental diagram (FD). It is shown that the results differ drastically from the numerical simulations especially in case of large buffer sizes. Thus, a more sophisticated technique has to be considered. In contrast to the MF approach where correlations are completely neglected the n-cluster approximation is applied in order to obtain better results. It is shown exemplarily for buffer size $B = 2$ that this complex approximation method provides much better results compared to the MF approach even in case of a cluster length of $n = 2$.

Thereon, in the *fourth chapters* the AMOP with open boundary conditions is investigated in the context of boundary induced phase transitions. This model was successfully introduced to simulate the basic properties of Ping-experiment time-series and thus could help to get a deeper insight into the nature of Internet congestions.
First, the model with deterministic bulk movement is investigated. Here, the only stochastic elements are the inflow respectively the outflow rates. A straightforward inflow strategy is chosen capable to provide the complete range of possible system flows. An analytically exact representation of the system flow for deterministic inflows and stochastic outflows respectively deterministic outflows and stochastic inflows is given in dependence of the buffer size. Therefore, the probability distribution of the occupation number of the first respectively last side is considered. It is shown that in contrast to the outflow the system inflow is strongly influenced by the buffer size. Hence, the phase diagram of the AMOP with deterministic particle movement is analyzed by means of analytical considerations and numerical simulations. It turns out that the buffer size drastically influences the shape of the phase diagram. Clearly, it is shown that the free flow phase is strongly reduced at the expense of the jammed phase compared to smaller buffers.

Regarding stochastic system dynamics the phase diagram is derived completely by Monte-Carlo simulations. Conform to the results known from the ASEP and other DLG models in the vicinity of noise a third phase arises. This maximum current phase is entered for inflows and outflows providing a higher capacity than the internal system dynamics. As in the considerations of deterministic bulk movement the shape of the phase diagram is strongly influenced by the buffer size. Here, the jammed phase and even the free-flow phase are both increased at the expense of the maximum current phase.
Furthermore, it is shown that the system flow within the phases is increased with rising buffers at the same set of inflow and outflow parameters. However, regarding the benefit of flow provided by the increase of the buffer size the gain rapidly converges to zero. In the context of reasonable hardware extensions this result is of prime importance since buffer extensions obviously provide larger system flows but on the other hand enlarge the processing time. Moreover, beyond a certain point the profit gained by increased buffer sizes vanishes and a further extension becomes uneconomic.

In the *last chapter* a more realistic inflow strategy is introduced with the intention to include flow control policies known from real Internet transport protocols and hence improve the stability of high flow states respectively data transmissions. As in reality the new *fall back* inflow strategy implies the communication between the two connection partners in order to adjust a reliable transmission rate.
In the model this is realized by interacting boundaries, i.e, the first and the last site communicate in so far that the inflow into the first site is adjusted in dependence of the state of the last one. Precisely, two new model parameters α_- and T_B are introduced. A reduced inflow rate α_- that is applied if more than a dedicated amount T_B of particles is present in the last site. Thus, an emerging jamming at the right boundary will dissolve due to the reduction of the inflow respectively the sending rate.
By means of numerical simulations it is shown that the fall back rule implies highly complex dynamics compared to the generic inflow strategy. Furthermore, the analysis of the phase diagram reveals the existence of two new phases in case of deterministic and stochastic particle movement. Both phases are characterized by a microscopic striped pattern of alternating high and low density regimes.
In the context of flow control policies the arising new jammed phase is of special interest since jams induced at the end of the chain dissolve due to the utilization of the reduced inflow rate. Hence, the system is prevented from a complete jamming. Furthermore, it becomes apparent that the mean velocity in this striped jammed phase is strongly enlarged compared to the model with generic inflow strategy for the same set of inflow and outflow parameters.
As a result for real flow control policies it is confirmed that the fall back policy is a useful and powerful strategy in order to prevent a system from a complete jamming. Nevertheless, this is performed at the expense of a reduced inflow. Here, arising jams are reduced and thus the effective transmission of a fixed amount of data packets is also reduced compared to the generic strategy. Moreover, the established connection becomes more stable and thus more reliable.

Recapitulating this, there are some further questions that should be analyzed in future.
With regard to the model dynamics it was shown that the AMOP can directly be related to extensively studied CA models like the ASEP and the ARAP. Unfortunately, an exact analytical representation could not be derived with the help of successfully applied standard techniques as the matrix product ansatz or advanced MF approaches. Here, the

finite buffer size, i.e., the finite state space of single sites introduces strong correlations and thus major difficulties. Thus, the complex dynamics are mostly analyzed by Monte-Carlo simulations. However, because of the relevance for real world problems systems equipped with restricted state spaces should be further analyzed.
Regarding open boundary conditions it was shown that the choice of the inflow strategies exhibit strong influences onto the system dynamics. As demonstrated, slight changes in the inflow rule sets are capable to provide a more stable system flow and strongly reduces the appearance of completely jammed system states. Thus, in terms of boundary induced effects the influence of various inflow strategies and scenarios should be investigated further more.
With respect to more realistic model dynamics concerning the appearance of jamming within the system, model extensions implementing absorption and annihilation at each site might be analyzed. In particular, the extension of the model in two dimensions is of prime interest.
Because of the high performance and the ability to reproduce the statistical features of Internet data transport the AMOP might help to investigate complex network topologies. Routing strategies and changes in the topology could be analyzed effectively in order to find and eliminate vulnerabilities.

Finally, it has to be stressed that a further analysis could help to improve the performance of the Internet.

Bibliography

[1] Internet mapping project. *http://www.opte.org*.

[2] Network simulator vers. 2. *http://www.isi.edu/nsnam/ns*.

[3] Requests for comments. *www.isc.org*.

[4] Abry, P., and Veitch, D. Wavelet analysis of long-range dependence traffic. *IEEE Trans. Information Theory 44*, 1 (1998), 2–15.

[5] Albert, R., and Barabasi, A. L. Topology of evolving networks: Local events and universality. *PRL 85*, 24 (2000), 5234–5237.

[6] Albert, R., and Barabasi, A. L. Statistical mechanics of complex networks. *Rev. Mod. Phys. 74*, 47 (2002).

[7] Antal, T., and Schütz, G. M. Asymmetric exclusion process with next-nearest-neighbor interaction: Some comments on traffic flow and a nonequilibrium reentrance transition. *Phys. Rev. E 62* (2000), 83–89.

[8] Appert, C., and Santen, L. Boundary induced phase transitions in driven lattice gases with metastable states. *Phys. Rev. Lett. 86* (2001), 2498–2501.

[9] Bak, P., Tang, C., and Wiesenfeld, K. Self-organized criticality. *Phys. Rev. A 38* (1988), 364–374.

[10] Bantay, P., and Janosi, I. M. Avalanche dynamics from anomalous diffusion. *Phys. Rev. Lett. 68* (1992), 2058–2061.

[11] Barabasi, A., and Stanley, H. E. *Fractal Concepts in Surface Growth*. Cambridge Univ. Press, Cambridge, 1995.

[12] Barabasi, A. L., and Albert, R. Emergence of scaling in random networks. *Science 286* (1999), 509–512.

[13] Barabasi, A. L., Albert, R., and Jeong, H. Mean-field theory for scale-free random networks. *Physica A 272*, 173 (1999).

[14] Barlović, R. Metastabile Zustände in Zellularautomatenmodellen für den Straßenverkehr. *Diplomarbeit, Gerhard-Mercator Universität Duisburg, Germany* (1998).

[15] Barlović, R., Huisinga, T., Schadschneider, A., and Schreckenberg, M. Open boundaries in a cellular automaton model for traffic flow with metastable states. *Phys. Rev. E 66* (2002), 046113.

[16] Barlović, R., Santen, L., Schadschneider, A., and Schreckenberg, M. Metastable states in CA models for traffic flow. In *Traffic and Granular Flow '97* (Singapore, 1998), M. Schreckenberg and D. Wolf, Eds., Springer, pp. 335–340.

[17] Barlović, R., Santen, L., Schadschneider, A., and Schreckenberg, M. Metastable states in cellular automata for traffic flow. *Eur. Phys. J. B 5* (1998), 793–800.

[18] Barlović, R., Schadschneider, A., and Schreckenberg, M. Random walk theory of jamming in a cellular automaton model for traffic flow. *Physica A 294* (2001), 525–538.

[19] Ben-Avraham, D., and Köhler, J. Mean-field (n,m)-cluster approximation for lattice models. *Phys. Rev. A 45* (1992), 8358.

[20] Cheybani, S., Kertész, J., and Schreckenberg, M. The nondeterministic Nagel-Schreckenberg traffic model with open boundary conditions. *Phys. Rev. E 63* (2001), 016108.

[21] Cheybani, S., Kertész, J., and Schreckenberg, M. Stochastic boundary conditions in the deterministic Nagel-Schreckenberg traffic model. *Phys. Rev. E 63* (2001), 016107.

[22] Chopard, B., and Droz, M., Eds. *Cellular automata modelling of physical systems*. Cambridge University Press, 1998.

[23] Chowdhury, D., Santen, L., and Schadschneider, A. Statistical physics of vehicular traffic and some related systems. *Physics Reports 329* (2000), 199–329.

[24] Chrobok, R., Kaumann, O., Wahle, J., and Schreckenberg, M. Three categories of traffic data: Historical, current, and predictive. *IFAC00* (2000), 250–255.

[25] Coppersmith, S. N., h. Liu, C., Majumdar, S., Narayan, O., and Witten, T. A. Model for force fluctuations in bead packs. *PRE 53* (1996), 4673.

[26] Crovella, M., and Bestavros, A. Self-similarity in world wide web traffic: Evidence and possible causes. In *IEEE/ACM Transactions on Networking* (1996), vol. 4, p. 209.

[27] Crovella, M., and Bestavros, A. Self-similarity in world wide web traffic: Evidence and possible causes. In *IEEE/ACM Transactions on Networking* (1997), vol. 5, pp. 835–846.

[28] Csabai, I. 1/f noise in computer network traffic. *J. Phys. A 27* (1994), 417–419.

[29] Davis, E., and Heiss, W. Random-phase approximation and broken symmetry. *J. Phys. G: Nucl. Phys. 12* (1986), 805–820.

[30] Derrida, B., Domany, E., and Mukamel, D. An exact solution of an one-dimensional asymmetric exclusion model with open boundaries. *J. Phys. A 26* (1992), 667.

[31] Derrida, B., and Evans, M. R. Bethe ansatz solution for a defect particle in asymmetric exclusion process. *JPA 32* (1999), 4833–4850.

[32] Derrida, B., Evans, M. R., Hakim, V., and Pasquier, V. Exact solution of a 1D asymmetric exclusion model using a matrix formulation. *J. Phys. A 26* (1993), 1493.

[33] Derrida, B., and Mallick, K. Exact diffusion constant for the one-dimensional partially asymmetric exclusion model. *J. Phys. A 30* (1993), 1031.

[34] Domb, C., and Lebowitz, J. L., Eds. *Phase Transition and Critical Phenomena*, vol. 19. Academic Press, New York, 2000.

[35] Domb, C., and Lebowitz, J. L., Eds. *Statistical Mechanics of Driven Diffusive Systems*, vol. 117. Academic Press, London, 2000.

[36] Dorogovtsev, S. N., and Mendes, J. F. F. Effect of the accelerating growth of communications networks on their structure. *PRE 63*, 025101 (2001).

[37] Dorogovtsev, S. N., and Mendes, J. F. F. Evolution of networks. *Adv. Phys. 51*, 1079 (2002).

[38] Dorogovtsev, S. N., and Mendes, J. F. F. *Evolution of Networks: From biological nets to the Internet and WWW*. Oxford University Press, Oxford, 2003.

[39] Evans, M. R. Bose-Einstein condensation in disordered exclusion models and relation to traffic flow. *Europhys. Lett. 36* (1996), 13–18.

[40] Evans, M. R. Exact steady states of disordered hopping particle models with parallel and ordered sequential dynamics. *J. Phys. A 30* (1997), 5669–5685.

[41] Evans, M. R. Phase transitions in one-dimensional nonequilibrium systems. *Braz. J. Phys. 30* (2000), 42–57.

[42] Evans, M. R., Rajewsky, N., and Speer, E. R. Exact solution of a cellular automaton for traffic. *J. Stat. Phys. 95* (1999), 45–96.

[43] Faloutsos, M., Faloutsos, P., and Faloutsos, C. On power-law relationship of the internet topology. *Comput. Common. Rev. 28* (1999), 44.

[44] Feldmann, A., Gilbert, A. C., Willinger, W., and Kurtz, T. G. The changing nature of network traffic: Scaling phenomena. *ACM Computer Communication Review 28* (1998), 5–29.

[45] Feller, W. *An Introduction to Probability Theory and Its Applications*. Wiley Series, 1968.

[46] Fukuda, K. *Phase Transition Phenomena in Internet Traffic: Observations and Possible Causes*. Phd thesis, Department of Computer Science, Keio University, Feb 1999.

[47] Fukuda, K., Takayasu, H., and Takayasu, M. Spatial and temporal behavior of congestion in intemet traffic. *Fractals 7* (1999), 23.

[48] Fukui, M., Sugiyama, Y., Schreckenberg, M., and Wolf, D., Eds. *Traffic and Granular Flow '01* (Heidelberg, 2003), Springer.

[49] Gardner, M. The fantastic combinations of john conway's new solitaire game "life". *Sc. American 220* (1970), 120–123.

[50] Gutowitz, H., Victor, J., and Knight, B. Local structure theory for cellular automata. *Physica D 28* (1987), 18.

[51] Hager, J. S., Krug, J., Popkov, V., and Schütz, G. M. Minimal current phase and universal boundary layers in driven diffusive systems. *Phys. Rev. E 63* (2001), 056110.

[52] Helbing, D., Herrmann, H., Schreckenberg, M., and Wolf, D., Eds. *Traffic and Granular Flow '99* (Heidelberg, 2000), Springer.

[53] Huberman, B. A., and Lukose, R. M. Social dilemmas and internet congestions. *Science 277*, 25 (1997), 535–537.

[54] Huisinga, T. Simulation des Datentransports im Internet mittels eines eindimensionalen Zellularautomatenmodells. *Diploma Thesis, Universität Duisburg, Germany* (2000).

[55] Huisinga, T., Barlović, R., Knospe, W., Schadschneider, A., and Schreckenberg, M. A microscopic model for packet transport in the internet. *PA 294* (2001), 249–256.

[56] Huisinga, T., Barlović, R., Knospe, W., Schadschneider, A., and Schreckenberg, M. Microscopic modeling of packet transport in the internet. In *Traffic and Granular Flow '01* (Heidelberg, 2003), M. Fukui, Y. Sugiyama, M. Schreckenberg, and D. Wolf, Eds., Springer.

[57] Huisinga, T., Barlović, R., Knospe, W., Schadschneider, A., and Schreckenberg, M. Microscopic modeling of packet transport in the internet. In *Traffic and Granular Flow '01* (New York, 2003), M. Fukui, Y. Sugiyama, M. Schreckenberg, and D. Wolf, Eds., Springer, pp. 401–406.

[58] Huisinga, T., Barlović, R., Schadschneider, A., and Schreckenberg, M. Phase diagram of a ca model for intent data tarnsport. In *Traffic and Granular Flow '03* (New York, 2005), M. Fukui, Y. Sugiyama, M. Schreckenberg, and D. Wolf, Eds., Springer, pp. 401–406.

[59] Huisinga, T., Barlović, R., Schadschneider, A., and Schreckenberg, M. Phase diagram of a discrete mass transport model with buffer restriction and open boundaries. *to appear in PA* (2005).

[60] Hurst, H. Long-term storage capacity of reservoirs. *Transactions of the American Society of Civil Engineers 116* (1951), 770–799.

[61] Hurst, H. E., Black, R., and Sinaika, Y. M. *Long-Term Storage in Reservoirs: An experimental Study.* Constable, London, 1965.

[62] Juhasz, R., and Santen, L. Dynamics of an exclusion process with creation and annihilation. *J. Phys. A: Math. Gen. 37* (2004), 3933–3944.

[63] Kadanoff, L. P. Built upon sand: Theoretical ideas inspired by granular flows. *Rev. Mod. Phys. 71* (1999), 435–444.

[64] Katz, S., Lebowitz, J. L., and Spohn, H. Phase transitions in stationary non equilibrium states of model lattice systems. *PRB 28* (1983), 1655–1658.

[65] Katz, S., Lebowitz, J. L., and Spohn, H. Stationary nonequilibrium states for stochastic lattice gas models of ionic superconductors. *JSP 34* (1984), 497.

[66] Kikuchi, R. Path probability method. *Prog. Theor. Phys. Suppl. 35*, 1 (1966).

[67] Kleinrock, L. *Queuing Theory, Volume II: Computer Applications.* John Wiley & Sons, 1976.

[68] Klümper, A., Schadschneider, A., and Zittartz, J. Equivalence and solution of anisotropic spin-1 models and generalized t-j fermion models in one dimension. *JPA 24* (1991), 955.

[69] Klüpfel, H. A cellular automata model for crowd movement and egress simulation. *Ph.D. Thesis, Universität Duisburg, Germany* (2002).

[70] Kolomeisky, A. B. Exact solution for a partially asymmetric exclusion model with two species. *Physica A 245* (1997), 523.

[71] Kolomeisky, A. B., Schütz, G. M., Kolomeisky, E. B., and Straley, J. P. Phase diagram of one-dimensional driven lattice gases with open boundaries. *J. Phys. A 31* (1998), 6911–6919.

[72] Krug, J. Boundary-induced phase transitions in driven diffusive systems. *Phys. Rev. Lett. 67* (1991), 1882–1885.

[73] Krug, J., and Garcia, J. Asymmetric particle systems on r. *JSP 99* (2000), 31.

[74] Kurose, J., and Ross, K. *Computer Networking. A Top-Down Approach Featuring the Internet.* Addison Wesley Longman, 2001.

[75] Lee, H. K., Barlović, R., Schreckenberg, M., and Kim, D. Mechanical restriction versus human overreaction triggering congested traffic states. *PRL 92*, 38702 (2004).

[76] Lee, J. Density waves in the flows of granular media. *Phys. Rev. E 49* (1994), 281.

[77] Leland, W. E., Taqqu, M. S., Willinger, W., and Wilson, D. V. On the self-similar nature of ethernet traffic(extended version). In *IEEE/ACM Transactions on Networking* (1994), vol. 2, pp. 1–15.

[78] Leland, W. E., and Willson, D. V. High time-resolution measurement and analysis of lan traffic: Implications for lan interconnection. In *INFOCOM91 IEEE* (1991).

[79] Liggett, T. M. *Interacting Particles.* Springer, 1985.

[80] MacDonald, J. T., and Gibbs, J. H. Kinetics of biopolymerization on nucleic acid templates. *Biopolymers 7* (1969), 707.

[81] Mandelbrot, B. B. *The Fractal Geometry of Nature.* Freeman, New York, 1983.

[82] Nagel, K., and Schreckenberg, M. A cellular automaton model for freeway traffic. *J. Physique I 2* (1992), 2221–2229.

[83] Nelson, R. *Probability, Stochastic Processes, and Queuing Theory.* Springer-Verlag, New York, 1998.

[84] Park, K., and Willinger, W. Self-similar network traffic: An overview. In *Self-Similar Network Traffic and Performance Evaluation* (2000), Wiley-Interscience, pp. 1–39.

[85] Pastor-Satorras, R., Vazquez, A., and Vespignani, A. Dynamical and correlation properties of the internet. *PRL 87*, 2587011 (2001).

[86] Pastor-Satorras, R., Vazquez, A., and Vespignani, A. Immunization of complex networks. *PRE 65*, 066130 (2002).

[87] Pastor-Satorras, R., and Vespignani, A. Epidemic spreading in scale-free networks. *PRL 86*, 3200 (2001).

[88] Pastor-Satorras, R., and Vespignani, A. *Evolution and Structure of the Internet. A Statistical Physics Approach.* Cambridge University Press, Cambridge, 2003.

[89] Paxon, V., and Floyd, S. Wide area traffic: The failure of poisson modeling. In *IEEE/ACM Transactions on Networking* (1995), vol. 3, p. 226.

[90] Paxon, V., and Floyd, S. Why we don't know how to simulate the internet. In *Proceedings of the 1997 Winter Simulation Conference* (1997).

[91] Peterson, L., and Davie, B. *Computer Networks. A system Approach.* Academic Press, 2000.

[92] Popkov, V., and Schütz, G. M. Steady-state selection in driven diffusive systems with open boundaries. *Europhys. Lett 48* (1999), 257–263.

[93] Press, W. H., Teukolsky, S. A., Vetterling, W. T., and Flannery, B. P. *Numerical Recipes in C++.* Cambridge University Press, 2002.

[94] Preston, K. J., and Duff, M. J. B., Eds. *Modern Cellular Automata: Theory and Applications.* New York: Plenum, 1984.

[95] Rajesh, R., and Majumdar, S. N. Conserved mass models and particle systems in one dimension. *JSP 99* (2000), 943.

[96] Rajewsky, N., Santen, L., Schadschneider, A., and Schreckenberg, M. The asymmetric exclusion process: Comparison of update procedures. *J. Stat. Phys. 92* (1998), 151.

[97] Rajewsky, N., Schadschneider, A., and Schreckenberg, M. The asymmetric exclusion model with sequential update. *J. Phys. A 29*, 12 (1996), L305.

[98] Riedi, R. H., and Willinger, W. Toward an improved understanding of network traffic dynamics. In *Self-similar Network Traffic and Performance Evaluation* (2000), Park and Willinger, Eds., Wiley.

[99] Schadschneider, A., and Schreckenberg, M. Cellular automaton models and traffic flow. *J. Phys. A 26* (1993), L679.

[100] Schadschneider, A., and Schreckenberg, M. Car-oriented mean-field theory for traffic flow models. *J. Phys. A 30* (1997), L69.

[101] Schreckenberg, M., Schadschneider, A., Nagel, K., and Ito, N. Discrete stochastic models for traffic flow. *Phys. Rev. E 51* (1995), 2939–2949.

[102] Schreckenberg, M., and Wolf, D., Eds. *Traffic and Granular Flow '97* (Singapore, 1998), Springer.

[103] Spitzer, F. Interaction of markov processes. *Advances in Math. 5* (1970), 246–290.

[104] Spohn, H. *Large Scale dynamics of Interacting Particles*. Springer, 1991.

[105] Stauffer, D. Computer simulations of cellular automata. *J. Phys. A 24* (1991), 909–927.

[106] Strogatz, S. H. Exploring complex networks. *Nature 410*, 268 (2001).

[107] Takayasu, M., Sato, T., and Takayasu, H. Evidence for a dynamic phase transition in information traffic. *Phys. Rev. E 1* (1995), 1.

[108] Takayasu, M., and Takayasu, H. 1/f-noise in a traffic flow model. *Fractals 1* (1993), 860–866.

[109] Takayasu, M., Takayasu, H., and Fukuda, K. Application of statistical physics to the internet traffics. *Physica A 274* (1999), 144.

[110] Takayasu, M., Takayasu, H., and Fukuda, K. Dynamic phase transition observed in the internet traffic flow. *Physica A 277* (2000), 248.

[111] Takayasu, M., Takayasu, H., and Sato, T. Critical behaviors and 1/f noise in computer networks. *Physica A 233* (1996), 924–934.

[112] v. Hakim, and Nadal, J.-P. Exact results for a 2d directed animals on a strip of finite width. *JPA 16* (1983), 213–218.

[113] Veres, A., Kenesi, Z., Molnar, S., and Vattay, G. On the propagation of long-range dependence in the internet. In *SIGCOMM* (2000).

[114] von Neumann, J., and Burks, A. W. *Theory of Self-Reproducing Automata*. Univ. of Illinois Press, Urbana, IL, 1966.

[115] W. Foster, I. G. F. B. Small pc-network simulation - performance case study. *Simulation News Europe* (2004).

[116] Watts, D. J., and Strogatz, S. H. Collective dynamics of small-world networks. *Nature 393* (1998), 440–442.

[117] Willinger, W., Taqqu, M. S., Sherman, R., and Willson, D. V. Self-similarity through high- variability: Statistical analysis of ethernet lan traffic at the source level. In *IEEE/ACM Transaction on Networking* (1997), vol. 5, pp. 71–86.

[118] Woelki, M. Steady states of discrete mass transport models. Master's thesis, University Duisburg-Essen, 2005.

[119] Wolf, D., Schreckenberg, M., and Bachem, A., Eds. *Traffic and Granular Flow* (Singapore, 1996), World Scientific.

[120] Wolf, D. E., and Grassberger, P. *Friction, Arching, Contact Dynamics*. World Scientific, Singapore, 1997.

[121] Wolfram, S. Universality and complexity in cellular automata. *Physica D 10*, 1 (1984), 35.

[122] Wolfram, S. *Theory and Applications of Cellular Automata*. World Scientific, Singapore, 1986.

[123] Wolfram, S. *A New Kind of Science*. Wolfram Media, Inc, Ilinois,USA, 2002.

[124] Zia, R. K. P., Evans, M. R., and Majumdar, S. N. Construction of the factorized steady state distribution in models of mass transport. *J. stat. Mech. L10001* (2004).

[125] Zielen, F., and Schadschneider, A. Exact mean-field solutions of the asymmetric random average process. *JSP 106*, 1/2 (2002), 173–185.

[126] Zielen, F., and Schadschneider, A. Matrix product approach for the asymmetric random average process. *JPA 36* (2003), 3709–2723.

Zusammenfassung und Ausblick

Die vorliegende Arbeit beschäftigt sich mit der detaillierten Analyse eines eindimensionalen diskreten Massentransport-Modells, des Asymmetric Multi Occupation Process (AMOP), zur Simulation von Internet-Datentransport.

Es handelt sich hierbei um ein so genanntes getriebenes System, d.h. der stationäre Zustand ist kein Gleichgewichtszustand. In der modernen statistischen Physik ist die Analyse dieser Nichtgleichgewichts-Prozesse, im thermischen Gleichgewicht oder nicht, zu einem wichtigen Forschungszweig gewachsen. Nicht zuletzt aufgrund der Tatsache, dass viele interdisziplinäre Problemstellungen auf Nichtgleichgewichts-Prozesse zurückzuführen sind. Beispiele hierfür finden sich in den unterschiedlichsten Forschungsfeldern wie der Modellierung von Straßenverkehr, der Proteinsynthese oder, wie im Fall des AMOP mit offenen Randbedingungen, in der Simulation und Analyse von Datentransportprozessen im Internet.

Das erste Kapitel dieser Arbeit gibt eine Einführung in die Thematik. Im zweiten Kapitel werden die wichtigsten empirischen Erkenntnisse vorgestellt und ein Überblick über die elementaren Methoden zur statistischen Datenanalyse gegeben. Im Folgenden werden die bekanntesten Simulationsmodelle für Internet-Transportprozesse dargestellt. Schließlich werden die relevantesten Zellularautomaten-Modelle zur Simulation von Nichtgleichgewichts-Prozessen und deren analytische Beschreibungen vorgestellt. Hierbei liegt das Augenmerk auf dem wohl bekanntesten diskreten Transportmodell, dem Asymmetric Simple Exclusion Process (ASEP) sowie dessen Lösung mit Hilfe des Matrix-Produkt-Ansatzes für stochastische Systeme. Desweiteren wird das Basismodell eines Massentransport-Prozesses vorgestellt: der Asymmetric Random Average Process (ARAP). Auch hier ist es möglich den stationären Zustand mittels des Matrix-Produkt-Ansatzes zu bestimmen. Weitere Untersuchungen haben gezeigt, dass der ARAP ebenfalls mit Hilfe des Mean-Field (MF)-Ansatzes exakt lösbar ist.

Das dritte Kapitel dieser Arbeit befasst sich mit der Untersuchung des AMOP unter Berücksichtigung periodischer Randbedingungen. Hierbei ist die Beschreibung des stationären Zustandes von besonderem Interesse. In diesem Zusammenhang wird das Fundamentaldiagramm (FD) sowohl unter Berücksichtigung deterministischer als auch stochastischer Dynamik mit Hilfe von analytischen Beschreibungen und numerischen Simulationen untersucht. Als Basis für die analytische Beschreibung dient hierbei der MF-Ansatz. Es wird gezeigt, dass der AMOP im Gegensatz zum ARAP im Fall stochastischer Dynamik nicht exakt mittels MF-Ansatz lösbar ist. Aufgrund der Beschränkung der Besetzungszahl auf den einzelnen Gitterplätzen müssen bei der analytischen Beschreibung Korrelationen berücksichtigt werden, die im Mean-Field-Ansatz gänzlich vernachlässigt sind. Exemplarisch wird gezeigt, dass die n-Cluster-Approximation für den Fall einer maximalen Zweifachbesetzung der Zellen deutlich bessere Ergebnisse liefert, als der MF-Ansatz.

Im vierten Kapitel wird der Einfluss offener Randbedingungen auf die Dynamik des AMOP untersucht. Es ist bekannt, dass offen getriebene Systeme so genannte randinduzierte Phasenübergänge aufweisen. Im Hinblick auf die Abhängigkeit des Phasendiagramms von Zufluss- und Ausflussraten sowie der maximalen Besetzungszahl eines Gitterplatzes wird zuerst der AMOP mit deterministischer Dynamik analysiert. In diesem Zusammenhang wird mittels analytischer Rechnungen gezeigt, dass der Systemfluss sowohl für deterministischen Zufluss und stochastischen Ausfluss als auch im umgekehrten Fall exakt bestimmt werden kann. Somit ist es möglich, das Phasendiagramm des deterministischen AMOP mit offenen Randbedingungen durch analytische Untersuchungen zu bestimmen. Ferner wird gezeigt, dass die Erhöhung der maximalen Besetzungszahl eine deutliche Vergrößerung der gestauten Phase mit sich bringt, während andererseits die Freifluss-Phase verkleinert ist.
Im Fall stochastischer Dynamik zeigt das durch Monte-Carlo Simulationen ermittelte Phasendiagramm ebenfalls eine Abhängigkeit von der gewählten maximalen Besetzungszahl eines Gitterplatzes. So ist die Maximalstromphase, d.h. die Phase in der der Fluss unabhängig von der Zufluss- und Ausflussrate und nur durch die Sprungwahrscheinlichkeit bestimmt wird, für steigende maximale Besetzungszahlen deutlich reduziert. Andererseits sind die gestaute und die Freiflussphase in gleichem Maße vergrößert. In Bezug auf den maximalen Fluss in der jeweiligen Phase ist jedoch zu sagen, dass dieser mit steigender maximaler Besetzungszahl zwar anwächst, andererseits der Zuwachs jedoch stetig gegen Null strebt.
In Hinblick auf reale Hardware-Erweiterungen zeigt dies, dass ein Kapazitätsausbau nur bei gleichzeitiger Erhöhung der Verarbeitungsgeschwindigkeit sinnvoll ist. Zu beachten ist ferner, dass die nachfolgenden Knotenpunkte ebenfalls die erhöhte Kapazität bewältigen, da sonst diese eine neue Engstelle darstellen und hier neue Datenverluste drohen, die schließlich zum Zusammenbruch der Verbindung führen können.

Im fünften der Arbeit wird der Einfluss einfacher Flusssteuerungsmechanismen auf die Dynamik des AMOP vorgestellt. Ziel ist es, existierende Hochflusszustände im System zu stabilisieren. Die hierzu implementierte *Fall-Back*-Zufluss-Strategie beruht auf der Kommunikation bzw. der Interaktion der Ränder. So wird der Zufluss in das System vom Zustand des letzten Gitterplatzes bestimmt, d.h. im Falle einer Störung am Ende des Systems wird der Zufluss deutlich reduziert. Das mit Hilfe von Monte-Carlo-Simulationen ermittelte Phasendiagramm zeigt zwei neue Phasen, die sowohl im Fall deterministischer als auch stochastischer Bewegung existieren. Es handelt sich hierbei jeweils um eine Freifluss- und eine Stau-Phase die sich durch ihre mikroskopische Struktur von den bekannten Phasen unterscheiden. Als wichtigstes Ergebnis ist festzuhalten, dass die vollständig gestaute Phase zugunsten der neuen gestauten Hochflussphase verkleinert ist.
Im Hinblick auf die Stabilität von Hochflusszuständen zeigt sich, dass die Einführung der Fall-Back Strategie einen deutlichen Vorteil birgt. So findet man im Vergleich zur generischen Zufluss Strategie, dass aufgrund der durch die Fall-Back-Regel induzierten reduzierten Zuflussrate die Übertragung einer festen Anzahl an Paketen deutlich schneller bewältigt werden kann.

Abschließend ist zu sagen, dass die vorgestellten Modelluntersuchungen einen tiefen Einblick in die Dynamik des AMOP geben. Insbesondere Effekte wie durch Randbedingungen induzierte Phasenübergänge konnten umfassend dargelegt werden. Trotz der offensichtlichen Nähe zu bekannten diskreten Transportprozessen wie dem ASEP und dem ARAP konnte keine analytisch exakte Lösung der Dynamik mit Hilfe bekannter Methoden präsentiert werden. In diesem Zusammenhang sollten neue Ansätze untersucht werden,

um eine analytisch exakte Beschreibung der stationären Zustände zu erlangen.
Im Hinblick auf Flussoptimierungsstrategien in offenen getriebenen Systemen konnte gezeigt werden, dass mit Hilfe einfacher Regelsätze eine deutliche Steigerung des Flusses zu finden ist. Dies könnte ebenfalls als Ansatzpunkt weiterer Forschung dienen. Die Entwicklung und Untersuchung verfeinerter Zufluss-Strategien sollte hierbei im Mittelpunkt stehen.
Auch könnte bei weiteren Untersuchungen die Analyse realistischerer Szenarien, wie Zufluss und Abfluss von Teilchen an allen Gitterplätzen (großkanonische Betrachtung) und schließlich die Erweiterung des Modells auf zwei Dimensionen, im Mittelpunkt stehen. Aufgrund der numerischen Effizienz des AMOP könnten hierbei neue Routenwahlverfahren evaluiert oder komplexe Netzwerk-Topologien auf Schwachstellen hin analysiert werden.

Kurzfassung

Die Analyse komplexer stochastischer Prozesse mittels diskreter Simulationsmodelle, so genannter Zellulärer Automaten, erfreut sich einer wachsenden Beliebtheit. In der vorliegenden Arbeit wird der Asymmetric Multi Occupation Process (AMOP) untersucht. Es handelt sich hierbei um ein diskretes stochastisches Modell, welches auf einem eindimensionalen Gitter definiert ist. Insbesondere lässt sich der AMOP in die Klasse der Massentransport-Modelle einordnen. Diese zeichnen sich durch die Mehrfachbesetzung der einzelnen Gitterplätze aus. Als Besonderheit weist das untersuchte Modell eine Beschränkung der Besetzungszahl eines jeden Gitterplatzes auf. Anzumerken ist hierbei, dass der AMOP unter Berücksichtigung offener Ränder zur Simulation des Internet-Datentransports eingeführt und erfolgreich angewendet wurde.

Der erste Teil dieser Arbeit beschäftigt sich mit der Untersuchung des AMOP unter Berücksichtigung periodischer Randbedingungen. Besonderes Augenmerk liegt hierbei auf der Beschreibung des stationären Zustandes. Verifiziert werden die Ergebnisse aus numerischen Simulationen mit analytischen Näherungsverfahren wie dem Mean-Field-Ansatz oder der n-Cluster-Approximation.
Der Einfluss offener Randbedingungen auf die Dynamik des Systems wird im zweiten Teil der Arbeit untersucht. Ziel ist es, mit Hilfe von analytischen Betrachtungen und Monte-Carlo-Simulationen den Einfluss verschiedener maximaler Besetzungszahlen auf das Phasendiagram zu analysieren. Es kann gezeigt werden, dass sowohl im Falle deterministischer als auch stochastischer Dynamik die Stauphase mit steigender maximaler Besetzungszahl deutlich anwächst. Im ersten Fall auf Kosten der Freiflussphase, im zweiten Fall auf Kosten der Maximalstromphase.
Im dritten Teil wird letztlich der Einfluss von interagierenden Randbedingungen auf die Modelldynamik untersucht. Hierzu wird eine neue *Fall-Back*-Einfüll-Strategie implementiert, die als Besonderheit interagierende Ränder aufweist. So ist der Zufluss in das Gitter insbesondere von der Besetzungszahl des letzten Gitterplatzes abhängig. Das mit Hilfe numerischer Simulationen ermittelte Phasendiagramm zeigt sowohl für deterministische als auch stochastische Dynamik die Existenz zweier neuer Phasen. Es handelt sich hierbei um eine weitere gestaute und eine weitere Freiflussphase, die sich in ihren mikroskopischen Eigenschaften von den bereits bekannten Phasen abgrenzen. Es stellt sich heraus, dass insbesondere die vollständig gestaute Phase zugunsten der neuen gestauten Hochflussphase deutlich verkleinert ist.

Danksagung

An dieser Stelle möchte ich mich bei den vielen Menschen bedanken, die zum Gelingen dieser Arbeit beigetragen haben.

Mein erster Dank gebührt Herrn Prof. Dr. Michael Schreckenberg für die Betreuung der Arbeit und die Schaffung idealer Arbeitsbedingungen.

Bei Herrn Dr. Robert Barlović und Herrn Priv.-Doz. Dr. Andreas Schadschneider bedanke ich mich für freundschaftliche Zusammenarbeit, fachliche Anregungen und unzählige Diskussionen.

Mein weiterer Dank gilt den Mitarbeitern des gesamten Lehrstuhls Physik von Transport und Verkehr. Die gelöste Arbeitsatmosphäre hat viel zum Gelingen der Arbeit beigetragen. Besonders hervorzuheben sind Frau Dr. Dahm-Courths und Herr Andreas Pottmeier. Ich werde die Gespräche in den Kaffeepausen sehr vermissen.

Ganz besonders bedanke ich mich bei Herrn Dr. Robert Barlović, der mir während des Studiums und der Promotion ein echter Freund geworden ist.

Für das sorgfältige Korrekturlesen des Manuskripts bedanke ich mich bei Dr. Robert Barlović, Priv.-Doz. Dr. Andreas Schadschneider und Andreas Pottmeier.

Ein großer Dank gebührt meinen Eltern Christa und Wolfgang sowie meine Schwester Kerstin, die mich nicht nur während meiner Ausbildung stets unterstützt haben.

Nicht zuletzt bedanke ich mich bei meiner Traumfrau Angela, die mir stets ein liebevoller Ansporn war und somit ganz besonders zum Gelingen dieser Arbeit beigetragen hat.

Lebenslauf

Persönliche Daten

Name:	Huisinga
Vorname:	Torsten
Geburtsdatum:	03 August 1972
Geburtsort:	Düsseldorf
Familienstand:	ledig
Staatsangehörigkeit:	deutsch

Schulausbildung

1979-1983	Friederich von Spee Grundschule Düsseldorf-Angermund
1983-1992	Erzbischöfliches Suitbertus-Gymnasium Düsseldorf-Kaiserswerth, Abschluss: Abitur

Grundwehrdienst

1992-1993	Freiherr vom Stein Kaserne Coesfeld

Hochschulstudium

Okt. 1993	Immatrikulation an der Gerhard-Mercator Universität Duisburg, Studiengang Physik (DII)
1993 2000	Abschluß der Diplomarbeit bei Prof. Dr. Michael Schreckenberg
Seit 2000	Anfertigung der vorliegenden Dissertation unter Anleitung von Prof. Dr. Michael Schreckenberg

Arbeitsverhältnisse

1998 – 2000	Studentische Hilfskraft am Lehrstuhl Physik von Transport und Verkehr der Gerhard-Mercator Universität Duisburg
seit 2000	Wissenschaftlicher Angestellter am Lehrstuhl Physik von Transport und Verkehr der Gerhard-Mercator Universität Duisburg

Erklärung

Ich versichere, dass ich die von mir vorgelegte Dissertation selbständig angefertigt, die benutzten Quellen und Hilfsmittel vollständig angegeben und die Stellen der Arbeit – einschließlich der Abbildungen –, die anderen Werken im Wortlaut oder dem Sinn nach entnommen sind, in jedem Einzelfall als Entlehnung kenntlich gemacht habe; dass diese Dissertation noch keiner anderen Fakultät oder Universität zur Prüfung vorgelegen hat; dass sie – abgesehen von unten angegebenen Teilpublikationen – noch nicht veröffentlich worden ist sowie, dass ich eine solche Veröffentlichung vor Abschluß des Promotionsverfahrens nicht vornehmen werde. Die Bestimmungen dieser Promotionsordnung sind mir bekannt. Die von mir vorgelegte Dissertation ist von Herrn Professor Dr. Michael Schreckenberg betreut worden.

Duisburg, den 29. Juli 2005

Teilpublikationen

T. Huisinga, R. Barlović, W. Knospe, A. Schadschneider and M. Schreckenberg, A microscopic model for packet transport in the Internet, Physica A, **294**, 249-256, (2001)

T. Huisinga, R. Barlović,W. Knospe, A. Schadschneider and M. Schreckenberg, Microscopic Modeling of Packet Transport in the Internet, *Traffic and Granular Flow '01*, M. Fukui, Y. Sugiyama, M. Schreckenberg and D.E. Wolf, Springer, Heidelberg (2003)

R. Barlović, T. Huisinga, A. Schadschneider, and M. Schreckenberg, Open boundaries in a cellular automaton model for traffic flow with metastable states, Phys. Rev. E, **66**, 046113 (2002)

T. Huisinga, R. Barlović, A. Schadschneider and M. Schreckenberg, Phase Diagram of a CA model for Intent Data Tarnsport, in *Traffic and Granular Flow '03*, M. Fukui and Y. Sugiyama and M. Schreckenberg and D.E. Wolf, Springer, New York (2005)